MODELING KINETICS AND THERMODYNAMICS OF AMINE BASED FUEL AND OXIDIZER INTERACTIONS

A THESIS SUBMITTED TO
THE GRADUATE SCHOOL OF NATURAL AND APPLIED SCIENCES
OF
MIDDLE EAST TECHNICAL UNIVERSITY

BY

MELİKE ÖZKAN ÖZER

IN PARTIAL FULFILLMENT OF THE REQUIREMENTS
FOR
THE DEGREE OF MASTER OF SCIENCE
IN
CHEMICAL ENGINEERING

SEPTEMBER 2021

Approval of the thesis:

MODELING KINETICS AND THERMODYNAMICS OF AMINE BASED FUEL AND OXIDIZER INTERACTIONS

submitted by **MELİKE ÖZKAN ÖZER** in partial fulfillment of the requirements for the degree of **Master of Science** i**n Chemical Engineering, Middle East Technical University** by,

Prof. Dr. Halil Kalıpçılar
Dean, Graduate School of **Natural and Applied Sciences** _____

Prof. Dr. Pınar Çalık
Head of the Department, **Chemical Engineering** _____

Prof. Dr. Deniz Üner
Supervisor, **Chemical Engineering, METU** _____

Prof. Dr. Viktorya Aviyente
Co-Supervisor, **Chemistry, Boğaziçi University** _____

Examining Committee Members:

Prof. Dr. Halil Kalıpçılar
Chemical Engineering, METU _____

Prof. Dr. Deniz Üner
Chemical Engineering, METU _____

Prof. Dr. Viktorya Aviyente
Chemistry, Boğaziçi University _____

Assoc. Prof. Dr. Çerağ Dilek Hacıhabiboğlu
Chemical Engineering, METU _____

Assoc. Prof. Dr. Selis Önel
Chemical Engineering, Hacettepe University _____

Date: 24.09.2021

I hereby declare that all information in this document has been obtained and presented in accordance with academic rules and ethical conduct. I also declare that, as required by these rules and conduct, I have fully cited and referenced all material and results that are not original to this work.

Name Last name : Melike Özkan Özer

Signature :

ABSTRACT

MODELING KINETICS AND THERMODYNAMICS OF AMINE BASED FUEL AND OXIDIZER INTERACTIONS

Özkan Özer, Melike
Master of Science, Chemical Engineering
Supervisor: Prof. Dr. Deniz Üner
Co-Supervisor: Prof. Dr. Viktorya Aviyente

September 2021, 154 pages

This study is conducted to develop a model for the parameters that determine the ignition delay time during hypergolic combustion of liquid bipropellants in rocket engines. Hypergolic combustion utilizes the heat of mixing between the fuel and the oxidizer for ignition. A model study is conducted in order to understand the role of heat of mixing on the final temperature and final distribution of species between a vapor and a liquid phase. Water and nitric acid were selected as model compounds, due to the availability of the data and similarity of the system to binary liquid propellants. In order to be able to generalize the conclusions, alternative methods were used to obtain mixture state energies and vapor-liquid equilibrium data.

Two constant Margules, van Laar and UNIFAC binary activity coefficient models were used to estimate both excess Gibbs free energy of the selected mixture and its vapor-liquid equilibrium. Moreover, density functional theory (DFT) estimations were performed using Gaussian09 software to estimate enthalpy, entropy, Gibbs free energy and binding energy upon mixing.

The predictions were compared to the experimental data. A simple calorimetry system was constructed to measure the mixing enthalpy. The measured values are compared with the estimations.

The experimental heat of mixing data was compared with DFT results. Although the estimations showed similar behavior in trend, it was shown that the estimations by DFT is almost eight times larger in magnitude than experimental results. Estimation models were also used and compared with the experimental data.

The methodology developed in this study can be extended to estimate the behavior of binary liquid propellants and their ignition delay times.

Keywords: Mixing Enthalpy, Binary Activity Coefficients, Hypergolic Ignition

ÖZ

AMİN BAZLI YANICI VE OKSİTLEYİCİ ETKİLEŞİMİNİN KİNETİK VE TERMODİNAMİĞİNİN MODELLENMESİ

Özkan Özer, Melike
Yüksek Lisans, Kimya Mühendisliği
Tez Yöneticisi: Prof. Dr. Deniz Üner
Ortak Tez Yöneticisi: Dr. Viktorya Aviyente

Eylül 2021, 154 sayfa

Bu çalışmada, roket motorlarında kullanılan hipergolik sıvı yakıt çiftlerinin yanması öncesindeki alevlenme gecikmesi zamanı üzerinde etkili parametreler modellenmesi çalışılmıştır. Hipergolik yanma, hipergolik sıvı yakıt çiftinin karışması esnasında açığa çıkan ısı enerjisi ile buhar fazına geçen yakıt çiftinin gaz fazı reaksiyonları ile başlamaktadır. Karışım ısısının karışımın son sıcaklığı ve türlerin sıvı ve buhar fazlarındaki dağılımındaki rolünü anlamak için bir model çalışması yürütülmüştür. Hipergolik yakıt çiftine benzerliği ve literatür verilerinin erişilebilirliği göz önünde bulundurularak su ve nitrik asit model bileşenleri olarak seçilmiştir.

Seçilen ikili sıvı karışımlarının artık molar Gibbs serbest enerjilerini ve sistemin sıvı – buhar dengesini tahmin etmek için iki katsayılı Margules, van Laar ve UNIFAC ikili aktivite katsayısı modelleri kullanılmıştır. Bununla birlikte, karışım esnasındaki entalpi, entropi, Gibbs serbest enerjisi ve bağlanma enerjilerinin tahmin edilmesi için yoğunluk fonksiyonel teorisi (DFT) tabanlı Gaussian09 yazılımı ile hesaplamalar yapılmıştır.

Bileşenlerin karışım ısısını ölçmek için basit bir kalorimetre sistemi kurulmuştur. Bu deneylerden elde edilen veriler, tahminler ile kıyaslanmıştır.

Deneysel veri ve DFT yöntemleri ile elde edilen veri karşılaştırılmıştır. Her iki yöntemle elde edilen karışım ısılarının kompozisyona bağlı benzer eğilim gösterdiği görülmekle birlikte DFT ile elde edilmiş tahminlerin kalorimetre ile elde edilmiş verilerden yaklaşık 8 kat daha büyük olduğu görülmüştür.

Bu çalışmada ortaya çıkarılan yöntem, yakıt çiftinin karışım ve sıvı – buhar faz davranışlarını ve alevlenme gecikmesini tahmin etmek amacı ile genişletilebilir.

Anahtar Kelimeler: Karışım Isısı, İkili Aktivite Katsayıları, Hipergolik Alevlenme

To My Beloved Country, Türkiye,

To My Beloved Family,

To My Love,

To My Future.

ACKNOWLEDGEMENTS

First of all, I would like to express my deepest gratitude to my supervisor Prof. Dr. Deniz Üner for encouraging and guiding me throughout the period of my graduate studies on such an important topic for the future of our country. Her vision, experiences and never-ending support helped me to overcome the difficulties and to seek for new solutions, gave me confidence and taught me how to think.

I want to thank to my co-supervisor Prof. Dr. Viktorya Aviyente for making me familiar with quantum chemical methods, which was a very new area for me. I also want to thank for her and her assistant İpek Munar for her valuable contributions to my work by performing DFT calculations and providing data to my work and answering my questions with a valuable guidance.

I am grateful that Roketsan A.Ş. has given me the opportunity to conduct graduate studies on my profession and supported my works by providing me time, knowledge and equipment necessary to do some parts of my studies.

I also would like to thank to my manager Hacı Eşiyok and my colleagues Ahmet, Kerem, Kaan, Gizem, Uğur, Adil and Erdi for supporting me in research and experiments.

My greatest gratitude is for my family; my mom Emine, my dad Bülent, my sister Zeynep and my in-laws Akif and Nimet, for always giving me support, tolerate my rush and never stopping to care with me during this period of time. My grandfather Mehmet deserves a big appreciation for supporting me up to now since I started to kindergarten. I also would like to thank to my furry babies Fiona and Frodo for staying with me and relaxing me through the stressful times.

Finally, I would like to thank my dear husband Görkem for loving and supporting me in all occasions. He has also a slice on the pie by guiding me on programming languages. He is simply the key of my happiness and success.

TABLE OF CONTENTS

LIST OF TABLES

TABLES

LIST OF FIGURES

FIGURES

LIST OF ABBREVIATIONS

ABBREVIATIONS

ASOG: Analytical Solutions of Groups

a.u.: Hartree Arbitrary Unit

B3LYP: Becke 3-Parameter, Lee, Yang and Parr Functional

B.E. : Binding Energy of Molecules

CAGR: Compound Annual Growth Rate

CI: Connectivity Index

COSMO-RS: Conductor-like Screening Model for Real Solvents

DFT: Density Functional Theory

IDT: Ignition Delay Time

IRFNA: Inhibited Red Fuming Nitric Acid

LLE: Liquid – Liquid Equilibrium

LNG: Liquid Natural Gas

LOX: Liquid Oxygen

MMH: Monomethyl Hydrazine

NIST: National Institute of Standards and Technology

NRTL: Non-Random Two Liquid

NTO: Nitrogen Tetroxide

PCC: Pearson Correlation Coefficient

PM6: Semi Empirical Parametric Model Number 6

PTFE: Polytetrafluoroethylene

RFNA: Red Fuming Nitric Acid

UDMH: Unsymmetrical Dimethyl Hydrazine

UNIFAC: Unified Activity Coefficient

UNIQUAC: Universal Quasi-Chemical

VLE: Vapor – Liquid Equilibrium

WFNA: White Fuming Nitric Acid

LIST OF SYMBOLS

SYMBOLS

A_i *: polynomial coefficients*

a_i^**: activity of component i*

a_i^{*IM}*: activity of component i in an ideal mixture*

a_{mn} *: UNIFAC group interaction parameters of groups m and n in Kelvin*

C_p *: heat capacity*

C_p^{mix}*: heat capacity of mixture*

C_p^i *: heat capacity of component i*

D_{ab} *: binary mass diffusivity*

E *: energy generated by an arbitrary process*

$E[\rho]$ *: exact ground-state energy*

E_K *: total kinetic energy*

$E_{P;e,N}$ *: electron-nucleus potential energy*

$E_{P;e,e}$ *: electron-electron potential energy*

$E_{XC}[\rho]$*: exchange-correlation energy*

f_i*: fugacity of component i*

f_i^{IM}*: fugacity of component i in an ideal mixture*

φ_i *: molar property of component i*

φ_i^* *: partial molar property of component I*

ΔG_{mix}^{IM} : *molar Gibbs free energy change of an ideal mixture*

δ^v: *atomic index for a single atom or vertex*

G_i : *molar Gibbs free energy of component i*

G_i^* : *partial molar Gibbs free energy of component i*

G_i^{*IM} : *partial molar excess Gibbs free energy of component i in an ideal mixture*

G_i^{*ex} : *partial molar excess Gibbs free energy of component i*

G^{ex} : *excess molar Gibbs free energy of mixture*

$G_i^{*ex\,\infty}$: *excess molar Gibbs free energy of component I at infinite dilution*

ΔH_{mix}^{IM} : *molar enthalpy change of an ideal mixture*

ΔH_{mix} : *enthalpy of mixing*

ΔH_i^{vap} : *molar heat of vaporization of component i*

H_i : *molar enthalpy of component i*

H^{ex} : *excess molar enthalpy of mixture*

N_H : *number of hydrogens atoms attached to the atom*

ψ : *wavefunction*

P : *pressure*

P^0 : *reference state pressure*

P_c : *critical pressure*

P_i^{vap} : *vapor pressure of component i at a specified temperature*

Q_{vap} : *heat required to evaporate the liquid mixture components*

Q_{auto} : *heat required to start auto-ignition at liquid phase*

ρ : *electron density*

R : *ideal gas constant*

R_k : *UNIFAC volume parameter of group k*

Q_k : *UNIFAC surface area parameter of group k*

ΔS_{mix}^{IM} : *molar entropy change of an ideal mixture*

S_i : *molar entropy of component i*

S^{ex} : *excess entropy of mixture*

T : *Temperature*

T^0 : *reference state temperature*

T_{auto}^{i} : *auto-ignition temperature of component i*

T_c : *critical temperature*

t_i : *time at the* i^{th}*instant*

τ : *number of type of the hydrogen suppressed graphs*

$U(a-b)$: *bond energy between molecules a and b*

ΔV_{mix}^{IM} : *molar volume change of an ideal mixture*

V_i : *molar volume of component i*

V^{ex} : *excess entropy of mixture*

V_i : *molar volume of component i*

x_i : *liquid phase mol fraction of component i*

y_i : *vapor phase mol fraction of component i*

γ_i : *activity coefficient of component i*

γ_i^{∞} : *activity coefficient of component i at infinite dilution*

γ_i^{az} : *activity coefficient of component i at the azeotrope point*

Z : *atomic number*

Z^v : *number of valance electrons in a single atom*

CHAPTER 1

INTRODUCTION

1.1 Types of Propellants

By definition, a propellant is any material in gas, liquid, or solid phase which is expanded to transfer motion to another object or a substance (Britannica, 1998). In a rocket engine, which is basically a reaction chamber, the main component to combust is called “propellant”, which is the reaction mass in the rocket. In rocket propulsion systems, there are main types of energetic fuels classified as solid, liquid and hybrid propellants. A subtype can also be defined as gelled propellant.

In a rocket engine, the required thrust is obtained by its propulsion system. Obeying the Newton’s third law of motion, the acceleration is given by the oppositely directed momentum of the heated combustion gases.

The type of propellant focused in this work is liquid propellants. Liquid propellants are energetic materials used in rocket engines to obtain a target thrust value, the required force to move any spacecraft in the air, for maneuvering and attitude control in space applications. When compared with the mostly used propellant type in the recent history, solid propellants, the standout features of the liquid propellants are higher mass density and higher specific impulse. According to the number of reactant types, liquid propellants are grouped as liquid monopropellants, liquid bipropellants and very rarely liquid tripropellants. Liquid monopropellants are single energetic materials and they combust by a catalytic agent. Some of the liquid bipropellants are cryogenic liquids.

According to the Rocket Propulsion Market Report, Global Forecast to 2027 (Wadhwani & Saha, 2021), during the period of the forecast, the share of liquid propellants is expected to increase at a compound annual growth rate (CAGR) of larger than 7%. The reason for this growth can be said to be the capability of yielding very high efficiency and specific impulse. As NASA stated that as well as being American space programs' signature fuel, liquid propellants are also preferred by other countries, which are doing satellite launch business. With the developments in space applications by the investments of big companies in R&D fields, the market share of liquid propellants is expected to grow in the following years.

In this industrial report of Rocket Propulsion Market, the forecast including liquid propellants is given in Figure 1.1 below. The forecast covers leading countries in the industry of rocket propulsion: U.S., India, France, Russia, Japan, New Zealand, Iran, Ukraine and China (Wadhwani & Saha, 2021).

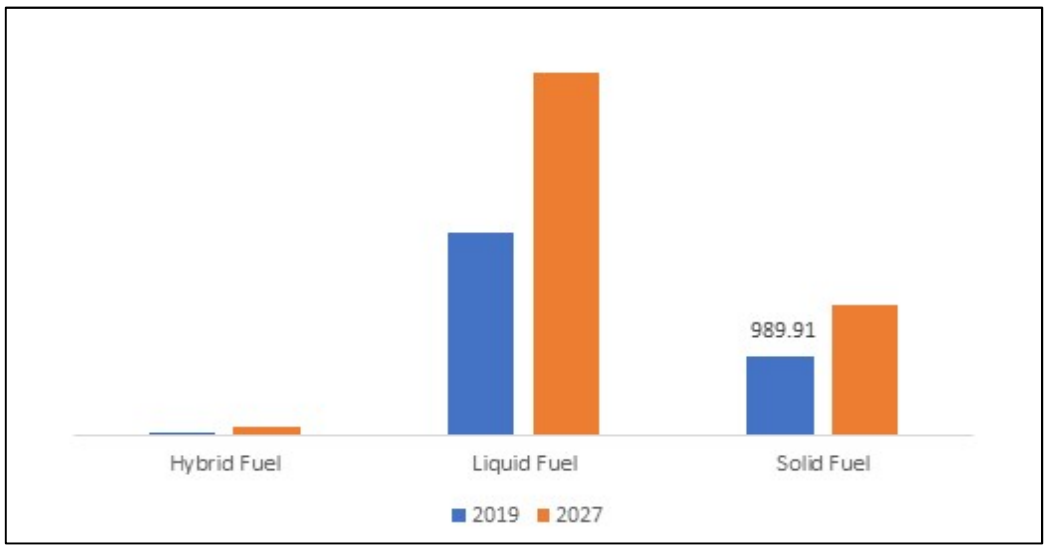

Figure 1.1. Rocket propulsion market size (in millions of USD) classified by the fuel type, 2019 data and 2027 forecast (Wadhwani & Saha, 2021).

Liquid bipropellants are promising due to their many benefits other than the ability to ignite without an ignition source, called as hypergolicity: simplicity of the system, storability, and high engine performance. Surely, they have some disadvantages with

the benefits: difficult handling and toxicity (Dennis, Son, & Pourpoint, 2012). However, some newly used green liquid bipropellants offer more nature friendly applications.

For any propulsion system, there are various important measurable properties such as the thrust per weight of the propellant (specific impulse) and adiabatic flame temperature of the propellant (Davis & Yılmaz, 2014). With those quantifiable properties, there is one more important indicator of performance of the hypergolic fuel and oxidizer combinations is the duration between contact of surfaces and ignition of the flame (Mays, Farmer, & Smith, 2010). According to Blevins et al. (2004), in hypergolic systems, ignition of the propellant occurs at the instant of heat generation of the system becomes greater than the heat absorption of the surrounding media, which enables a sustainable thermochemical combustion (Blevins, Gostowski, & Chianese, 2004).

There are also some disadvantages regarding the engine systems, too. While hypergolic ignition offers an ease to fire the rocket engine, it may offer some problematic features. The main problem of hypergolic ignition is the time delay, of the order of milliseconds. According to Thomas and Cantwell (2017), for hypergolic propulsion systems, a typical target value of the ignition delay time is around 10 ms (Thomas & Cantwell, 2017). The time elapsed between the formation instant of the liquid-liquid interface of the fuel and oxidizer and the instant ignition starts, called the ignition delay time. It is a very important issue when designing a liquid propellant rocket engine for the engine performance, integrity and security.

1.2 Hypergolic Propellants and Hypergolic Ignition

Typically, in commonly used combustion systems, in order to trigger the series of combustion reactions, it is needed to provide an ignition source, such as a spark (Turns, 2000). On the contrary to any combustion systems, there is a material class

yielding ignition without requiring any ignition source. Those are liquid bipropellants, fuel and oxidizer couples, and they do not require either a complex ignition source or a catalytic agent. Liquid bipropellants ignite upon the formation of liquid-liquid mass transfer interface. Simply, the ignition occurs in contact of the propellant surfaces, also known as hypergolic ignition. In the hypergolic ignition case, the well-known fire triangle between heat, fuel and oxidizer becomes the fire line between only fuel and oxidizer constituents.

The hypergolic ignition feature of the propellants is a very important tool for multiple restart requiring engines and thrust controlled rocket applications (Sardeshmukh, Heister, Wang, & Sankaran, 2013). A very long ignition delay time can cause a 'hard-start' problem, which results in accumulation of unburned propellant couple in the combustion chamber, and a sudden ignition with damaging pressure generation (Holtzmann, 1969). According to Black et al. (2018), while long ignition time delays may result in catastrophic hard starts, relatively shorter ignition delay times can lead to damage in the injectors (Black, Drolet, & Pourpoint, 2018). According to Thomas and Cantwell (2017), the common acceptable target ignition delay time upper limit is around 10 ms for the hypergolic bipropellants (Thomas & Cantwell, 2017).

According to Pourpoint and Anderson (2005), the hypergolic ignition of the liquid propellants is not exactly instantaneous. There exists a time delay, which is a combination of physical delay time including physical processes such as mixing, surface tension, diffusion and atomization, and chemical delay time, which is driven by the chemical potential and kinetics of reactions (Pourpoint & Anderson, 2005). In the chemical delay time the radicals and other intermediates necessary for the ignition evolve up to a critical concentration (Naidja, Krishna, Butcher, & Mahajan, 2002). The studies revealed that an important amount time is involved in ignition delay time due to mixing process and heating the liquids up to boiling point (Davis & Yılmaz, 2014). However, according to Davis and Yılmaz (2014), the chemical ignition delay time is rather preferred by researchers since this approach eliminates the factors by mixing process affecting the reaction delay time. It is basically a measure of the time

between the vaporization of the propellant and appearance of the flame. Thus, this approach minimizes the physical mixing factors of preignition time (Davis & Yılmaz, 2014). Hence, the mixing issues are not that important for the chemical ignition delay time, which is rather in relation with physical delay time.

1.3 Ignition Delay Time and Mechanism of Hypergolic Ignition

As stated in Section before, the ignition delay time can be expressed as the physical and chemical ignition delay time. The physical interactions and issues of transport phenomena such as mixing, atomization and evaporation cause the physical ignition delay time. On the other hand, the chemical delay time is directly a consequence of chemical kinetics. According to Izato et al. (2021), in a bipropellant thruster system, condensed-phase reactions are the initial aspect of the ignition process (Izato, Shiota, & Miyake, 2021)

The hypergolic ignition process described before, can be divided into four stages:

1. Momentum of the dropping/impinging liquids,
2. Mixing of liquid reactants,
3. Condensed phase reactions,
4. Gas phase reactions between the reactant vapors.

Kilpatrick and Baker Jr. (1955) suggests that, the ignition step occurs fast proportional to the speed of mixing for their hydrazine – nitric acid system. Therefore, the following steps to mixing are very fast comparing to mixing process, such as initial ignition reactions (Kilpatrick & Baker Jr., 1955). According to Blevins et al. (2004), since these fuel and oxidizer mix in the form of liquid, necessarily the pioneering reactions are in liquid phase (Blevins, Gostowski, & Chianese, 2004). As they pointed out, the total heat released upon mixing is considered to be the triggering step of the phase change to gas and consequently the gas phase combustion reactions.

In this work, only two stages of hypergolic ignition is explained: non-ideal mixing and vaporization of liquids and initial ignition reactions.

1.3.1 Non-ideal Mixing of Hypergolic Liquids

Liquid phase mixing is a very important step of hypergolic ignition. When two droplets of miscible liquids a and b come into contact on their surfaces in absence of any external forces, initially it is necessary to break the surface tension of both liquids. After breaking the surface tension, the molecules contacting molecules of a and b leave the bulk phase and migrate through the other liquid. This process of migration is called as diffusion of liquids (Incropera, Lavine, Bergman, & Dewitt, 2011). The liquid-liquid interface and diffusion of liquids through each other is simply illustrated in Figure 1.2.

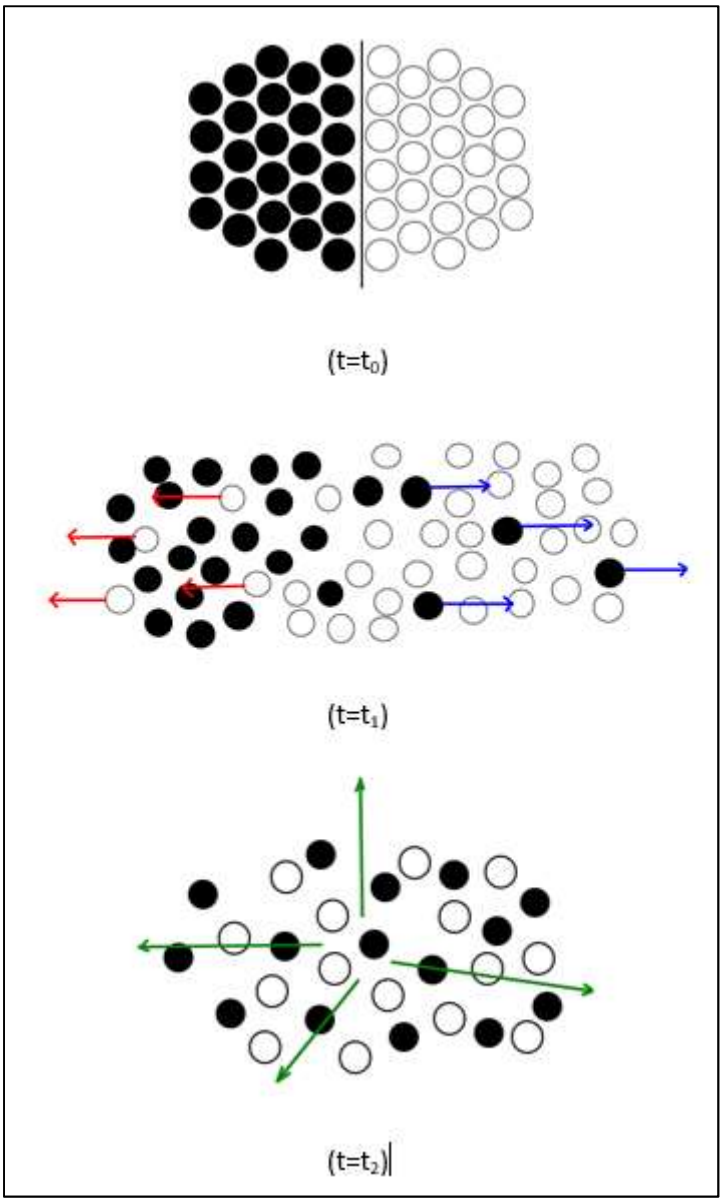

Figure 1.2. Liquid – liquid interface of liquids a and b (t_0), binary liquid mixing of a and b (t_1) and mixture of a and b and evolution of heat and vaporization (t_2)

The rate of this migration of molecule a into liquid b, is named as the binary mass diffusivity of liquid a in liquid b, D_{ab} (Incropera, Lavine, Bergman, & Dewitt, 2011). The mass diffusivity is a function of temperature, viscosity of liquid, particle size and geometry. In this study, regarding the scope of the work, the case of diffusion is not explained in detail.

In addition to diffusive mass transfer, in mixing tests for propellants, some other external energies ease the mixing process. These can be the potential energy of the droplet dropped at a certain height or the momentum of two impinging liquid jets.

Regardless of which path it takes, either dropping or impinging, the mixing process is the key step of hypergolic ignition. For hypergolic couples, the combustion starts at the gas phase. Thus, first it is necessary to change phase of liquids to gas. According to Black et al., the ignition of monomethyl hydrazine (MMH) and red fuming nitric acid (RFNA) includes two phases. First, liquid phase interactions locally cause a temperature rise at interacting sites and this rise starts boiling and aerosol formation. Just after that, by the vaporization – limited gas phase reactions, a rapid temperature rise occurs and brings the gas phase mixture to point of ignition (Black, Drolet, & Pourpoint, 2018).

As a consequence of non-ideal mixing of liquids, an amount of heat is released from the binary liquid mixture to surroundings for exothermic mixing which is demonstrated in Figure 1.2 at time t_2. In order to have an ignition in gas phase, this heat output from the mixing is consumed by vaporization of liquids, possibly temperature rise of the liquids up to auto-ignition point of the fuel and the energy barrier of the initial ignition reactions. The heat requirement can be summarized with the following equations.

For evaporation of liquids, the mixture needs heat proportional to latent heat requirement of the components,

$$Q_{vap} = x_1 \Delta H_1^{vap} + x_2 \Delta H_2^{vap} \quad (1)$$

In addition, in favorable conditions the ignition can start at the liquid phase (Sardeshmukh, Heister, Wang, & Sankaran, 2013). When the liquid phase ignition is also taken into account, the temperature of the flammable liquid should reach to its auto ignition point, which is the lowest temperature for the liquid in air must be heated to start a self-sustaining combustion regardless of a heating source (Nolan, 2014). The heat required to have ignition in the liquid phase is given by,

$$Q_{auto} = x_1 C_p^1 (T_{auto}^1 - T) + x_2 C_p^2 (T_{auto}^1 - T) \quad (2)$$

Since the liquids generally mix in an air environment in laboratory and engine conditions, auto-ignition of liquids is a considerable issue for the case of propellants. According to (Li, Qian, Haoyang, Guijun, & Zhu, 2021), even in some cases of laminar flow, the auto-ignition kinetics is faster than mixing (Li, Qian, Haoyang, Guijun, & Zhu, 2021). Therefore, it should also be in the energy balance and to ensure the complete evaporation and ignition of the liquid mixture, the total heat requirement should be balanced by the heat of mixing.

$$\Delta H_{mix} \geq Q_{vap} + Q_{auto} \quad (3)$$

Remembering that both sides of the equation are functions of composition at constant temperature, there must be a specific composition or a valid composition interval.

In this study, this methodology is applied to a model system of hydrazine (N_2H_4) and NTO (N_2O_4). The thermophysical properties for this couple is given in Table 1.1. The resulting heat requirements for evaporation and ignition, and the mixing enthalpy changing with composition were calculated and compared for sufficiency.

Table 1.1 Properties of hydrazine and nitrogen tetroxide. (NIST) (Lide, 2007) (ILO, 2009)

	N_2H_4	**N_2O_4**
Latent Heat of Vaporization (kJ/mol)	44.50	38.12
Heat Capacity (J/mol.K)	98.83	145.95
Auto-ignition Temperature (K)	543.15	-

Therefore, the net heat required to ensure ignition both at liquid and gas phases is calculated by equation 3.

The heat of mixing is obtained by UNIFAC excess molar Gibbs free energy calculation in scope of regular solution assumption. The model system includes liquid mixture of hydrazine (N_2H_4) and NTO (N_2O_4). The heat of mixing is calculated by UNIFAC binary activity coefficient model. The missing functional group in interaction parameters were calculated using CI -connectivity index- method. In order to meet the heat input requirements for evaporation and ignition, the heat of mixing data was multiplied by 30. Otherwise, the heat of mixing curve would be out of the comparison range.

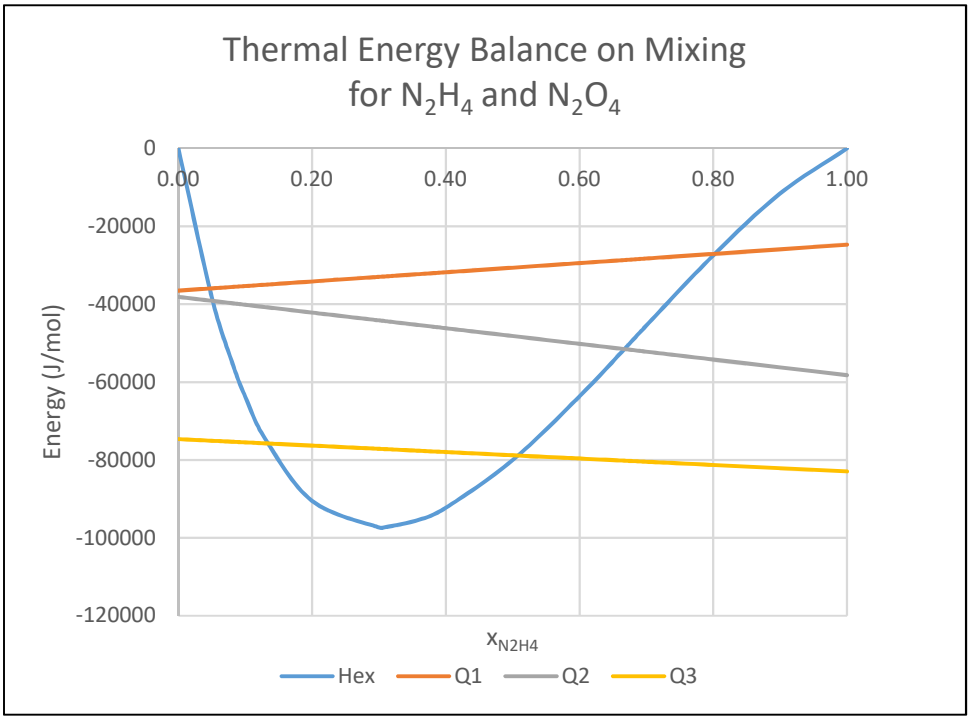

Figure 1.3. Thermal energy analysis for ignition of hydrazine – nitrogen tetroxide couple

In the Figure 1.3, for the composition range lying between the heat of mixing curve and Q_1 line, $x_1 = 0.05 - 0.80$, indicates an interval to make self-ignition of the liquid fuel possible in proper conditions. Similarly, for the composition range lying between the heat of mixing curve and Q_2 line, $x_1 = 0.05 - 0.67$, it can be understood that the vaporization of liquids is ensured by just the heat of mixing of liquids at constant temperature. For the composition range lying between the heat of mixing

and Q_3 line, $x_1 = 0.13 - 0.50$, the heat of mixing is sufficient to supply energy for both vaporization of liquids and start an auto-ignition for the liquid fuel. Which can be indicated as the *safe region* for combustion. From that point on, the heat released from the liquid phase auto-ignition may also start the gas phase reactions.

The complete combustion reaction for hydrazine and NTO can be simplified as,

$$2N_2H_4 + N_2O_4 \rightarrow 3N_2 + 4H_2O \quad (4)$$

Regarding the stoichiometric ratio in gas phase for complete combustion, the vapor phase composition, $y_1 = 0.67$ should be provided. With Raoult's Law, the required liquid composition for stoichiometric vapor composition at 20 ˚C is $x_1 = 0.36$, which is already lying in the safe region.

The same procedure can be conducted for any combustible liquids to predict the liquid composition interval that facilitates the heat evolution sufficient for steps of ignition.

1.3.2 Hypergolic Ignition Reactions

After liquid phase mixing, the evolved heat supplies the energy for both evaporation of molecules and triggering the vapor phase reactions. The vapor phase reactions can be explained in three steps.

- In the first step of the hypergolic ignition mechanism, there occurs instantaneous neutralization reactions just upon contact of the liquid surfaces. In other words, after the mixing of liquids, the neutralization takes place. Generally, these type of reactions are simple, single step reactions with relatively low energies of activation. With neutralization reactions, a significant amount of heat is released to the liquid media. Therefore, this heat facilitates a rapid evaporation of the liquid fuel and the oxidizer so that the gas phase ignition reactions can start.

- The acidic oxidizer, nitric acid, is an inorganic compound having a nitro group. In inorganic chemistry, nitration is expressed as the process in which a nitro group is presented to an organic molecule. Here in the hypergolic propellants case, the nitro group of the oxidizer is presented to the amine based fuel. This step is generally considered as that the slower reactions take place, because of the relatively slow nitration process. However, their contribution to heat release is quite significant. In addition, at the nitration step, some critical species for the ignition are produced. Furthermore, according to Liu et al. (Liu, Dashgupta, Zybin, & Goddard, 2011), the amount of heat released from the salt formation and the rate at which the reaction between the fuel molecule and NO_2 have a great influence on the ignition delay time.

  The simple general expression of nitration and hydrogen abstraction from fuels is given below.

$$Fuel\ molecule + NO_2 \cdot \rightarrow Fuel\ radical + \ HONO$$

- The oxidation step is started after nitration. At high temperatures, oxidation triggers highly exothermic runaway reactions. From this point on, the combustion reactions begin and continues very fast up to the complete combustion products evolve. The combustion reaction mechanism and complete combustion products are specific to the fuel and oxidizer couple.

To summarize the reasons of overall delay, here is an example work done by Black et al: in accordance with the steps explained above, according to Black et al. (2018), the similar steps were observed with three stages of temperature profiles acquired from the drop test experimental analysis of monomethyl hydrazine (MMH) and several types of nitric acid (Black, Drolet, & Pourpoint, 2018). They described the first stage as the region at which the temperature raises to boiling point of the reactant from the ambient temperature. Similarly, the second stage was the slower temperature rise from the boiling point to the initial combustion reactions. Finally, the third stage is described as the temperature rise up to the flame temperature, which is very

high compared to the first two stages. They also stated that the evolution of the products at the first stage is the source of the heat that is required for the evolution of the gas phase species to take part in the subsequent ignition reactions as stated in the neutralization step above. However, they stated that the scientists were not able to specify the experimental energy of activation of the first stage reactions because of the effect of condensation. Under these circumstances, the assumption was to take the energy of activation low at room temperature. Since the reaction intermediate evolves at room temperature, hence non-igniting conditions, it was concluded that the energy of activation should be smaller than the energy of activation of the ignition reactions.

Since the combustion reactions are very fast compared to the liquid phase mixing, the liquid phase mixing process can be said to be the rate determining step of overall ignition process. Therefore, it can be assumed that the ignition delay time is a consequence of the duration for two liquids to mix with each other up to a concentration where the heat release due to mixing is sufficient enough to start the ignition reactions.

With this aim, in combustion science ignition delay time measurements are done for the hypergolic liquids. Due to the importance of mixing on ignition delay time, for physical ignition delay time measurement, all methods include a forced mixing on hypergolic liquids. They can be either dropping from a definite height or forcing the liquids through injectors to impinge.

1.4 Measurement of Ignition Delay Time

Ignition delay time is measured either by a stationary drop test (mixing tests) or by impinging jet tests (or engine tests). Both of them use a similar approach, which is using a high-speed camera recording the scene during the time elapses between the first contact of the liquid surfaces and the flame ignition.

Firstly, drop tests are done in a way that reactant liquid is dropped from a definite height onto the second reactant, which is stationary in the ground. Those techniques are applied to develop the mixing process of the reactant pairs. However, in impinging jets tests (engine tests), both the fuel and the oxidizer are separately injected into the chamber, that is, both are in motion and having a kinetic energy. These techniques are used to develop the mixing rates and to provide a quick simulation of the engine conditions. This technique can also be applied on a small scale rocket engine which is equipped with required measurement units to measure the ignition delay time (Mays, Farmer, & Smith, 2010).

1.4.1 Drop/Mixing Test

In a typical drop test, it is usually required to drop around 1 mL of the hypergolic fuel onto a pool of oxidizer, or vice versa. In this technique, a light sensor operates whose light beam is located just above the pool surface. When this light beam is broken by the fuel drop, upon the surface contact, the camera starts to record the scene. A photocell detects the ignition and marks when the measurement is finished. This technique is limited by the lines of sight of mixing (Mays, Farmer, & Smith, 2010). A simple sketch of the general design of an drop/mixing test setup is shown in Figure 1.4.

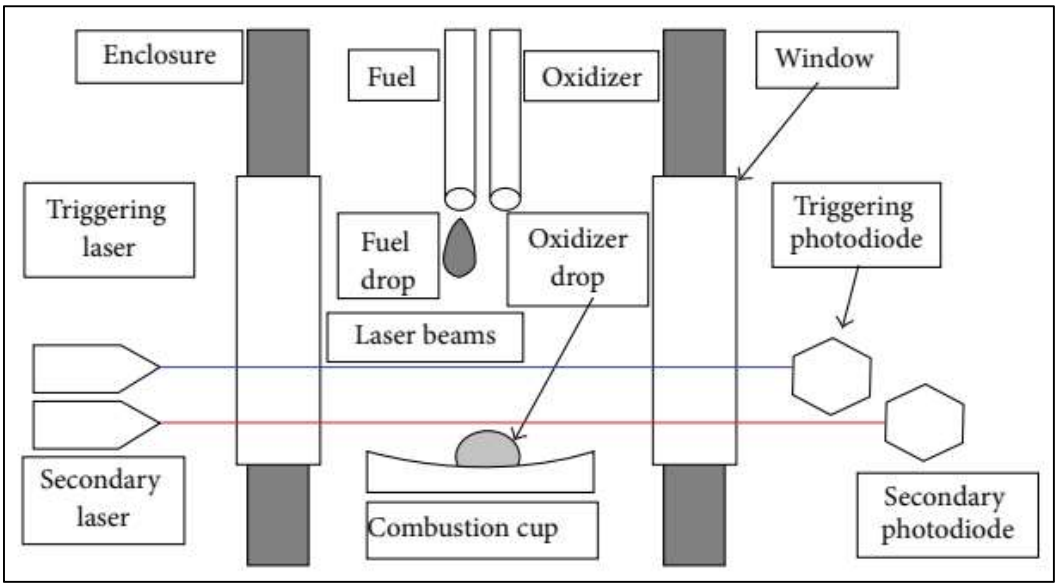

Figure 1.4. A simple demonstration of an ignition delay time measurement of hypergolic bipropellants (Davis & Yılmaz, 2014).

Davis and Yılmaz (2014) stated that, because of the continuous evaporation of the mixture of propellant fluids, if there are fluctuations in the laser signal, they are also recorded by the software and it defines an onset of chemical delay time measurement (Davis & Yılmaz, 2014). At that instant, when the laser signal is once boosted by the heat and light production, this is called the ignition point in an optical manner.

In drop tests, ignition delay time depends strongly on temperature, pressure and the ratios of the mixing propellants. It also depends on the nature of the initial reactions in liquid phase. According to Sangiovanni & Kesten (1977), ignition delay is also related to concentration of ambient oxygen, relative velocity of the fuel droplet, size of the fuel droplet and type of the fuel (Sangiovanni & Kesten, 1977). According to Zarbo et al. (2015), ignition delay time is also related with the humidity of ambient air, thus ambient air composition (Zarbo, Belal, & Pourpoint, 2015).

Unlike the impinging jets technique, drop testing techniques do not ensure sufficient conditions for mixing. According to Pourpoint et al. (2005), the method of injection, surface tension, viscosity and miscibility of the liquids also have a major influence on ignition delay time (Pourpoint & Anderson, 2005).

For a series of repeatable and logical ignition delay time experiments and reliable results, the drop test should ensure feasible environmental conditions. However, drop test technique differs from other ignition phenomena because of the exclusion of aggressive and dangerous mixing and thermal transitions (Blevins, Gostowski, & Chianese, 2004).

1.4.2 Impinging Jets (or Engine Test) Technique

Another method to measure ignition delay time is impinging jets technique. In this technique, the separate fuel and oxidizer jets are forcedly injected onto each other. In the injection process, the angle of the jets and the degree of atomization can be modified for a specific test. In the impinging jets technique, according to Davis and Yılmaz (2014), ignition point is the instant at which pressure of combustion chamber reaches 90% of its steady-state value (Davis & Yılmaz, 2014). Similarly, in the drop test technique, the time interval between the mixing of the propellants and the appearance of the first flame is measured in impinging jets technique. The difference is that in the impinging test technique this interval includes the combined jet formation as the beginning while it is the contact of the surfaces of the fuel drop and the oxidizer in the pool. Ignition delay is measured from the extent of the combined jet just before the entrance of the combustion zone. The whole process is conducted utilizing photography similarly in the case of drop test technique. In this technique, according to Mays et al. (2012), the size of the unignited combined jet is proportional to the duration of the ignition delay (Mays, Farmer, & Smith, 2010).

Each injection method significantly decreases the time of mixing. Because of this ease of mixing and shortage of mixing time, the recorded ignition delay time in the injection test is remarkably shorter than that of in the drop test operated with the same fuel and oxidizer combination. This is because of the reduction of the surface tension and the increase in mass diffusion of the propellant couple. Therefore, the surface tension is broken much easier and mixing occurs much faster than that in the

drop test. (Mays, Farmer, & Smith, 2010). A simple sketch of the general design of an impinging jets test setup is shown in Figure 1.5.

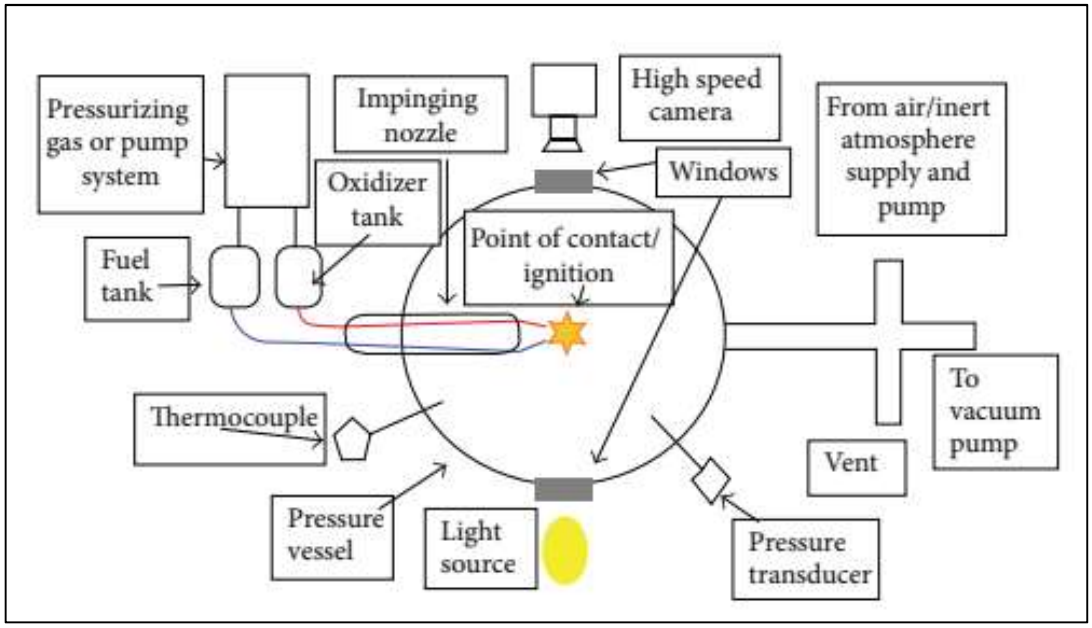

Figure 1.5. A simple demonstration of an impinging jet reactor ignition delay test of hypergolic bipropellants (Davis & Yılmaz, 2014).

Due to the better mixing conditions and closeness of the measured ignition delay time in the injection test to the real hypergolic ignition delay time in a rocket engine, impinging jets/engine tests are rather chosen than drop tests.

The ultimate inference of this work is to find ways to decrease the ignition delay time. In order to do this, it is aimed to put forth the best interpretation of the effects of temperature, pressure and composition of the mixture components on ignition delay time. To model the ignition delay time as a function of temperature, pressure and composition, the experimental data was modeled by one of the most widely used and very successful quantum chemical method, Density Functional Theory (DFT). Mathematical modeling of the acquired data was done using different type of mathematical expressions and polynomial fittings.

1.5 A Brief Introduction on Density Functional Theory

Density Functional Theory, DFT, is a quantum chemical modeling method. It is one of the basic computational methods applied in chemistry, biochemistry, condensed matter, physics and material science. DFT studies the electronic or nuclear structure of systems including atoms, molecules and condensed phase materials. According to Bretonnet (2017), with a very low cost of computation and acceptable accuracy, DFT is used for prediction of various properties like energies of atomization and binding, size and shape of molecules, energy barriers for different transitions and processes and crystal structures of materials (Bretonnet, 2017). Computational DFT codes are utilized for research of the structural, electronic and magnetic properties of molecules, materials and defects.

DFT enables to solve Schrödinger equation for an N-body system, which is a linear partial differential equation used to model the wave function of a quantum mechanical system. A functional is in definition, a function of a function, which indicates the energy of the molecule is a function of the electron density, which is a function of position. In DFT, the electron density is used as the fundamental property. The DFT technique deals with electron density (ρ) rather than wavefunction (ψ). The functional term of DFT indicates that the energy of the molecule is a function of electron density $E[\rho]$ and electron density is the function of position, $\rho(r)$. The exact ground-state energy of an n-electron molecule shown in the equation below (Atkins & de Paula, 2006).

$$E[\rho] = E_K + E_{P;e,N} + E_{P;e,e} + E_{XC}[\rho] \tag{5}$$

where E_K is total kinetic energy, $E_{P;e,N}$ is electron-nucleus potential energy, $E_{P;e,e}$ is electron-electron potential energy and $E_{XC}[\rho]$ is exchange-correlation energy, where all the spin effects are included.

The electron density of orbitals is calculated from the equation below (Atkins & de Paula, 2006) (Gosh, Verma, Cramer, Gagliardi, & Truhlar, 2018).

$$\rho(r) = \sum_{i=1}^{N} |\psi_i(r)|^2 \tag{6}$$

where ψ_i represents i^{th} occupied Kohn-Sham orbital.

The basic phenomenon in DFT, the electrons are not only influenced by particles of its own nuclei in their lattices, but also influenced by the other electrons. Therefore, the energies are a result of not only physical interactions (van der Waals forces, hydrogen bonds, dipole interactions) but also stronger chemical interactions. Actually, DFT does not count what interaction to have. It only makes predictions over electrons present in the system (Atkins & de Paula, 2006).

DFT has several areas in application and many advantages:

- Structure prediction of the atoms, molecules, ions and complexes
- Determination of phase stability
- Determination of thermodynamic, electronic and kinetic properties
- Property prediction and screening
- Providing a base for optical properties by determining electrical properties
- Enabling accurate calculations including an enormous number of electrons

According To Atkins & de Paula (2006), for the prediction of molecular properties, molecular orbital computations give only approximate results with some deviations. Those deviations come from experimental values that increase with the molecule size. Therefore, computational chemistry aims to obtain an insight for the trends of molecular properties at the first sight. That is, the ultimate accuracy is not the essential concern of computational chemistry (Atkins & de Paula, 2006).

In this work, DFT is used for obtaining quantum chemical results of complexation interactions. With DFT, the complexation energies were presented for nitric acid – water and fuel – oxidizer systems.

1.6 Information on Hypergolic Bipropellants

Hypergolic bipropellants are the fuel and oxidizer couples that instantly ignite upon contact of the liquid surfaces. Hypergolic bipropellants can be either regular liquids, gels or cryogenic liquids. While liquid and cryogenic liquid bipropellants are very broadly used especially in space applications, gelled hypergolic bipropellants are still under development and not very commonly used up to now.

Cryogenic (low boiling) liquid bipropellants are actually cooled and pressurized gases. Some examples of cryogenic fuels are liquid hydrogen, liquid natural gases (LNG, representatively liquid methane). and oxidizers are liquid oxygen (LOX), and not very commonly used liquid fluorine. These cryogenic bipropellants are not storable. Thus, propellants are filled into the propellant tanks just before the launch.

Liquid fuels are ignitable/combustible energetic materials. They can be exploited in order to convert their chemical energy into mechanical energy. Mostly, this mechanical energy is needed as kinetic energy in propulsion systems.

For the liquid bipropellants, there are common fuels such as hydrazine (N_2H_4), unsymmetrical dimethyl hydrazine (UDMH), monomethyl hydrazine (MMH), gasoline, kerosene, aniline, methanol, ethanol, anhydrous ammonia and variable types of hydrocarbon mixtures (i.e. RP-1, RP-3).

Liquid oxidizers are liquids which are willing to donate an oxygen to other molecules. They are also able to chemically oxidize the burnable materials to increase the possibility of a spontaneous fire or even an explosion. In propulsion systems, commonly used oxidizers are nitric acid, nitrogen tetroxide (N_2O_4), nitrous oxide (N_2O), hydrogen peroxide (concentrated, >90%), ammonium perchlorate, chlorine trifluoride (ClF_3), fluorine (not very preferred), ozone and oxygen bifluoride.

Not all the mathematical combinations of liquid fuels and liquid oxidizers are hypergolic. That is, hypergolicity is simply specific to the propellant couple. For example;

while nitrogen tetroxide (N_2O_4) and hydrazine (N_2H_4) liquid propellant couple is hypergolic, hydrogen peroxide and N_2H_4 couple is not hypergolic. Because, the hypergolicity is depending on the physical and chemical interactions between molecules of the constituent liquid components.

For both liquid fuels and oxidizers, there are common desired properties. These are, hypergolicity, high specific impulse, robustness, reliability, storability, larger operation interval (low freezing point and high boiling point), lower self-ignition temperature for fuels, chemical stability, low toxicity, environmentally non-hazardous and no carcinogenicity (Black, Drolet, & Pourpoint, 2018), (Davis & Yılmaz, 2014).

In this study, fuel of undisclosed identity due to the confidentiality issues and nitric acid (HNO_3) were selected to examine their kinetics and thermodynamics of their hypergolic interaction. This hypergolic couple plays a very important role on the environmental sustainability.

1.6.1 Nitric Acid (HNO_3) as Hypergolic Oxidizer

Nitric acid is one of the most commonly used hypergolic oxidizer used in both military and space applications in propulsion systems. It has a variety of derivatives. The most concentrated one, WFNA, white fuming nitric acid contains at least 98% pure nitric acid and the complement is water. It has a yellowish colorless appearance. The other type is the second place concentrated one, RFNA, red fuming nitric acid which is the most common type of nitric acid. It is a mixture containing between 5 – 20 % of dissolved nitrogen dioxide which causes the reddish-brown fumes that are poisonous (Sutton & Biblarz, 2016). When comparing the two types of the nitric acid, RFNA is rather storable, less corrosive for many types of tank materials and more energetic than WFNA. Although it is less corrosive than WFNA, still has important corrosion issues with many metal tank materials. In order to overcome this corrosive behavior, a third type of nitric acid was generated, IRFNA, inhibited red fuming nitric acid. It is obtained by addition of a very minute amount of hydrogen fluoride,

less than 1%, to RFNA. The fluorine ion involves in the formation of a fluoride layer on the surface of the tank material; thus, contribute to reduce the corrosion in several tank materials (Sutton & Biblarz, 2016). Therefore, increases its storability.

Table 1.2 Properties of the selected oxidizer, Nitric Acid (NIST) (Thiemann, Scheibler, & Wiegand, 2000) (Duisman & Stern, 1969) (Lide, CRC handbook of chemistry and physics, 2004)

Oxidizer Property	**Value**
Density (g/cm^3) (@20ºC)	1.500
Viscosity (Pa.s) (@20ºC)	0.0012
Vapor pressure (bar) (@20ºC)	0.06
Normal boiling point (ºC)	83
Normal freezing point (ºC)	-41.6

In addition to storability features, nitric acid derivatives offer a broad range of operation temperatures due to their very low freezing point and relatively high boiling point temperatures. Some of the possible hypergolic fuels with nitric acid are hydrazine and derivatives, kerosene, anilines, amines and xylidines.

CHAPTER 2

THERMODYNAMIC THEORY OF MIXTURES

2.1 Ideal and Non-ideal Mixture Theories

A mixture is an assembly of the molecules of different types of substances in solid, liquid or gas phase without causing a chemical reaction. A mixture can be taken into account as an ideal mixture if the following conditions are satisfied by the mixture: homogeneity of the mixture, equal sizes of the molecules of the component molecules and magnitude equality in forces of like molecules and unlike molecules in the mixture (Tosun, 2012).

In ideal mixtures, the molecules act like regular billiard balls with similar sizes. Due to the constant and similar sizes, the molecules always occupy same amount of volumes both in the mixture and in pure liquid. Therefore, the volume of the liquid mixture is always equal to the sum of volumes of the pure liquids. That is, there is no volume change for the ideal mixture.

When molecules of two pure liquids face a mix through each other, a and b, the bonds between identical molecules, $a-a$ and $b-b$, break and new bonds between non-identical molecules, $a-b$, are formed. In addition, the momentum of collision of $a-a$ and $b-b$ are similar to that of $a-b$. Similarly as in the volume issue, since the collision energies and energies of broken $a-a$, $b-b$ bonds are equal in magnitude with newly formed $a-b$ bonds, there is no net energy yielded. Therefore, the enthalpy of the mixture is equal to the sum of enthalpies of the pure liquids and no energy is released or taken during the mixing process. That is, the enthalpy change for ideal mixing is equal to zero.

In short, when two liquids form a mixture, the final mixture volume is equal to sum of the initial volumes of the components in ideal mixtures. Similarly, the enthalpy of the final mixture is equal to sum of that of components.

$$H_{mix}(T,P,x) = x_1 H_1(T,P) + x_2 H_2(T,P) \tag{7}$$

$$V_{mix}(T,P,x) = x_1 V_1(T,P) + x_2 V_2(T,P) \tag{8}$$

Ideal mixtures are very rare over a wide concentration range. Some examples are heptane – hexane, methylbenzene – benzene and 1-propanol – 2-propanol. Thus, over more general ranges, $x_i = 0 \ldots 1$, many of the mixtures exhibit "non-ideal" behaviors.

While ideal mixtures are composed of molecules act like ideal balls and yield no volume and energy change, in non-ideal mixtures, the molecules are quite far from the ideality. They are generally different in sizes. Also, in non-ideal mixtures like molecular interactions, $a - a$ and $b - b$, can be weaker or stronger than unlike molecular interactions, $a - b$, but not equal. Therefore the net energy of the system during mixing process is not equal to zero. For non-ideal mixtures, there is always an amount of energy taken or released.

In case of ideal mixtures or ideal solutions, Lewis-Randall Rule which is relating the phase change escaping tendency to mole fraction and Raoult's Law which is relating the partial pressures to mole fraction can be utilized to relate vapor-liquid equilibrium to pressure as seen in equations below.

$$f_i^{IM} = x_i f_i \tag{9}$$

$$y_i P = x_i P_i^{vap} \tag{10}$$

In non-ideal case, the mixtures do not follow the Raoult's law, positive or negative deviations observed depending on the strength of the like or unlike molecular interactions. When like molecular interactions are stronger than unlike molecular interactions, $U(a-a)$ or $U(b-b) > U(a-b)$, the system exhibits a positive deviation

from Raoult's Law. For this case, the vapor pressure of the mixture is greater than that estimated by the Raoult's law:

$$P > \sum x_i P_i^{vap} \tag{11}$$

In the opposite case, when like molecular interactions are weaker than unlike molecular interactions, $U(a-b) > U(a-a)$ or $U(b-b)$, the system exhibits a negative deviation from Raoult's Law. For this case, the vapor pressure of the mixture is less than that estimated from the Raoult's Law:

$$P < \sum x_i P_i^{vap} \tag{12}$$

While positive deviation from Raoult's Law implying phase change to gas, simply evaporation of the liquid in the mixture is easier, negative deviation from Raoult's Law implies evaporation of the liquid in the mixture is harder than expected. Generally, in positive deviation case, because that the molecules repel each other, absorption of heat and an increase in volume of the system is observed during mixing. Oppositely, in negative deviation case, because of that the molecules attract each other, a heat release and decrease in system volume is observed.

It is also necessary to interpret vapor phase in terms of liquid composition, temperature and pressure, because the hypergolic combustion reactions start at the vapor phase as explained before. With this consideration, vapor-liquid equilibria is also explained in detail.

Unlike to ideal mixtures, for non-ideal mixtures the intensive thermodynamic properties cannot directly be expressed with mole fractions. In order to overcome this restriction, the quantities should be expressed as partial molar properties which are explained in detail in the next section.

2.2 Partial Molar Properties

In order to interpret the thermodynamic state of a substance, there are thermodynamic state properties like enthalpy, entropy, Gibbs free energy, Helmholtz free energy, molar mass and molar volume. While temperature, pressure and density are intensive properties, i.e., property is independent of the size of the system, total volume, potential energy and enthalpy are extensive properties, i.e., they depend on the size of the system. When an extensive property is expressed in a molar or mass basis, it is called a molar or specific property.

Unlikely to ideal systems, partial molar properties are used to express the intensive properties of the mixture. By definition, when temperature, pressure and mole numbers of other components are constant, the rate of change of a property with respect to changing number of moles of a component, i, is called a partial molar property, φ_i^*.

$$\varphi_i^* = \left(\frac{\partial \varphi_{mix}}{\partial n_i}\right)_{T,P,n_{j\neq i}} \tag{13}$$

Being an intensive property, generally a partial molar property depends on temperature, pressure and mixture composition. As seen from equation 13, partial molar properties are calculated at constant temperature, pressure and number of moles. Therefore, calculation of partial molar Gibbs free energy requires an isothermal heat of mixing data. Due to constraints in experimental conditions, easier approaches, e.g. adiabatic heat of mixing data can be collected. In the thermodynamic landscape, it is possible to relate properties with different constraints to each other either through the use of Maxwell relations or through Legendre transformations (Modell & Reid, 1974). In order to have an accurate transformation, in addition to thermochemical data, such as heats or heat capacities, an accurate model of $P - V - T$ relationship is also needed.

In a closed system, an energy interaction of E generated by arbitrary process is to be measured. The amount of energy measured depends strongly on the system constraints. By combining the first and second laws of thermodynamics under constant temperature and pressure gives,

$$\left(\frac{dU}{dt}\right)_V = E + Q - P\left(\frac{\partial V}{\partial t}\right)_P \tag{14}$$

And,

$$Q = T\left(\frac{dS}{dt}\right)_V \tag{15}$$

Such that,

$$E = \left(\frac{d(U - TS + PV)}{dt}\right)_V = \frac{dG}{dt} \tag{16}$$

for a constant temperature and constant pressure system. Under constant pressure and constant entropy constraints, the system is represented by the following relations,

$$\left(\frac{dU}{dt}\right)_V = E - P\left(\frac{\partial V}{\partial t}\right)_P \tag{17}$$

$$E = \left(\frac{d(U + PV)}{dt}\right)_V = \frac{dH}{dt} \tag{18}$$

In order to calculate partial molar properties of a component in a mixture, the system should be under the conditions of constant temperature and constant pressure while

the number of moles of the other component is constant. Therefore, a calorimetry system normally requires a constant temperature –therefore non-adiabatic- construction. Under the conditions satisfying the regular solution theory, which assumes the entropy change of the mixture is equal to entropy change of the ideal mixture, hence the excess Gibbs free energy is directly equal to the excess mixing enthalpy. Therefore, if the entropy change of this process is negligible, the energy measured by these two processes with two different constraints will be equal:

$$E = \frac{dG}{dt} = \frac{dH}{dt} \tag{19}$$

This condition is an underlying principle of the regular solution theory also.

$$G^{ex} = H^{ex} = U^{ex} \tag{20}$$

Therefore, the partial molar properties of a component in a mixture can be calculated through this approximation.

2.3 Excess Mixture Properties of Non-ideal Mixtures

In non-ideal mixtures, it is not easy to predict the mixture properties as in the ideal mixtures. As stated before, in ideal mixtures, the sum of the component properties is equal to the mixture property. The final volume of the mixture is always equal to the sum of pure liquid volumes and the final mixture internal is equal to the sum of the pure liquid internal energies.

However, in non-ideal mixture case, the final mixture property is either larger or less than sum of initial component properties. At the same temperature, pressure and composition for the same mixture, the difference between exact property (non-ideal mixture property) and the ideal mixture property is called as the excess mixture property. Since initial sum and final value of properties are equal, excess mixture volume and excess mixture enthalpy are zero for an ideal mixture.

$$\varphi^{ex}(T,P,x_i) = \varphi_{mix}(T,P,x_i) - \varphi^{IM}_{mix}(T,P,x_i) \tag{21}$$

For molar volume, enthalpy, entropy and Gibbs free energy of a mixture, excess properties are;

$$V^{ex} = \Delta V_{mix} - \Delta V^{IM}_{mix} \tag{22}$$

$$H^{ex} = \Delta H_{mix} - \Delta H^{IM}_{mix} \tag{23}$$

$$G^{ex} = \Delta G_{mix} - \Delta G^{IM}_{mix} \tag{24}$$

$$S^{ex} = \Delta S_{mix} - \Delta S^{IM}_{mix} \tag{25}$$

For an ideal mixture, $\Delta V^{IM}_{mix} = 0$ and $\Delta H^{IM}_{mix} = 0$ as mentioned before. For ideal mixture Gibbs free energy is expressed as,

$$\Delta G^{IM}_{mix} = RT \sum_{i=1}^{k} x_i ln x_i \tag{26}$$

Since, Gibbs free energy can be expressed in a relation with enthalpy and entropy,

$$\Delta G^{IM}_{mix} = \Delta H^{IM}_{mix} - T\Delta S^{IM}_{mix} \tag{27}$$

Excess Gibbs free energy can be considered as the basis function to estimate the other excess properties.

$$d\left(\frac{G^{ex}}{RT}\right) = \frac{-H^{ex}}{RT^2}dT + \frac{V^{ex}}{RT}dP + \sum_{i=1}^{k} ln\gamma_i dn_i \tag{28}$$

Equation 28 implies that, the excess Gibbs energy is a function of temperature, pressure and number of moles. Partial derivative of excess Gibbs free energy with respect to temperature, pressure and number of moles respectively gives the excess enthalpy, excess molar volume and component activity coefficients as expressed in equations below.

$$\left[\frac{\partial(G^{ex}/RT)}{\partial T}\right]_{P,n_i} = \frac{-H^{ex}}{RT^2} \tag{29}$$

$$\left[\frac{\partial(G^{ex}/RT)}{\partial P}\right]_{T,n_i} = \frac{V^{ex}}{RT} \tag{30}$$

$$\left[\frac{\partial(G^{ex}/RT)}{\partial n_i}\right]_{T,P,n_{j\neq i}} = ln\gamma_i \tag{31}$$

Substituting $\Delta H_{mix}^{IM} = 0$ and using equation 26 in equation 27, entropy change of an ideal mixture is expressed as,

$$\Delta S_{mix}^{IM} = -R\sum_{i=1}^{k} x_i lnx_i \tag{23}$$

Summarizing all of the excess property equations above, excess mixture properties are expressed as in the equations below.

$$V^{ex} = \Delta V_{mix} \tag{32}$$

$$H^{ex} = \Delta H_{mix} \tag{33}$$

$$G^{ex} = \Delta G_{mix} - RT\sum_{i=1}^{k} x_i lnx_i \tag{34}$$

$$S^{ex} = \Delta S_{mix} + R\sum_{i=1}^{k} x_i lnx_i \tag{35}$$

As explained with non-ideal mixtures, the energy of the whole system can change during mixing. Assuming no mechanical energies are involved in the mixing process, from now on, the energy release or gain can be regarded as the heat release or heat gain for the system. In the case of the final internal energy of the mixture is less than the sum of the internal energies of the constituent pure liquids, a considerable amount of heat can be released from the system to the surroundings.

In the case of mixing of hypergolic propellants, this possible heat release can be an important stage of the hypergolic ignition. The significant amount of heat release can be a direct trigger factor for the initial ignition reaction. As explained in before, combustion of the hypergolic propellants starts with the initial gas phase reactions. It is important to comprehend the conditions where the heat release is sufficient enough to enable evaporation of the liquids and trigger the initial gas phase reactions and start the combustion reactions.

2.3.1 Regular Solution Theory

Regular solution theory is a concept, which requires only pure component thermophysical data for predicting thermodynamic properties of the solutions. According to Sandler (2006), in prediction of activity coefficients, regular solution theory exhibits a very good qualitative prediction ability while it is not that good in quantitative prediction (Sandler, 2006).

As mentioned before, in ideal mixtures, the enthalpy of mixing is equal to zero and entropy of mixing is given below,

$$\Delta S_{mix}^{IM} = -R \sum_{i=1}^{k} x_i ln x_i \tag{36}$$

Therefore, the mixing Gibbs free energy is directly equal to;

$$\Delta G_{mix}^{IM} = -T\Delta S_{mix}^{IM} = RT\sum_{i=1}^{k} x_i ln x_i \tag{37}$$

In this case, since component mole fractions are always between 0 and unity, entropy of mixing is always obtained as positive. Hence, because of the minus sign on the $T\Delta S$ term, the ideal mixture Gibbs free energy is always obtained as negative.

However, in *regular solution theory*, which is firstly introduced by an American scientist Joel Henry Hildebrand in 1927, ΔH_{mix} and ΔG_{mix} are expressed considering unequal interactions between the molecules of like and unlike species. In chemistry literature, when entropy of mixing of a solution is directly equal to entropy of mixing of an ideal solution and its enthalpy of mixing is not equal to zero, thus not equal to that of an ideal mixture, this solution is called a regular solution (Atkins & de Paula, 2006). Regular solution theory is a subject of non-ideality to overcome the calculations much easier. The purpose of this theory provides an easier prediction method for the thermodynamic properties of binary or multicomponent solutions. The ease is due to that method requires only the pure component data. According to Praustnitz (1958), there is actually no valid theory, which completely predicts the thermodynamic properties of the solution from the pure component molecular property data. However, at definite and restricted conditions, some theoretical ways exist which can give very well approximated results of predictions. He also stated that, most satisfactory method of all mentioned is the regular solution theory (Prausnitz, 1958).

Regular solution theory is basically developed for mixtures of non-polar liquids and non-polar gases (Prausnitz, 1958). In addition, regular solutions are assumed to be formed by components which are randomly mixed with no specifically strong interactions (Atkins & de Paula, 2006). Furthermore, their diversions from ideal solutions are only at moderate levels (Simon & McQuarrie, 1997). Besides, the total volume of the solution can also be directly equal to sum of the pure component volumes in regular solutions. However, this assumption does not strictly dedicate a direct additivity. For a more realistic system representation, it is better to calculate the total

volume from the partial molar volumes of mixture components. In fact, regular solution theory is more suitable for the systems showing positive deviation from Raoult's Law. Even though the nitric acid – water and fuel – oxidizer sytems show negative deviation, it was still considered the shortest way to reach logical conclusions on the effect of composition on mixing of nitric acid – water and fuel – oxidizer systems. For the nitric acid – water and fuel – oxidizer systems, the structures of molecules of the constituent liquids are assumed to be preserved.

For regular mixtures, since the entropy of mixture is directly equal to that of an ideal mixture and the same expression is valid for the total volume of the mixture; the excess entropy and the excess molar volumes of the regular mixtures turns out to be zero;

$$S^{ex} = \Delta S_{mix} - \Delta S_{mix}^{IM} = 0 \tag{38}$$

$$V^{ex} = \Delta V_{mix} - \Delta V_{mix}^{IM} = 0 \tag{39}$$

Regarding the zero excess mixing entropy for the regular mixture, for excess enthalpy of mixing and excess Gibbs free energy of mixing, the energy equation becomes;

$$G^{ex} = U^{ex} + PV^{ex} - TS^{ex} = U^{ex} \tag{40}$$

$$U^{ex} = H^{ex} - PV^{ex} - TS^{ex} = H^{ex} \tag{41}$$

In fact, acid solutions consist of ions; therefore, the modeling requires to use much more complicated theories to model the ion – ion interactions. However, for the first approximations simpler models used with the assumption of regular solution theory.

2.4 Binary Activity Coefficients and Their Relations to Thermodynamic Properties

Activity, *a*, is a phase changing tendency of a substance which is related to chemical potential, thus fugacity, *f*. Activity is also called the "*active concentration*" of a solution. The activity indicates the degree of activeness of the liquid is relative to a specified reference state. That is,

$$a_i^*(T,P,x_i) = \frac{f_i^*(T,P,x_i)}{f_i(T^0,P^0,x_i)} \tag{42}$$

The value of the activity coefficient depends on the specific choice of reference state and it is dependent on temperature, pressure and mixture composition, i.e. $\gamma_i(T,P,x_i)$. With the utilization of Lewis-Randall Rule[1] to definition of activity, for an ideal mixture,

$$a_i^{*IM} = x_i \tag{43}$$

Being the measure of deviation from ideal mixture, activity coefficient, γ_i is defined as,

$$\gamma_i = a_i^*/x_i \tag{44}$$

By re-defining the Raoult's Law to an extended form that includes activity coefficients,

$$y_i P = x_i P_i^{vap} \gamma_i \tag{45}$$

---

[1] *Lewis-Randall Rule* indicates that the fugacity of component i in an ideal mixture can be calculated by multiplying the pure component fugacity by its mole fraction.

$$f_i^*(T,P,x_i) = x_i f_i(T^0,P^0,x_i)$$

Where y_i represents vapor phase mole fraction of species i and x_i is the liquid phase mole fraction,

It can be said that for a mixture exhibiting positive deviation from Raoult's Law, the activity coefficient of component i is greater than unity, i.e. $\gamma_i > 1$. On the other hand, for a mixture exhibiting negative deviation from Raoult's Law, the activity coefficient of component i is less than unity, i.e. $\gamma_i < 1$.

Activity coefficients are directly related to the partial molar excess Gibbs energies of the components. By definition G_i^{*ex} is given as ,

$$G_i^{*ex} = G_i^* - G_i^{*IM} = RTln\left(\frac{f_i^*}{f_i^{*IM}}\right) = RTln\gamma_i \tag{46}$$

Summing partial molar excess Gibbs energies of components gives the molar excess Gibbs energy of the mixture as,

$$G_i^{ex} = \sum_{i=1}^{k} x_i G_i^{*ex} \tag{47}$$

$$G^{ex} = RT \sum_{i=1}^{k} x_i ln\gamma_i \tag{48}$$

In this work, this direct thermodynamic relation of activity coefficients to excess molar Gibbs energies offers an advantage to estimate activity coefficients from excess Gibbs energy data or vice versa.

2.4.1 Binary Activity Coefficient Models

The approach of model-based solutions provides a very quick evaluation of many process alternatives (reaction, phase equilibrium, physical properties, etc.). Thus, using predictive models for large ranges of applications is a very practical way which offers satisfying results and acceptable uncertainties.

Binary activity coefficient models are some mathematical equations which relate the activity coefficient of a binary system to its temperature, pressure and composition. Binary activity coefficients are grouped into three main groups in principle. These are empirical binary activity coefficient models, local composition binary activity coefficient models and group contribution binary activity coefficient models.

Empirical models simply relate the excess Gibbs free energy to the composition with the help of the experimental data. The experimental data is fitted into a Redlich-Kister Type expanded equation, which is a form of polynomial regression, as shown below.

$$\frac{G^{ex}}{x_1 x_2} = \sum_{i=1}^{N} A_i \, (x_1 - x_2)^{i-1} \tag{49}$$

One-Constant Margules, Two-Constant Margules, van Laar equations are some examples of the empirical binary activity coefficient models. In those kind of models, the excess Gibbs free energy of the mixture is expressed as a function of both x_1 and x_2, as shown in the equation below.

$$\frac{G^{ex}}{RT} = x_1 x_2 f(x_1, x_2) \tag{50}$$

Exactly One-Constant Margules and Two-Constant Margules equations are some linear forms of Redlich-Kister expansion, where $i = 1$ and $i = 2$. After the modeling of excess Gibbs free energy as a function of both $x_1$and x_2, the activity coefficients are determined in relation with the excess Gibbs free energy.

$$\frac{G_i^{*ex}}{RT} = \left[\frac{\partial(G^{ex}/RT)}{\partial n_i}\right]_{T,P,n_{j\neq i}} = ln\gamma_i \tag{51}$$

The other group of binary activity coefficient models is the local composition binary activity coefficient models. These models are based on the local composition theory. Local composition theory states that the mixture interactions depend strongly on the composition of the mixture, that is, the cross interaction parameter, $a_{ij} = a_{ji}(x_i)$ depends on the mixture composition. Thus, it can be said that, there might be possible strong deviations of local compositions from the bulk composition of the mixture. This hypothesis is based on that, the energetic differences in the mixture lead to non-randomness, which causes the breakdown of quadratic mixing rules. This group of binary activity coefficient models includes NRTL (Non-Random Two Liquid) model, UNIQUAC (Unified Quasi-Chemical) model and Wilson equation.

The final group is the group contribution binary activity coefficient models. Group contribution theory is based on the idea which implies that the sum of the individual contributions of groups represents the comprising molecule. In group contribution models, in the calculation of activity coefficients, the interaction of individual functional groups is taken into account. Some of the group contribution binary activity coefficient models are ASOG (Analytical Solutions of Groups), UNIFAC (Unified Activity Coefficients) and modified-UNIFAC (UNIFAC Dortmund). UNIFAC group contribution activity coefficient model is the other activity coefficient model to estimate the binary activity coefficients of the fuel and oxidizer mixture. In this work, UNIFAC local composition binary activity coefficient model is one of the ways that was used to calculate the activity coefficients of the fuel and oxidizer mixture.

2.4.2 Calculation of Binary Activity Coefficients

According to the extended form of Raoult's Law, at a known temperature and pressure conditions, binary activity coefficients are calculated using experimental vapor-liquid equilibrium data of a binary mixture.

$$\gamma_i = \frac{y_i P}{x_i P_i^{vap}} \tag{52}$$

However, in the absence of experimental vapor-liquid equilibrium data there are some predictive models to estimate binary activity coefficients. In this work, UNIFAC activity coefficient model is introduced and utilized. In addition, Two Constant Margules and van Laar equations were utilized in data fitting procedures and azeotrope point calculations.

2.4.3 Estimation of Binary Activity Coefficients By UNIFAC Model

As explained before, activity coefficients are a measure of escaping tendency of a substance from liquid phase to gas phase, which is a function of temperature, pressure and composition.

When the vapor-liquid equilibrium data is available for binary or ternary mixtures, activity coefficients can be directly calculated using a suitable model with the help of vapor pressure data of the components using equation 45.

UNIFAC (Unified Activity Coefficients) activity coefficient model is a group contribution method. It is an estimation method of unknown activity coefficients of a binary system of an unknown vapor-liquid equilibrium data. It considers the mixture is composed of several functional groups and each group attracts other groups differently. According to Fredenslund et al. (1975), it is considered to be a reliable and very fast route for prediction of activity coefficients of substances in liquid phase (Fredenslund, Jones, & Praustnitz, 1975). According to Rasmussen & Gmehling (1991), the success of UNIFAC group contribution binary activity coefficients model

is due to the availability of the data on volumes of functional groups, $R_{i,}$ surface areas of functional groups, $Q_{i,}$ and the availability of group interaction parameters, a_{mn} and a_{nm} (Gmehling, Rasmussen, & Fredenslund, 1982). For the case of our amine fuel and acidic oxidizer, some of the UNIFAC parameters are missing. In other words, truly some of them are not available in the literature.

Being a well-known and the most successful group contribution liquid phase activity coefficients prediction method for mixtures, UNIFAC group contribution model has been utilized in several different thermodynamic and physical properties. These are prediction of vapor-liquid, liquid-liquid and solid-liquid equilibria, prediction of flash points of liquid solvent mixtures, determination of gas solubility in liquids, determination of pure vapor pressures, estimation of activities in polymeric mixtures and estimation of excess mixing enthalpies for non-ideal mixtures (Gonzalez, Abildskov, Gani, Rousseaux, & Le Bert, 2007).

UNIFAC group contribution activity coefficients are composed of a combinatorial activity coefficient and a residual activity coefficient, as stated in the equation below.

$$ln\gamma_i = ln\gamma_i^C + \ln \gamma_i^R \tag{53}$$

For the mixtures composed of alkanes only, the residual excess Gibbs free energy is assumed to be zero (Larsen, Rasmussen, & Fredenslund, 1987). Thus, the residual activity coefficient is assumed to be unity. The combinatorial part of the activity coefficient is only dependent on binary liquid composition, volume and the surface area of the molecules (or groups) of the liquid mixture. Therefore, it is not very difficult to obtain combinatorial activity coefficients in the absence of experimental data. The equation, which gives a direct calculation of combinatorial activity coefficient, is given in the equation below.

$$ln\gamma_i^C = \ln\left(\frac{\Phi_i}{x_i}\right) + 5q_i \ln\left(\frac{\theta_i}{\Phi_i}\right) + l_i - \frac{\Phi_i}{x_i}\sum_j x_j\, l_j \tag{54}$$

Where,

$$\Phi_i = \frac{x_i\, r_i}{\sum_j x_j\, r_j} \tag{55}$$

$$\theta_i = \frac{x_i\, q_i}{\sum_j x_j\, q_j} \tag{56}$$

The molecular volume and the surface area of the substances are calculated by the equations below.

$$r_i = \sum_k v_k^{(i)} R_k \tag{57}$$

$$q_i = \sum_k v_k^{(i)} Q_k \tag{58}$$

Where, x_i is the liquid phase composition of the mixture, R_k is the surface area parameter and Q_k is the volume parameter of functional groups.

In the presence of surface area and volume parameters with a known liquid composition, calculation of the combinatorial part of the activity coefficient is rather easier than the residual part, because it does not take the functional group interactions into account. However, the residual part of the activity coefficients includes both molecular geometry and the intermolecular (or subgroup) interactions.

The residual part of the binary activity coefficient is given by the equation below.

$$ln\gamma_i^R = \sum_k v_k^{(i)}[ln\Gamma_k - ln\Gamma_k^{(i)}] \tag{59}$$

Where,

$$ln\Gamma_k\left(\text{or } ln\Gamma_k^{(i)}\right) = Q_k\left[1 - \ln\left(\sum_m \theta_m\psi_{mk}\right) - \sum_m \frac{\theta_m\psi_{km}}{\sum_n \theta_n\psi_{nm}}\right] \tag{60}$$

$$\theta_m = \frac{Q_m X_m}{\sum_n Q_n X_n} \tag{61}$$

$$X_m = \frac{\sum_j v_m^{(j)} x_j}{\sum_j \sum_n v_n^{(j)} x_j} \tag{62}$$

Where θ_m is the area fraction of group m and X_m is the mole fraction of the group m in the mixture. The group interaction parameter, ψ_{km} is given by the equation,

$$\psi_{km} = \exp\left(-\frac{a_{mn}}{T}\right) \tag{63}$$

a_{mn} is the functional group interaction parameter of the groups m and n, indicating the intermolecular interactions from the group m to group n. There is also a_{nm}, which is the group interaction parameter, indicating the intermolecular interactions from the group n to group m. Even though they belong to the same functional group couple, m and n, a_{mn} and a_{nm} are not equal to each other. Because, the physical interaction of a functional group naturally can be different. For the identical

functional groups, the group interaction parameter a_{mn} is equal to zero by definition (Carreón-Calderón, Uribe-Vargas, & Aguayo, 2020).

In Modified-UNIFAC and many other activity coefficient methods, regarding the temperature dependence of activity coefficients, the group interaction parameter,a_{mn}, is dependent on temperature. For the sake of simplicity and comprehensibility, in this work, the group interaction parameters were taken into calculations as temperature independent constant values.

2.4.4 Consistency Evaluation of the Data

Gibbs-Duhem equation offers a very useful way to interrelate the quantities of partial molar properties of different components in a mixture by putting constraints between partial molar properties of species (Tosun, 2012). Simply that is, if partial molar property values of the first species is known, then Gibbs-Duhem equation can be easily applied to calculate the partial molar property of the second species in a binary mixture. Therefore, the Gibbs-Duhem equation can be used to evaluate the thermodynamic consistency/accuracy of the predictive methods.

The total property of an extensive thermodynamic property of a mixture, which is a function of temperature, pressure and number of moles of comprising components, can be expressed as sum of partial molar properties with contribution of number of moles,

$$\varphi_{mix} = \varphi_{mix}(T, P, n_i) \tag{64}$$

$$\varphi_{mix} = \sum_{i=1}^{k} n_i \varphi_i^* \tag{65}$$

By differentiating the expression of total property of an extensive property, the differential equation is obtained below.

$$d\varphi_{mix} = \sum_{i=1}^{k} n_i d\varphi_i^* + \sum_{i=1}^{k} \varphi_i^* dn_i$$

(66)

As, a total property of a mixture depends all of temperature, pressure and number of moles, the differential of the total property is given by,

$$d\varphi_{mix} = \left(\frac{\partial \varphi_{mix}}{\partial T}\right)_{P,n_j} dT + \left(\frac{\partial \varphi_{mix}}{\partial P}\right)_{T,n_j} dP + \sum_{i=1}^{k} \left(\frac{\partial \varphi_{mix}}{\partial n_i}\right)_{T,P,n_{j\neq i}} dn_i$$

(67)

where,

$$\left(\frac{\partial \varphi_{mix}}{\partial n_i}\right)_{T,P,n_{j\neq i}} = \varphi_i^*$$

(68)

From the equations above, at constant temperature and pressure conditions, depending only on number of moles, the differential of the total property simplifies into the equation below.

$$d\varphi_{mix} = \sum_{i=1}^{k} \varphi_i^* \, dn_i. \qquad \text{(69-a)}$$

And through equation 66,

$$d\varphi_{mix} = \sum_{i=1}^{k} n_i d\varphi_i^* + \sum_{i=1}^{k} \varphi_i^* dn_i$$

(69-b)

Equating (69-a) to (69-b) and canceling the identical terms leaves,

$$\sum_{i=1}^{k} n_i d\varphi_i^* = 0$$

(70)

Dividing each side of the equation by the total number of moles of species gives the expression for Gibbs-Duhem equation at constant temperature and constant pressure conditions,

$$\sum_{i=1}^{k} x_i d\varphi_i^* = 0 \tag{71}$$

Further, in the detail, for a binary mixture, the equation simplifies into,

$$x_1 d\varphi_1^* + x_2 d\varphi_2^* = 0 \tag{72}$$

For a binary mixture, if this equation is differentiated with respect to liquid composition of component 1, x_1, at constant temperature and pressure, that gives,

$$x_1 \frac{d\varphi_1^*}{dx_1} + x_2 \frac{d\varphi_2^*}{dx_1} = 0 \tag{73}$$

Activity coefficient of a species in the mixture is directly related to its partial molar excess Gibbs free energy.

$$G_i^{*ex} = G_i^* - G_i^{*IM} = RTln\left(\frac{f_i^*}{f_i^{*IM}}\right) = RTln\gamma_i \tag{74}$$

Therefore, for binary mixtures the Gibbs-Duhem equation could be utilized to evaluate the thermodynamic consistency of the resulting partial molar excess Gibbs free energies, thus, the thermodynamic consistency of activity coefficients.

$$x_1 \frac{dln\gamma_1}{dx_1} + x_2 \frac{dln\gamma_2}{dx_1} = 0 \tag{75}$$

In the example calculation in Appendix A, the Gibbs-Duhem equation was also applied.

2.5 Vapor-Liquid Equilibria in Relation with Binary Activity Coefficients

Since the hypergolic reactions start in the vapor phase, it is necessary to make a relation between liquid phase and vapor phase under same conditions. For most of the double phase mixtures, it is possible to determine the vapor-liquid equilibrium compositions experimentally. However, in some cases like in the hypergolic propellants, making experiments or finding a suitable experimental setup for the determination of composition can be very difficult, or almost impossible. In such a situation, the estimated activity coefficients can be very helpful.

Binary activity coefficients are determined either from the experimental VLE data or estimated by doing series of calculations including binary activity coefficient models.

2.5.1 Raoult's Law and Vapor – Liquid Equilibrium

For ideal mixtures, the total pressure is calculated directly from Raoult's Law.

$$P = \sum_{i=1}^{k} x_i P_i^{vap} \tag{76}$$

The total mixture pressure can be larger or smaller than the calculated pressure by Raoult's Law. As explained before, this is explained by positive and negative deviations from the Raoult's Law. For a given temperature, pressure and liquid composition conditions, with the calculated activity coefficients, vapor-liquid equilibrium compositions of a binary mixture can be estimated by utilizing the extended form of Raoult's Law.

$$y_i P = x_i P_i^{vap} \gamma_i \tag{77}$$

According to Tosun (2012), in case of the mixture components have different functional groups or if they are polar, like in the case of the systems oxidizer – water,

fuel – water and fuel – oxidizer, the physical interactions between the mixture components will lead to non-idealities in the mixture. Therefore for a binary mixture the total pressure equation turns into the equation below.

$$P = x_1 P_1^{vap} \gamma_1 + x_2 P_2^{vap} \gamma_2 \tag{78}$$

For a binary mixture, the previous equation of the total pressure, P, is the bubble point pressure, which can also be explained as in the equations below.

$$\sum_{i=1}^{k} y_i P = \sum_{i=1}^{k} x_i P_i^{vap} \gamma_i = P \sum_{i=1}^{k} y_i \tag{79}$$

Since, sum of the fractions in the vapor phase is equal to 1, that is;

$$\sum_{i=1}^{k} y_i = 1 \tag{80}$$

thus, the total pressure, P, is directly equal to sum of liquid mole fractions times the vapor pressure of the compound as shown in the equation below.

$$P = \sum_{i=1}^{k} x_i P_i^{vap} \gamma_i \tag{81}$$

The positive deviation from Raoult's Law is observed when activity coefficient of at least one component in the mixture is greater than 1, $\gamma_i > 1$, as it can be inferred from,

$$P > \sum_{i=1}^{k} x_i P_i^{vap} \tag{82}$$

Similarly, negative deviation is observed when activity coefficient of at least one component in the mixture is less than 1, $\gamma_i < 1$, as it can be inferred from,

$$P < \sum_{i=1}^{k} x_i P_i^{vap} \tag{83}$$

2.5.2 Bubble and Dew Point Binary Mixtures and Azeotrope Formation

Bubble point pressure and bubble point temperature of a liquid mixture, are the environmental conditions at which the first bubble appears as a result of changing either pressure or temperature. Similarly, dew point is the specific condition at which the first droplet appears for a vapor mixture.

In mixture systems, using the experimental liquid and vapor phase compositions as a function of pressure the pressure – composition diagrams are built at specific temperatures. The plot of pressure versus liquid phase composition is called the bubble point curve.

There is a specific point for the mixtures where the bubble and dew point temperatures coincide at constant temperature. This condition is called as the "azeotrope" and these kind of mixtures are called as azeotropic mixtures.

At constant temperature, when total pressure curve is plotted versus liquid composition, there exists either a minimum or a maximum point. To find out this extrema, the derivative of the total pressure with respect to liquid composition is set to be equal to zero. It should also be reminded that $x_1 = 1 - x_2$.

$$\left(\frac{\partial P}{\partial x_1}\right)_T = 0 \tag{84}$$

Thus,

$$P_1^{vap}\gamma_1\left(1+x_1\frac{\partial ln\gamma_1}{\partial x_1}\right)-P_2^{vap}\gamma_2\left(1+x_2\frac{\partial ln\gamma_2}{\partial x_2}\right)=0$$

(85)

Furthermore, the Gibbs-Duhem equation is given as,

$$x_1\frac{dln\gamma_1}{dx_1}+x_2\frac{dln\gamma_2}{dx_1}=0$$

(86)

Integration of the Gibbs-Duhem equation into the equation 85,

$$P_1^{vap}\gamma_1-P_2^{vap}\gamma_2=0 \tag{87}$$

In addition, the condition of vapor – liquid equilibrium for both components is given below.

$$x_1P_1^{vap}\gamma_1=y_1P \tag{88}$$

$$x_2P_2^{vap}\gamma_2=y_2P \tag{89}$$

Since $P_1^{vap}\gamma_1=P_2^{vap}\gamma_2$ from the Raoult's Law, the expression yields,

$$\frac{x_1}{x_2}=\frac{y_1}{y_2}$$

(90)

Keeping in mind that $x_1=1-x_2$,

$$\frac{x_1}{1-x_1}=\frac{y_1}{1-y_1}$$

(91)

Therefore, the equation simply reduces to $x_1=y_1$ and $x_2=y_2$, implying that, at these equilibrium conditions the composition of the liquid phase is same with the composition of the vapor phase. This condition results in an azeotrope. Which indicates a constant boiling case in the mixture. This is, the boiling reaches an extrema,

in the pressure curve, a constant boiling point. Hence separation of the two components cannot be completed at the distillation process. Since at the azeotrope, $x_i = y_i$, the activity coefficient can be directly written as the ratio of total pressure to vapor pressure,

$$\gamma_i = \frac{P}{P_i^{vap}} \tag{92}$$

In this work, both bubble and dew point temperature curves and the azeotrope condition were plotted and demonstrated for the mixtures nitric acid – water mixture in detail.

CHAPTER 3

METHODS

In order to obtain the heat upon mixing of nitric acid and water for a whole composition range, a calorimetry setup was used. In addition to calorimetry, DFT calculations were conducted for nitric acid – water system. DFT calculations were also done for the fuel – oxidizer system.

In this work, for the sake of simplicity and not to have a multicomponent mixture in the calculations, the nitric acid is attributed to be 100% pure nitric acid. For the necessary computations, the physical properties of it were compiled from different sources.

3.1 Method of Attack

In the initial phases of this study, a preliminary estimation approach was needed. In order to obtain accurate estimates of the heats of mixing, first, the process parameters were modeled with the existing thermodynamic mixing models. Furthermore, the accuracy of the approach is tested through mixing of nitric acid – water system. This approach could be extended to hypergolic propellants once proven feasible. In the first sight, van Laar and UNIFAC activity coefficient models were used to determine excess mixing properties. These values established a reference frame to supply inputs for the DFT calculations. The estimations of the DFT calculations were further tested by the experimental heat of mixing data collected as a part of this study.

The basis of the theory for the thermodynamic mixing models are previously given in detail in Chapter 2.

3.2 Calorimetry Experiments for Measurement of Heat of Mixing

In the scope of this work, the heat evolved upon mixing was measured through the temperature change upon mixing of oxidizer – water, fuel – water and diluted solutions of fuel and oxidizer systems in a coffee-cup calorimeter. Regarding the material incompatibility of fuel and oxidizer formulations, it was almost impossible to utilize commonly used sensitive and robust calorimeter setups. In order to have a feasible system for temperature rise upon mixing, the experimental setup was designed in a simpler manner than common idealized applications. The test setup is shown in Figure 3.1.

Figure 3.1. The coffee-cup calorimeter heat of mixing experimental test setup

In this experimental sequence, the coffee-cup calorimeter test setup was idealized to the best of our abilities. In order to make necessary idealization about adiabacity, the entire system was designed with the highest possible insulation. An inner glass beaker was tightly covered with a thick enough styrofoam jacket. The bottom cover

was also made of a thick styrofoam. The coffee-cup calorimeter system was left only with two tiny holes: one for the location of thermometer and the other for the oxidizer addition through. The ultimate target was to obtain an experimental dataset on enthalpy change upon mixing, depending on the mixture composition. Water used in the experiment was ultra-purified by Merck - Millipore Milli-Q® Direct 8/16 System. The environmental temperature was kept constant at 22 ˚C.

In this oxidizer – water, fuel – water and diluted oxidizer – diluted fuel mixing processes, some assumptions were made in order to idealize the systems as possible. The assumptions made are listed below:

- The calorimeter is perfectly adiabatic
- There is no change in the amount of water and oxidizer during the experiments (no evaporation of water)
- Densities of oxidizer, fuel and water were taken constant
- Heat capacities of oxidizer, fuel and water were taken constant
- Mixture molar heat capacities were taken as the molar average of the pure component heat capacities

The thermal and physical properties of the oxidizer, fuel and water used in the experiments are given in Table 3.1.

Table 3.1 Physical properties of oxidizer, fuel and water taken into account during the mixing experiments (NIST)

	Heat Capacity (Cp, J/mol.K)	**Density** (ρ, g/cm^3)
Oxidizer	55.49	1.564
Fuel	251.32	0.770
Water	75.29	1.000

During mixing processes, the mixture heat capacity was taken as the molar average of component heat capacities, as stated in assumptions part. Mixture heat capacities are calculated according to equation below.

$$C_p^{mix} = x_1 C_p^1 + x_2 C_p^2 + x_3 C_p^3 + \cdots \quad (93)$$

3.2.1 Enthalpy of Mixing of Nitric Acid – Water System

The coffee-cup calorimeter experimental setup was filled with constant volume of water (50 mL). Because of the security concerns, water was always taken in excess and addition of small amounts of oxidizer into a pool of excess water is preferred. A thermometer was located on top of the calorimeter system. Because of the concern of the material incompatibility of the oxidizer, a PTFE-coated glass thermometer was used to measure the temperature rise.

It was not possible to construct an entire heat of mixing versus concentration graph for the oxidizer – water mixture. Since injection of a small amount of water to the oxidizer results in highly aggressive evolution of heat dangerous for the given experimental system, the first experiment was started in the water rich area. Later on, injection of the oxidizer continued up to a possible point. The possibility line drawn by the excessive fume evolution upon mixing. After this point, the experiment was finished. With the same consideration, the second experiment was done with very little amounts of pool oxidizer. For the oxidizer – water system, the experimental scenario is given in Table 3.2.

Table 3.2 Conditions of temperature rise upon mixing experiments of oxidizer – water systems

Experiment No.	**1**	**2**
Pool liquid	Water	Oxidizer
Injected liquid	Oxidizer	Water
Fixed pool volume (mL)	50	2
Injection volume (mL)	1	0.001
Total addition (mL)	40	2.3

A picture of oxidizer injection to the coffee-cup calorimeter is given in Figure 3.2.

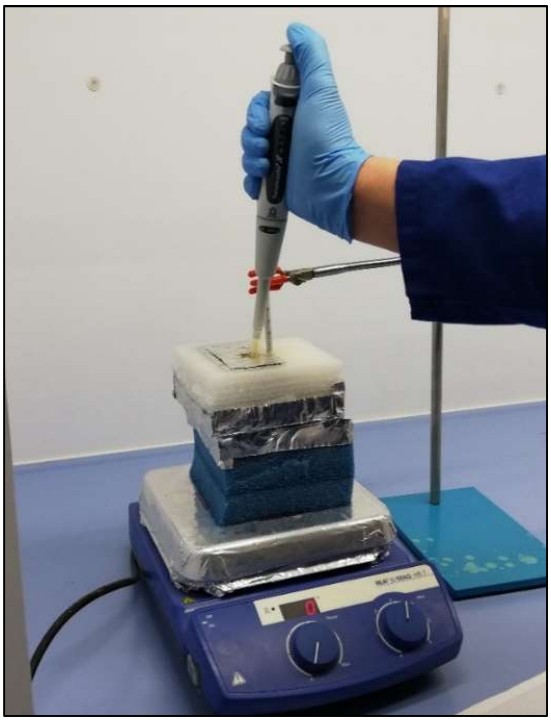

Figure 3.2. Injection of oxidizer into coffee-cup calorimeter

3.2.2 Enthalpy of Mixing of Fuel – Water System

By doing four separate experiments in different addition conditions, the excess enthalpy of mixing of the fuel – water system versus fuel concentration was constructed. The same experimental setup is used as in the oxidizer – water mixing process. The environmental conditions were again kept constant at 23 ˚C and atmospheric pressure. For a quicker temperature acquisition, a digital thermometer was used in fuel – water mixing temperature measurements.

Before the time t_0, the fuel and water were separately brought to thermal equilibrium with each other at 21 ˚C in a constant temperature water bath. At t_0, the fuel is started to be injected sequentially. At each addition step, the temperature is waited to come to an equilibrium state and then recorded. This procedure continued until all of the targeted amount of fuel was present in the mixture.

In order to make an entirely constructed composition – heat of mixing diagram, four separate mixing experiments were done. In first two experiments, water was taken in excess at the beginning and the fuel was started to be injected. The experimental scenario is given in Table 3.3.

Table 3.3 Conditions of temperature rise upon mixing experiments of fuel – water systems

Experiment No.	1	2	3	4
Pool liquid	Water	Water	Fuel	Fuel
Injected liquid	Fuel	Fuel	Water	Water
Fixed pool volume (mL)	50	50	50	50
Injection volume (mL)	1	5	1	5
Total addition	30	75	50	80

A picture of fuel injection to the coffee-cup calorimeter is given in Figure 3.3.

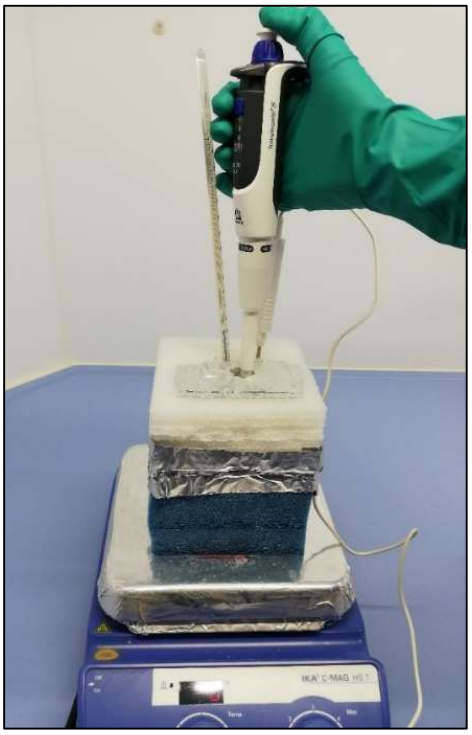

Figure 3.3. Injection of diluted fuel into coffee-cup calorimeter

3.2.3 Enthalpy of Mixing of Fuel – Oxidizer System

Due to the aggressive nature of the fuel and the oxidizer, it is impossible to mix pure components without an ignition. However, since this work includes the mixing issues of these materials, having the mixing in an inert media would give an idea about mixing enthalpies. Therefore, a set of mixing experiments were conducted in aqueous media. Diluted fuel solution was injected onto a 50 mL pool of diluted oxidizer (10% by volume of each) as 1 mL per injection. Similar in the oxidizer – water and fuel – water cases, the experiment was conducted in the coffee-cup calorimeter and the temperature rise was noted just after each injection. The experiment has the same assumptions that of oxidizer – water and fuel – water systems.

3.3 Quantum Chemical Calculations for Complexation Energy by Density Functional Theory

State functions of the fuel-oxidizer complexes would be obtained by computer simulations without causing any aggressive reactions or any explosions. For this purpose, quantum chemistry applications were utilized. Series of molecular simulations of fuel-oxidizer complex models were run in Gaussian09 software package. The calculations were done for both nitric acid – water system, having a comparable literature data on mixing, and the fuel – oxidizer system.

For both nitric acid – water and fuel – oxidizer systems, one of the components were put in the prior place and the other was added one by one to form complexes with different compositions. For example, the nitric acid molecule was put in interaction with water molecules one by one in a vacuum environment for the nitric acid – water system. Similarly, for the fuel – oxidizer system, fuel molecule was put in interaction with oxidizer molecules one by one in a vacuum environment. In DFT calculations, vacuum environment means that the dielectric constant of the environment is equal to zero. That is, no molecules other than the oxidizer and water atoms electrically affecting the complex focused.

In the data acquisition step, DFT computations were performed within Gaussian09 software package. For the geometry optimizations, the energy and frequency computations, the B3LYP functional and 6-31+G(d,p) basis set was used. As the solvation model, the conductor-like polarizable continuum model (CPCM) was used (Takano & Houk, 2005).

In this simulation, nitric acid first bound to a single water molecule. The resulting molar enthalpies, molar Gibbs free energies and molar entropies were calculated. From the complex and pure component molar enthalpy data, the molar binding energies could be calculated. These calculations were repeated for each step of water molecule addition.

$$B.E. = H_{complex} - (n_{NA} * H_{NA} + n_W * H_W) = H^{ex} \quad (94)$$

By utilizing regular solution theory,

$$H^{ex} = G^{ex} \quad (95)$$

Since it represents the enthalpy change over the complexation from pure components, conceptually, the binding energy can be considered as the enthalpy change among the complexation.

In utilization of quantum chemical complexation thermochemical data, the regular solution approach is used. Therefore, the binding enthalpy is considered as the Gibbs free energy change of the systems which are composed of pure liquids with the same nitric acid/water ratio.

3.4 Measurement of Ignition Delay Time

The mechanism of ignition and the methods for measuring ignition delay time are previously explained. In this work, an experimental setup was used for the drop test almost identical to the general design given in Figure 1.4. Also in this section, the hypergolicity and the mechanism of ignition are also briefly explained.

3.4.1 Ignition Delay Time Test Setup

As explained before, the drop test is simply performed by dropping fuel onto the oxidizer surface. Ignition delay time test setup (IDT) used in this work is customarily designed to observe the time delay between the first contact of the liquid fuel and oxidizer surfaces and the appearance of the first flame. The IDT test setup is mainly composed of a combustion room, a feeding unit, a temperature adjuster, a pressurizing unit, a control unit (the computer) and a camera system. Since the considerations of material compatibility of the propellant couple and temperature and pressure en-

durance, the whole chamber is made up from stainless steel. The chamber is illuminated for a better flame observation. The possible operating ranges and system features of the customarily designed ignition delay time test setup are given in Table 3.4.

Table 3.4 The features of the IDT experimental setup

System Features	
Temperature (˚C)	10 – 30
Pressure (bar)	0.5 – 10
Drop volume (µL)	5 – 10
Drop radius (mm)	0 – 2
Pool volume (µL)	200
İnjector height (mm)	50 - 100
Body material	Stainless Steel
Observation window material	Borosilicate glass
High speed camera	Phantom Miro C110

A plenary appearance of the structure of the ignition delay time experimental setup is given in Figure 3.4. In this experimental system, about 200 µL of oxidizer is put in a quartz pool, which has inner diameter of 22 mm and depth of 5 mm. On the top of the pool, there is an injector to provide the fuel drop which is fed by a syringe pump.

The principle of the ignition delay time measurement is quite straightforward, but not very simple. The liquid fuel is dropped onto the oxidizer pool through an injector connected to a syringe pump at the adjusted conditions. At the instant of the fuel drop appears, the high speed camera starts to record the whole scene.

Before starting the experiment, the chamber is purged with nitrogen gas. Due to its non-reactivity, nitrogen is also used for the pressurization of the chamber in ignition delay time measurements. In case of an undesired increase of pressure in the chamber, the excess nitrogen can be purged through a vacuum pump. The system can be pressurized in the interval of 0.5 – 10 bar with a 0.1 bar resolution. A vacuum ejector provides the vacuum condition up to 0.5 bar in the system. In order to be utilized, the vacuum ejector is connected to a compressor system.

Nitrogen is also used to prevent condensates on the observation and illumination glasses in order to keep them clean for the optical transmitting. In addition to these features, it is used for the utilization of the pneumatic equipment in the system.

The idea behind this test setup is to measure the ignition time delay by recording the whole ignition process with a high-speed camera. Behind a borosilicate glass which enables the optical access, the instant of the impingement over the pool, the mixing process, vapors and the first flame is all captured and recorded by a Phantom Miro C110 high speed camera. The camera captures 915 frames with a 1280x1024 resolution, 1295 frames with a 1280x720 resolution. The software embedded in the system, starts to record just before the collision and does not stop without seeing the flame. This sensitivity enables the observer correctly measure the ignition time delay as much as possible.

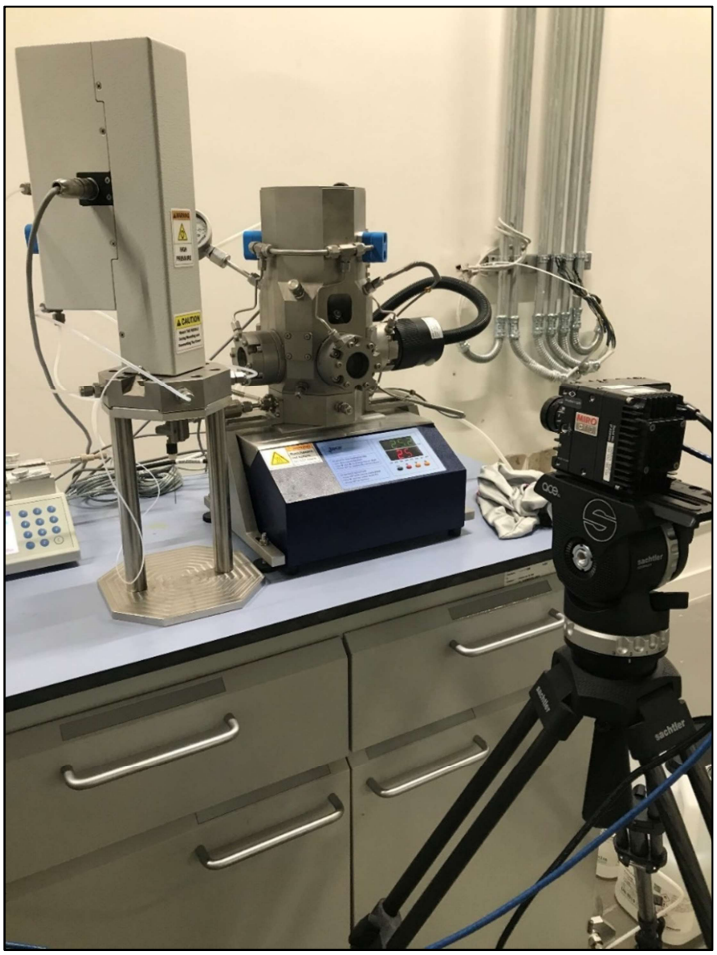

Figure 3.4. General view of ignition delay time experimental setup

The system temperature can be adjusted between 10 – 30 ˚C with a 1 ˚C resolution. The temperature is measured with three separately located thermocouples, one is located nearby the ignition zone, one is located in the chamber and the other is immersed in the oxidizer pool.

The injector is located on the top of the oxidizer pool whose height is adjustable between 50 – 100 mm. During the experiments, in order to eliminate the momentum at the collision effect, the injector height was kept at the minimum level, 50 mm.

Due to evaporation of the fuel at low pressures, this amount of droplet is considered to be changing between 5 – 10 µL for each injection. In order to be sure about the

maximum amount of fuel was provided, the drop volume of the injector was adjusted to 10 μL.

In the room, there is a quartz pool, the oxidizer pool, which is designed to keep the liquid oxidizer stable in the room without any spill. Besides, it provides the environment for the collision of fuel and oxidizer surfaces. A stainless steel syringe pump feeds the fuel to the combustion room through the tip of a stainless steel injector.

In the drop test experiments, it is better to put the oxidizer into the pool and the drop should be the fuel. Because of the flammable nature of the fuel, a counter action cannot be applied. For example, there cannot be a scenario that the oxidizer drop collides into a pool of fuel. This kind of a scenario would definitely lead to a continuous burning of the whole fuel in an air environment. However, since the oxidizer is not naturally flammable, the flame ends when the combustion of the single fuel drop completes. Thus, the system is designed in the way that the fuel drops onto a pool of the oxidizer.

In the Figure 3.5, the control panel of the IDT system is shown. The experiment is operated via this interface. The temperature and pressure conditions, tolerances and data acquisition parameters are set in this window before starting the experiment. Injection rate, drop volume and the injector height are also adjusted from the interface. During the experiment, the pressures at the transmitter and the pressure at the control valve can be observed instantly. In addition, the temperature values from the three separately located thermocouples can be directly read. The ignition chart frame shows the ignition scene via the high-resolution high-speed camera.

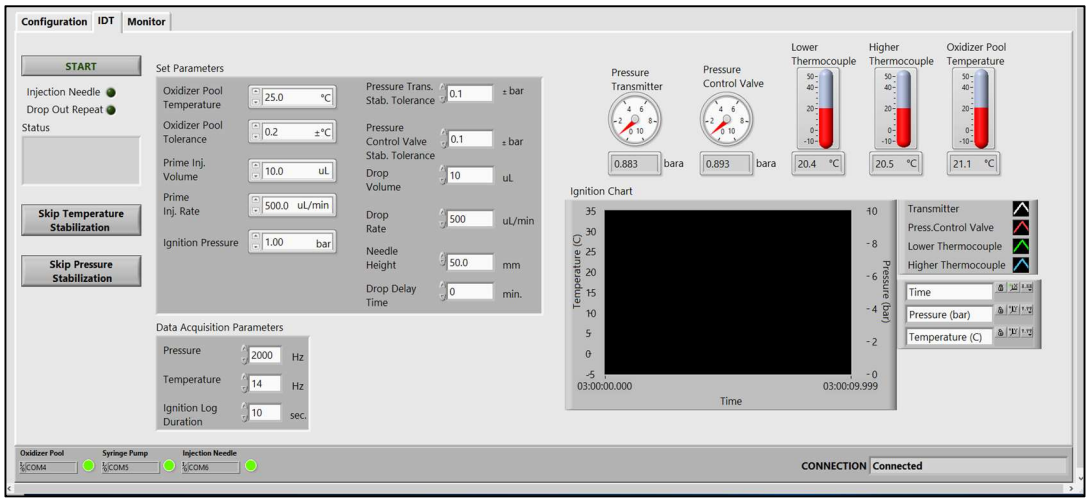

Figure 3.5. Control panel of the ignition delay time test setup

In the experiment, the test setup is heated to desired temperature and the pressure. Since the drop size of the fuel is kept constant, the composition is adjusted by changing the amount of oxidizer in the pool.

The instants of pre ignition, collision and ignition are captured by the high speed camera as shown in Figure 3.6.

Figure 3.6. The instants of dropping, collision, ignition and combustion in IDT

As in the experiments done in this work, according to Sangiovanni and Kesten (1977) in the ignition delay time experiment, the heat transfer due to radiation between the phases, gas and liquid, is neglected. In addition, heat conduction is assumed the only way of heat transfer on the body of droplet (Sangiovanni & Kesten, 1977).

CHAPTER 4

THEORY OF MIXTURES

4.1 van Laar Theory and Activity Coefficient and Excess Molar Gibbs Energy Estimation

According to Sandler (1986), van Laar theory is functionally equivalent to regular solution theory when α and β parameters are substituted by the molar volumes and solubilities (Sandler, 2006).

$$\alpha = \frac{V_1}{RT}(\delta_1 - \delta_2)^2 \tag{96}$$

$$\beta = \frac{V_2}{RT}(\delta_1 - \delta_2)^2 \tag{97}$$

In the van Laar theory, the basic assumptions are (Sandler, 2006),

- the constituent compounds of the binary mixture are in similar sizes and exhibit similar interaction energies,
- for both pure compounds and their liquid mixture, van der Waals equation of state can be used.

Depending on the regular solution theory, also in van Laar model, the excess molar entropy and the excess molar volume of the mixture are equal to zero. In this model, the molar excess Gibbs free energy of the mixture is represented as,

$$G^{ex} = RT \sum_{i=1}^{k} x_i ln\gamma_i \tag{98}$$

The activity coefficients of the components are given by,

$$ln\gamma_1 = \frac{\alpha}{\left(1 + \frac{\alpha}{\beta}\frac{x_1}{x_2}\right)^2} \tag{99}$$

$$ln\gamma_2 = \frac{\beta}{\left(1 + \frac{\beta}{\alpha}\frac{x_2}{x_1}\right)^2} \tag{100}$$

Where α and β are expressed as,

$$\alpha = \frac{b_1}{RT}\left[\frac{\sqrt{a_1}}{b_1} - \frac{\sqrt{a_2}}{b_2}\right]^2 \tag{101}$$

$$\beta = \frac{b_2}{RT}\left[\frac{\sqrt{a_1}}{b_1} - \frac{\sqrt{a_2}}{b_2}\right]^2 \tag{102}$$

where a_i and b_i can be directly calculated by van der Waals equation of state using pure molecular properties.

As stated by Sandler (2006), in case of presence of limited available data, van Laar coefficients α and β can also be calculated using activity coefficients at a single composition; therefore, the calculated van Laar parameters can be used to calculate the activity coefficients at all other molar compositions (Sandler, 2006).

Since $\gamma_i^{az} = P/P_i^{vap}$ at the azeotrope point, activity coefficients of the components can be directly calculated from the azeotrope point data. Hence, as the single point activity coefficients data are available at the azeotrope point, van Laar parameters can also be determined from the azeotrope point information.

$$\alpha = \left(1 + \frac{x_2}{x_1}\frac{ln\gamma_2^{az}}{ln\gamma_1^{az}}\right)^2 ln\gamma_1^{az} \tag{103}$$

$$\beta = \left(1 + \frac{x_1}{x_2}\frac{ln\gamma_1^{az}}{ln\gamma_2^{az}}\right)^2 ln\gamma_2^{az} \tag{104}$$

As explained before, at the azeotrope point the liquid composition is directly equal to the vapor composition, $x_1 = y_1$ and $x_2 = y_2$. Therefore, the equilibrium condition reduces to,

$$P_1^{vap}\gamma_1^{az} = P \tag{105}$$

$$P_2^{vap}\gamma_2^{az} = P \tag{106}$$

Hence, the azeotrope point activity coefficients could be directly calculated from the total pressure and vapor pressure data at the azeotrope point temperature.

From Matheswaran et al. (2007), the azeotrope composition and temperature of the nitric acid – water binary mixture at atmospheric pressure is given in Table 4.1 (Matheswaran, Kwon, Kim, & Moon, 2007).

Table 4.1 Azeotrope conditions of nitric acid – water binary mixture

Azeotrope Conditions	
$x_1 = y_1$ (HNO_3)	0.68
$x_2 = y_2$ (H_2O)	0.32
Temperature (^oC)	120.5
Pressure (atm)	1

4.2 UNIFAC Binary Activity Coefficients Model to Estimate Excess Molar Gibbs Energy

As the theory is explained before, UNIFAC binary activity coefficient model was used to estimate the excess molar Gibbs free energy of both nitric acid – water and fuel – oxidizer systems.

Functional group interaction parameters were estimated by CI-index method since they were not available for the fuel and oxidizer case. The fuel and oxidizer molecules are divided into three subgroups, which are G1, G2 and HNO_3. For this type of trial, the necessary volume and surface area parameters, R_k and Q_k were obtained from Dortmund Data Bank (NA, n.d.) for the fuel subgroups and water. For the acidic oxidizer, R_k and Q_k for the NO_3 group were taken from the work of Raatikainen & Laaksonen (2005) (Raatikainen & Laaksonen, 2005).

Table 4.2 UNIFAC surface area and volume parameters of the subgroups, R_k and Q_k

Subgroup	Volume, R_k	Surface Area, Q_k
G1	0.9011	0.8480
G2	0.9597	0.6240
NO_3	1.6400	1.6000
H_2O	0.9200	1.4000
OH	1.0000	1.2000

4.2.1 Estimation of Unknown Group Interaction Parameters

For many compounds or functional groups, there are group interaction parameter values that are assigned, published in different sources. Those functional group interaction parameters are obtained by regression of the binary vapor-liquid and liquid-

liquid equilibrium data. In order to get the group interaction parameters, it is first necessary to obtain the binary activity coefficient values from the experimental vapor-liquid and liquid-liquid equilibrium data.

Many of the group interaction parameters were studied separately, but they are collected in databases that are more comprehensive. However, there are only a few groups are available when considering all possible combinations of functional groups of a broad range of compounds.

While using group contribution models to calculate the mixture properties, is usually a deep frustration that there are missing parameters which is essential to have them in the calculation. Although a lot of compounds/functional groups are assigned a functional group interaction parameter value in different sources, very famous, successful and useful group contribution based activity coefficient estimation method, UNIFAC, also suffers from the absence of some important experimental functional group interaction parameter values, a_{mn}. For example, in order to estimate the compound or mixture properties, the contribution of the groups are required to represent the structure of the molecule of the compounds. For pure component properties, Gani et al. (2005), stated a group contribution approach. In this work, creation of the missing groups and estimation of their contributions to the whole molecule is done by setting valence connectivity indices (Gani, Harper, & Hostrup, 2005). This method, enables to estimate the missing group contributions without requirement of experimental data.

Gonzalez et al. (2007), offered an estimation method to calculate missing functional group interaction parameters, a_{mn}, of groups and subgroups of the constituent compounds in a liquid mixture (Gonzalez, Abildskov, Gani, Rousseaux, & Le Bert, 2007). This estimation method is called CI-UNIFAC method and it is based on connectivity indices explained in the work of Gani et al. (2005). In their work, atomic connectivity indices were used to predict pure component physical properties. On the other hand, in the work of Gonzalez et al. (2007), atomic and valance connectivity indices were used to estimate functional group interaction parameters, a_{mn}. In

parallel, by the use of UNIFAC model, it also enables to calculate the liquid phase binary activity coefficients. The current version of CI-UNIFAC method is only limited to UNIFAC groups, which are simply composed of carbon, oxygen, hydrogen and nitrogen (Gonzalez, Abildskov, Gani, Rousseaux, & Le Bert, 2007).

In this work, it is applied to the comprising compounds of the binary liquid mixture. With the same approach, the complexes were regarded as a whole molecule and the subgroups were taken into account in connectivity indices calculations. Group contribution methods regard the molecular structures as combination of smaller fragments (subgroups). Depending on this approach, the property of a molecule is simply considered a sum of properties of its fragments. The contribution values of the groups are usually found from the regression of experimental data, similarly in the case of group interaction parameters, a_{mn}. Supplement of these contribution data is very important, because in absence of any single data, the calculation of group interaction parameters, a_{mn}, cannot be expected to proceed.

4.2.1.1 Connectivity Indices, χ

The connectivity indices are formalisms defined using theoretical concepts and intended to define topological characteristics of structures of molecules. This molecular connectivity concept is first introduced by Kier and Hall (1987) (Kier & Hall, 1986). CI-index method then used by Gani (2005) in order to estimate contributions of groups to the properties of pure substances. In 2007, Gonzalez et al. used this concept to estimate the contributions of groups to interactions in mixtures (Gonzalez, Abildskov, Gani, Rousseaux, & Le Bert, 2007). The CI-index method starts with the construction of hydrogen suppressed molecular structure graph. That is, in the molecular structure, no hydrogens appear.

The hydrogen suppressed forms of the oxidizer molecule is;

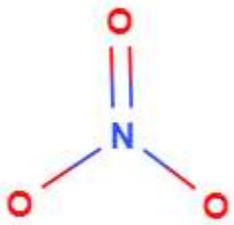

Figure 4.1. Hydrogen suppressed structure of oxidizer molecule

In hydrogen suppressed form, fuel molecule is taken into account as being formed from four G1 and two G2 groups. Nitric acid molecule is considered as formed of NO_3 group. In the hydrogen suppressed graph, the non-hydrogen atoms which were turned into vertices were symbolized by numbers. The chemical bonds which were turned into edges were symbolized by letters. In this representation, hydrogens and double bonds were hidden in the molecular structure. In the scope of this work, connectivity indices were calculated both for the fuel and the oxidizer molecules. For the sake of simplicity and confidentiality concerns, the connectivity index calculation of the oxidizer is explained only.

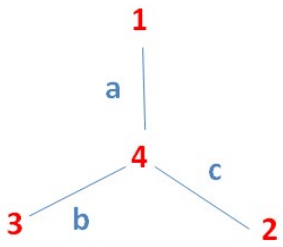

Figure 4.2. Hydrogen suppressed graph of the oxidizer molecule

In order to obtain the CI indices, first thing to do is to calculate atomic and bond indices of the molecules from the hydrogen suppressed graphs. The atomic index, δ^v, is defined for each single atom or vertex as in the equation below (Gonzalez, Abildskov, Gani, Rousseaux, & Le Bert, 2007),

$$\delta^v = \frac{(Z^v - N_H)}{(\mathrm{Z} - Z^v - 1)} \tag{107}$$

The related values and atomic indices for fuel and oxidizer molecules were calculated and are given in Table 4.3 below.

Table 4.3 Atomic indices values and atomic properties of the oxidizer molecule

Number of atom	1st	2nd	3rd	4th
Z	7	8	8	8
$\boldsymbol{Z^v}$	5	6	6	6
$\boldsymbol{N_H}$	0	0	1	0
$\boldsymbol{\delta^v}$	5	5	6	6

According to Gonzales et al. (2007), the atomic index is comprised of both the way that the atom attracts to atoms in its surroundings, the vertices, as well as the information on the atomic nature (Gonzalez, Abildskov, Gani, Rousseaux, & Le Bert, 2007). Those interactions are defined as connectivity indices of zeroth, first, second and nth order, $\chi^0, \chi^1, \chi^2 \ldots \chi^n$. The zeroth connectivity index is called the atomic index. The others are called as valance (bond) connectivity indices. The general expression to calculate nth order valance (bond) connectivity index of a molecule is given in the equation below.

$$\chi^n = \sum_{m}^{\tau} \prod_{i}^{\mu} (\delta^v{}_i)^{-1/2} \tag{108}$$

where τ is the number of type τ subgraphs of μ edges.

The atomic connectivity index, zeroth order, is calculated as in the equation below:

$$\chi^0 = \sum_i^{\omega} \frac{1}{\sqrt{\delta_i^v}} \tag{109}$$

where ω is the number of vertices in the hydrogen suppressed graph of molecule. For each of the bonds between atoms i and j, the first order bond index is calculated as expressed in the equation below.

$$\beta^v = \delta_i^v \delta_j^v \tag{110}$$

The calculated first order bond indices are used to calculate the first order valance (bond) indices as expressed in the equation below.

$$\chi^1 = \sum_i^{\tau} \frac{1}{\sqrt{\beta_i^v}} \tag{111}$$

For each path of two edges in the hydrogen suppressed graph, the second order valance bond indices are defined for the atoms i, j and k are present in the path,

$$\varepsilon^v = \delta_i^v \delta_j^v \delta_k^v \tag{112}$$

Similarly to zeroth and first order connectivity indices, the second order valance connectivity index is expressed as the sum of the paths of two edges in the hydrogen suppressed graph,

$$\chi^2 = \sum_i^{N} \frac{1}{\sqrt{\varepsilon_i^v}} \tag{113}$$

where N is the number of paths of two edges in the hydrogen suppressed graph.

According to Gonzales et al. (2007), since UNIFAC groups are in the type of first order, not very complex and therefore in a manageable level, for the fuel and oxidizer

molecules the CI indices were calculated up to first order (Gonzalez, Abildskov, Gani, Rousseaux, & Le Bert, 2007).

The CI indices for the oxidizer molecule are given in Table 4.4 below.

Table 4.4 CI indices for the oxidizer molecule

χ^0	1.7109
χ^1	0.5651
χ^2	0.0067

The group interaction parameters for the fuel and oxidizer system are calculated and the results are given in Table 4.5 below.

Table 4.5 Resulting group interaction parameters for the fuel and oxidizer system

Functional Group Pairs	a_{mn}
G1 – NO_3	930.841
G2 – NO_3	469.232
NO_3 – G1	-1075.918
NO_3– G2	-246.119
G1 – G2	-201.077
G2 – G1	120.917

A detailed calculation of the group interaction parameters for the nitric acid - water system is given in Appendix A.

4.3 Interpreting Quantum Chemical Energy Data and Modeling Binary Activity Coefficients

To model the activity coefficients as a function of composition, temperature and pressure, it is necessary to model the molar excess Gibbs energy of the complexes in the first step.

In order to utilize the excess Gibbs free energy data acquired from quantum chemical methods, it was required to fit the data into a useful and processible mathematical expression. Different types of data fitting models were applied.

$$G^{ex} = f(x_1, x_2) \tag{114}$$

On the other hand, with the fundamental excess property relation, all thermodynamic properties (excess Gibbs free energy, excess mixing enthalpy, excess molar volume change on mixing and excess partial molar Gibbs free energies, thus, activity coefficients) are related to each other in a mathematical basis. The fundamental excess property relation is given in the equation below.

$$d\left(\frac{G^{ex}}{RT}\right) = \frac{V^{ex}}{RT}dP - \frac{H^{ex}}{RT^2}dT + \sum_{i=1}^{k}\frac{G_i^{*ex}}{RT}dn_i \tag{115}$$

Starting from the fundamental excess property relation, by the tangent intercepts method, the equations below can directly give the individual activity coefficients of the components at a constant temperature and pressure in case of a binary system.

$$ln\gamma_1 = \frac{G^{ex}}{RT} - x_2\frac{d}{dx_2}\left(\frac{G^{ex}}{RT}\right) \tag{116}$$

$$ln\gamma_2 = \frac{G^{ex}}{RT} - x_1\frac{d}{dx_1}\left(\frac{G^{ex}}{RT}\right) \tag{117}$$

The excess Gibbs free energy data is expressed as a function of both x_1 and x_2 with the help of Redlich-Kister type mathematical expansion.

$$G^{ex} = x_1 x_2 \sum_{i=1}^{k} A_i (x_1 - x_2)^{i-1} \tag{118}$$

With the quantum chemical data, for a third order polynomial, $n = 4$, the molar excess Gibbs free energy of binary mixture of can be modeled as a function of x_1 and x_2 as in the equation below.

$$G^{ex} = x_1 x_2 (A_1 + A_2 (x_1 - x_2) + A_3 (x_1 - x_2)^2 + A_4 (x_1 - x_2)^3) \tag{119}$$

Partial differentiation of the fundamental excess property relation with respect to temperature at constant pressure and composition gives a relation to excess molar enthalpy of the mixture, an extension of Gibbs-Helmholtz equation.

$$\left(\frac{\partial}{\partial T} \left(\frac{G^{ex}}{T} \right) \right)_{P, x_j} = \frac{-H^{ex}}{T^2} \tag{120}$$

Partial differentiation of the fundamental excess property relation with respect to pressure at constant temperature and composition gives a relation to excess molar volume of the mixture,

$$\left(\frac{\partial G^{ex}}{\partial P} \right)_{T, x_j} = V^{ex} \tag{121}$$

Similarly, partial differentiation of the fundamental excess property relation with respect to number of moles of component *i* at constant temperature and pressure gives a relation to activity coefficients of the components in the mixture,

$$\left(\frac{\partial(G^{ex}/RT)}{\partial n_i}\right)_{T,P} = \frac{G_i^{*ex}}{RT} = ln\gamma_i \tag{122}$$

CHAPTER 5

RESULTS AND DISCUSSION

In this section, the results of experimental data, quantum chemical data and the results of estimation techniques were discussed.

5.1 Results of Calorimetry Experiments

For both the cases of oxidizer – water and fuel – water mixing experiments, the obtained heat of mixing data was fitted into different predictive models in order to calculate the resulting activity coefficients. Following the activity coefficients, it was required to estimate vapor composition of the gas phase.

In the data fitting process, the utilized fitting models are,

- Redlich-Kister type expansion (a type of polynomial regression)
- Two-constant Margules equation
- van Laar equation

5.1.1 Oxidizer – Water System

As explained before, in the adiabatic coffee-cup mixing experiment of oxidizer and water system, the oxidizer was added up to 40 mL into the mixture by 1 mL oxidizer per injection. In order to obtain heat of mixing data in the oxidizer rich phase 1 μL oxidizer was injected onto a 2 mL pool of oxidizer. The reason for that the oxidizer pool volume was taken very small compared to the first case of water pool is safety issues during the water addition onto the strong acid. The combined experimental data covering the broadest range of composition is plotted in Figure 5.1 below.

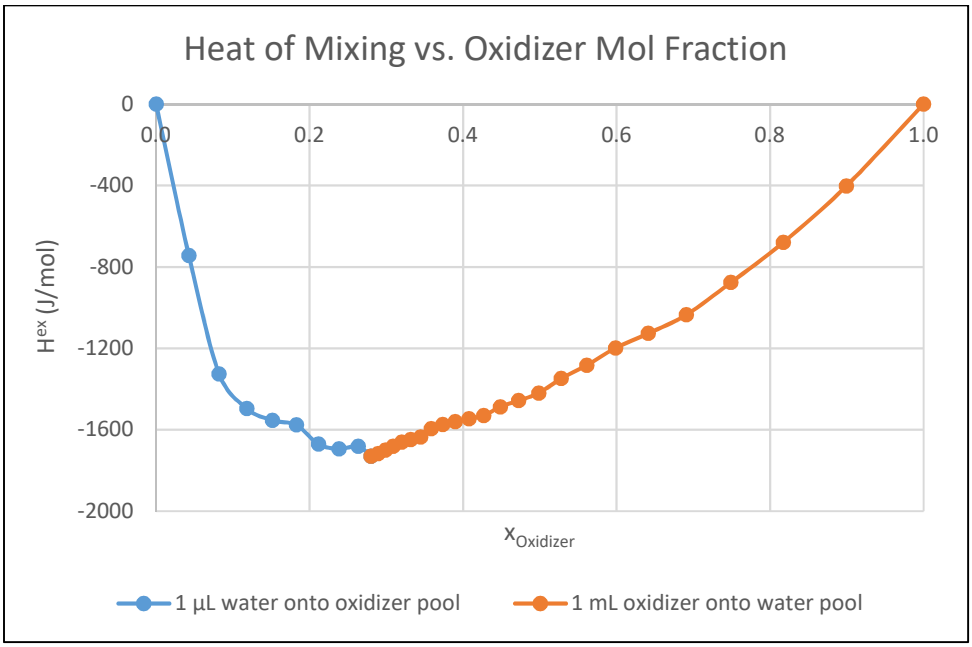

Figure 5.1 Comparison of coffee-cup calorimeter experiments for oxidizer – water mixture: 1 µL water per injection and 1 mL oxidizer per injection

For each of the experiments, the minima where the heat release has the highest value almost coincides at the same composition. The minimum can be said to be at the 26 % oxidizer, 74 % water composition by moles.

However, the maximum heat release is less for the 1 mL injection scenario than 5 mL injection scenario. This results in a little compression of the heat release curve. This is because the heat loss to the surroundings is a little larger in 1 mL injection scenario. Thus, the temperature of the solution could not be as high as that of 5 mL injection scenario. Therefore, it would have been better to model the 5 mL injection scenario with the least heat loss from the system.

In order to model activity coefficients as a function of composition, the experimental heat of mixing data is fitted into different models. The comparative plot of experimental data and results of different models is given in Figure 5.2 below.

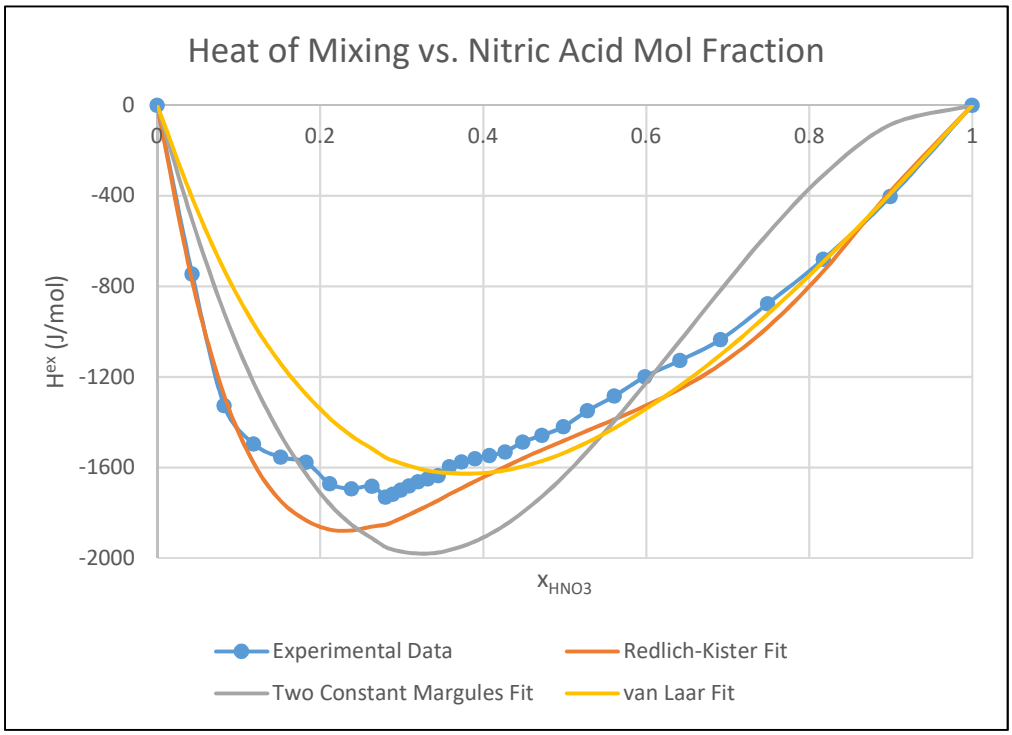

Figure 5.2 Comparison of experimental and fitted heat of mixing data for oxidizer - water mixture

In this experiment, there were no possibility to measure the pure compound enthalpies, Gibbs free energies and entropies. Also for the mixture, it was again unfeasible to measure mixture enthalpy, Gibbs free energy and entropy. Therefore, these restrictions canalized this experiment to be analyzed in a frame of regular solution approach. Thus, in the absence of other thermodynamic properties, the excess mixture enthalpy could have been utilized as the excess Gibbs free energy of the mixture, as shown in the equation below.

$$H^{ex} = \Delta H_{mix} = G^{ex} \tag{123}$$

After the fitting process, the necessary model parameters were obtained. The detailed calculation of the Redlich-Kister, Two-Constant Margules ad van Laar equations are given in Appendix C. Those equations are actually polynomials that are approximating models to an existing data.

The resulting model parameters are listed in Table 5.1 for the fitting models,

Table 5.1 Calculated model fitting parameters for G^{ex}

	Coefficients	Value
Redlich – Kister Expansion (for n=4)	A1	-2.24
	A2	1.07
	A3	-2.60
	A4	2.70
Two – Constant Margules Equation	A	-2.47
	B	2.62
van Laar Equation	A	-4.20
	B	-1.60

Following the calculation of model parameters, activity coefficients were calculated as a function of mixture composition. The resulting activity coefficients in comparison, are shown in Table 5.2 below.

Table 5.2 The activity coefficients calculated from different type of data fitting models

	Redlich Kister Fit		**Two Constant Margules Fit**		**Van Laar Fit**	
x_{HNO_3}	γ_{HNO_3}	γ_{H_2O}	γ_{HNO_3}	γ_{H_2O}	γ_{HNO_3}	γ_{H_2O}
1	1.00	1.00	1.00	0.00	1.00	0.20
0.90	0.91	0.77	0.97	0.03	0.99	0.23
0.82	0.79	0.70	0.97	0.03	0.97	0.26
0.75	0.71	0.67	0.97	0.03	0.95	0.28
0.69	0.68	0.65	0.96	0.04	0.91	0.31
0.64	0.68	0.64	0.96	0.04	0.88	0.34
0.60	0.70	0.63	0.95	0.05	0.84	0.36
0.56	0.75	0.62	0.95	0.05	0.80	0.39
0.53	0.80	0.62	0.94	0.06	0.76	0.41
0.50	0.88	0.62	0.93	0.07	0.72	0.43
0.47	0.96	0.62	0.92	0.08	0.69	0.45
0.45	1.04	0.62	0.90	0.10	0.65	0.48
0.43	1.13	0.63	0.89	0.11	0.62	0.50
0.41	1.23	0.63	0.87	0.13	0.59	0.52
0.39	1.33	0.64	0.85	0.15	0.56	0.53
0.37	1.43	0.64	0.82	0.18	0.53	0.55
0.36	1.53	0.65	0.80	0.20	0.50	0.57
0.34	1.62	0.66	0.77	0.23	0.48	0.58
0.33	1.72	0.66	0.74	0.26	0.45	0.60
0.32	1.81	0.67	0.71	0.29	0.43	0.61
0.31	1.89	0.68	0.67	0.33	0.41	0.63
0.30	1.98	0.69	0.64	0.36	0.39	0.64
0.29	2.06	0.69	0.61	0.39	0.37	0.65

Table 5.2 (continued)

0.28	2.13	0.70	0.57	0.43	0.36	0.66
0.26	2.26	0.71	0.50	0.50	0.33	0.69
0.24	2.45	0.74	0.39	0.61	0.28	0.72
0.21	2.62	0.77	0.27	0.73	0.23	0.76
0.18	2.74	0.81	0.16	0.84	0.19	0.80
0.15	2.74	0.85	0.08	0.92	0.14	0.85
0.12	2.59	0.89	0.03	0.97	0.10	0.90
0.08	2.22	0.94	0.01	0.99	0.06	0.94
0.04	1.66	0.98	0.00	1.00	0.03	0.98
0.00	1.00	1.00	0.00	1.00	0.02	1.00

It can be concluded that, even though four constant Redlich – Kister type polynomial was a good fit for the experimental excess enthalpy, it was not good enough to model activity coefficients. Similarly, two constant Margules and van Laar rather gave better predictions for activity coefficients while the excess enthalpy fits were not perfect. It is also seen that, two constant Margules fit gave maximum heat release upon mixing at liquid composition of $x_{HNO_3} = 0.33$ and van Laar fit gave it at the composition of $x_{HNO_3} = 0.37$.

5.1.2 Fuel – Water System

As explained before, in the fully adiabatic coffee-cup mixing experiment of fuel and water system, the fuel was added up to 75 mL into the mixture, either by 1 mL oxidizer per injection or 5 mL fuel per injection. The fuel rich side of the heat of mixing versus composition graph is constructed by the contribution of water injections on a fixed volume pool of fuel either by 1 mL water per injection or by 5 mL water per injection. By utilizing these four separate experiments, both the experimental data

are validated with each other and the entire heat of mixing versus composition plot at atmospheric pressure.

With the experimental data, the resulting enthalpy of mixing changing with composition is shown in Figure 5.3.

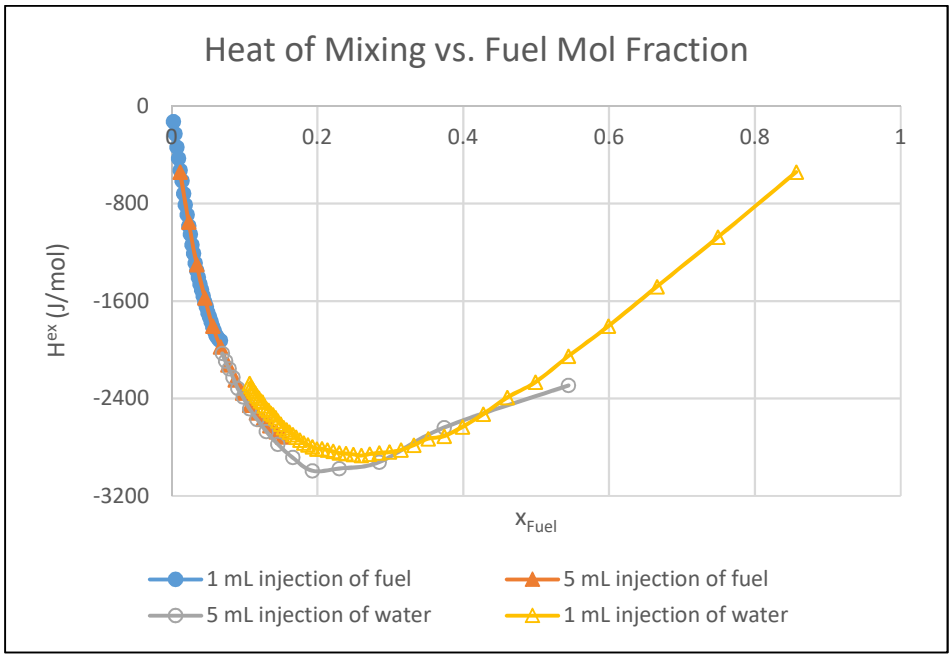

Figure 5.3 Comparison of coffee-cup calorimeter experiments for fuel – water mixture: 1 mL per injection and 5 mL per injection of fuel and water

As shown in Figure 5.3, the measurements seem to be in precision with only very small amount of differences. This implies that, the heat release is less in case of fuel – water mixing than oxidizer – water mixing. This might be because the transfer of the heat to surroundings by the fume of oxidizer leaking through.

Furthermore, the minimum is observed at the region where the fuel composition is 19 – 26 % by mole. The coincidence point of the minima may be missed due to unequal amounts of heat loss to the surroundings for 1 mL and 5 mL injection cases.

Similarly for the oxidizer – water system, in order to model activity coefficients as a function of composition, the experimental heat of mixing data is fitted into different

models. However, since the amount of data points is very large, Redlich-Kister polynomial and two-constant Margules equation gave very poor fitting for the experimental data. Therefore, the experimental data was modeled with van Laar equation regarding its reliability. The plot of experimental data and van Laar model fit is given in Figure 5.4.

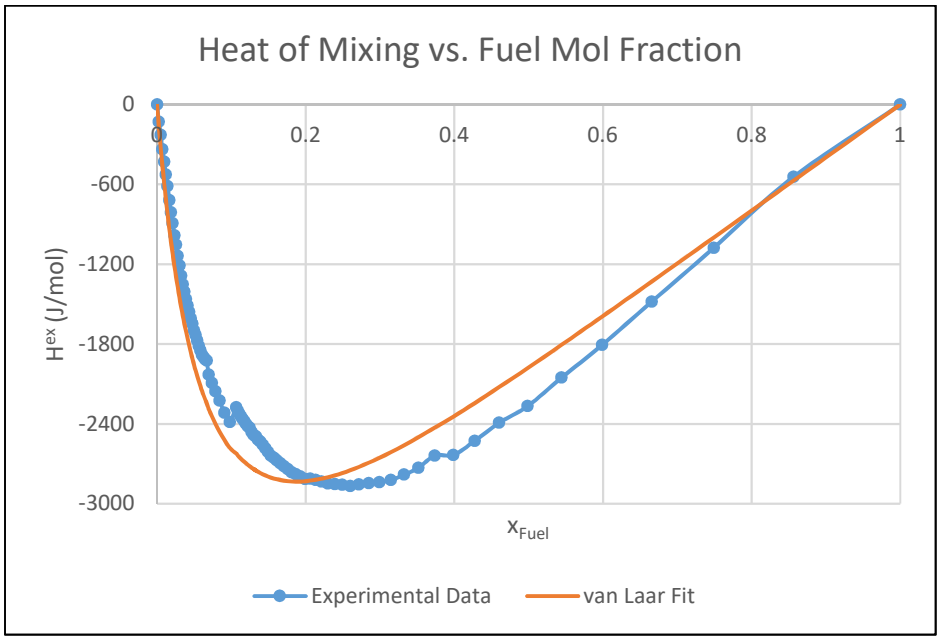

Figure 5.4 Comparison of experimental and fitted heat of mixing data

From the Figure 5.4, it can be said that the maximum heat release; therefore, the minimum excess Gibbs free energy is observed at the water rich side, at point where the mixture contains approximately 25% fuel by moles.

5.1.3 Diluted Fuel – Diluted Oxidizer System

As explained before, the heat of mixing for the diluted fuel and oxidizer system was measured. The experiment covered 50 mL of each solutions. 1 mL diluted fuel added onto diluted oxidizer per injection. The experiment covers data between $0.001 - 0.01$ % fuel by moles in the whole system. The experimental data are given in Appendix F.

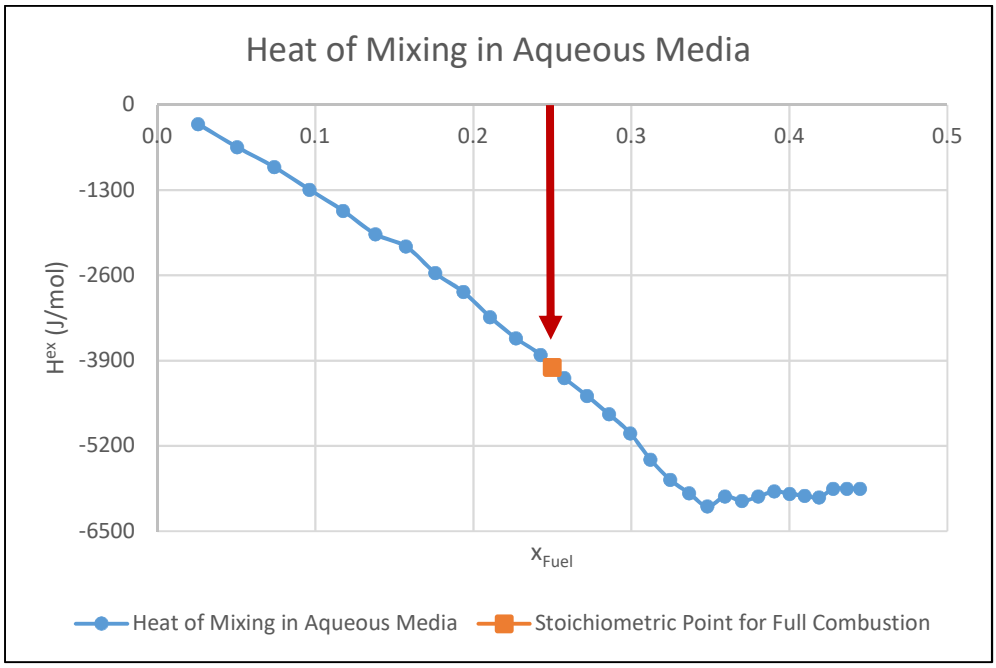

Figure 5.5 Heat of mixing result of the diluted fuel – diluted oxidizer system, 5 mL of diluted fuel per injection

In the case of diluted solutions, the maximum heat release, thus the minimum excess molar Gibbs free energy was observed at the point were the non-aqueous mixture contains 35 % fuel by moles. In this case, the heat of mixing is absorbed by the water environment, hence ignition is inhibited.

When the non-aqueous excess enthalpy of mixing is calculated from the temperature raise of all three components, the maximum heat release is observed when the fuel mole fraction is 0.36.

$$H_{mix}^{ex} = Q_{tot} - \left(C_p^{ox} n_{ox} \Delta T + C_p^{fuel} n_{fuel} \Delta T + C_p^{water} n_{water} \Delta T\right) \qquad (124)$$

According to the reaction of complete combustion of the fuel and the oxidizer, the stoichiometric ratio is $O/F = 8/1$. This mole fraction is also shown in the Figure 5.5.

5.2 Results of DFT Calculations

5.2.1 Nitric Acid – Water System

For nitric acid water system, the required excess Gibbs energy data is calculated from the state energies data obtained with computational chemistry applications, DFT. At 298.15 K and 1 bar conditions. The obtained quantum chemical data on molar thermodynamic properties are given in Table 5.3 below.

Table 5.3 Complexation thermodynamic properties of nitric acid – water system obtained by DFT (B3LYP/6-31+G(d,p)) in water, (CPCM)

	Structure of the Complex	**Enthalpy** (a.u.)	**Binding Energy** (kcal/mol HNO_3)	**Nitric Acid Mole Fraction**	**Gibbs Free Energy** (a.u.)	**Entropy** (cal/mol.K)
Pure	HNO_3	-280.88	0	1	-280.91	63.6
1st shell	HNO_3-H_2O	-357.31	-7.9	0.50	-357.35	80.7
	HNO_3-$2H_2O$	-433.73	-8.7	0.33	-433.78	107.5
	HNO_3-$3H_2O$	-510.15	-11.8	0.25	-510.21	119.2
	HNO_3-$4H_2O$	-586.57	-12.1	0.20	-586.66	145.4
2nd shell	HNO_3-$5H_2O$	-662.10	-18.3	0.17	-663.07	161.9
	HNO_3-$6H_2O$	-739.42	-22.2	0.14	-739.50	181.5
	HNO_3-$7H_2O$	-815.84	-25.3	0.13	-815.94	204.5
	HNO_3-$8H_2O$	-892.26	-28.1	0.11	-892.37	219.4
Pure	H_2O	-76.42	0	0	-76.44	45.1

The state energies data (enthalpy, binding energy, Gibbs free energy and entropy) are given in J/mol HNO_3 basis with the mole fractions in Table 5.4. The comparative

excess molar Gibbs energy plot with different polynomial fits is given in Appendix D.

Table 5.4 State energy data acquired for nitric acid water binary mixture by obtained by DFT (B3LYP/6-31+G(d,p)) in water, (CPCM), (in J/mol basis)

Complexes	**Nitric Acid Mole Fraction**	**Molar Enthalpy** (J/mol)	**Molar Gibbs Free Energy** (J/mol HNO_3)	**Molar Entropy** (J/mol)	**Binding Enthalpy** (J/mol)
H_2O	0.00	-200633807.6	-200690090.4	188.6	0.0
$1HNO_3$-$8H_2O$	0.11	-2342632235.0	-2342905962.0	917.2	-117750.9
$1HNO_3$-$7H_2O$	0.13	-2141986715.0	-2142241877.0	855.0	-106038.6
$1HNO_3$-$6H_2O$	0.14	-1941339572.0	-1941565975.0	758.6	-92703.7
$1HNO_3$-$5H_2O$	0.17	-1740689802.0	-1740891734.0	676.6	-76740.7
$1HNO_3$-$4H_2O$	0.20	-1540029931.0	-1540211282.0	607.7	-50677.4
$1HNO_3$-$3H_2O$	0.25	-1339394876.0	-1339543532.0	498.1	-49430.2
$1HNO_3$-$2H_2O$	0.33	-1138748185.0	-1138882285.0	449.3	-36546.9
$1HNO_3$-$1H_2O$	0.50	-938110996.2	-938211707.7	337.5	-33165.3
HNO_3	1.00	-737444023.3	-737523418.4	266.0	0.0

Since it represents the enthalpy change over the complexation from pure components, conceptually, the binding energy can be considered as the enthalpy change among the complexation.

In utilization of quantum chemical complexation thermochemical data, the regular solution approach is used. Therefore, the binding enthalpy is considered as the Gibbs free energy change of the systems which are composed of pure liquids with the same nitric acid/water ratio.

5.2.2 Fuel – Oxidizer System

Similar for the nitric acid – water system, the complexation energy data for the fuel – oxidizer system is obtained by DFT. The data was obtained by Gaussian09 software package with B3LYP functional for the optimization of the geometries and computations of energies and frequencies. The raw complexation energy data obtained for the fuel – oxidizer system is given in Table 5.5.

Table 5.5 Thermodynamic properties of fuel – oxidizer system obtained by (M06-2X/6-31+G(d,p) in nitric acid) ($\varepsilon = 50$, CPCM).

Structure of the Complex	**Enthalpy** (a.u.)	**Binding Energy** (kcal/mol)	**Oxidizer Mole Fraction**	**Gibbs Free Energy** (a.u.)	**Entropy** (cal/mol. K)
Fuel	-347.36	0.00	0.00	-347.41	99.5
2Fuel-1HNO_3	-975.53	-35.00	0.33	-975.62	175.6
3Fuel-2 HNO_3	-1603.7	-66.20	0.40	-1603.8	263.3
1Fuel-1HNO_3	-628.16	-28.10	0.50	-628.22	124.9
2Fuel-3HNO_3	-1537.1	-73.73	0.60	-1537.2	239.1
1Fuel-2HNO_3	-908.96	-52.90	0.67	-909.03	152.6
1Fuel-3HNO_3	-1189.7	-65.90	0.75	-1189.8	174.1
1Fuel-4HNO_3	-1470.5	-79.20	0.80	-1470.6	196.2
1Fuel-6HNO_3	-2032.1	-98.70	0.86	-2032.2	244.0
1Fuel-8HNO_3	-2593.6	-111.30	0.89	-2593.8	298.7
1Fuel-10HNO_3	-3155.2	-126.50	0.91	-3155.3	340.3
HNO_3	-280.76	0.00	1.00	-280.79	63.3

The binding energy used as the complexation enthalpy for the fuel – oxidizer complexes as stated in the equation 87. For the excess molar Gibbs energy and enthalpy of mixing, regular solution theory is applied during the calculations as stated before.

Similar for the nitric acid – water system, for fuel - oxidizer system the required excess Gibbs energy data is calculated from the state energies data obtained with DFT. At 298.15 K and 1 bar conditions, the state energies data are given in J/mol basis with the mole fractions in Table 5.6.

Table 5.6 Thermodynamic properties of fuel – oxidizer system obtained by DFT (M06-2X/6-31+G(d,p) in nitric acid) ($\varepsilon = 50$, CPCM).

Complexes	**Oxidizer Mole Fraction**	**Molar Enthalpy** (J/mol)	**Molar Gibbs Free Energy** (J/mol fuel)	**Molar Entropy** (J/mol.K)	**Binding Enthalpy** (J/mol)
Fuel	0.00	-911992803.1	-912116981.4	416.3	0
2Fuel-1HNO_3	0.33	-2561263630.0	-2561482641.0	734.7	-146440
3Fuel-2HNO_3	0.40	-4210518708.0	-4210847169.0	1101.7	-276980.8
1Fuel-1HNO_3	0.50	-1649242125.0	-1649397956.0	522.6	-117570.4
2Fuel-3HNO_3	0.60	-4035688879.0	-4035987149.0	1000.4	-308486.3
1Fuel-2HNO_3	0.67	-2386477326.0	-2386667743.0	638.5	-221333.6
1Fuel-3HNO_3	0.75	-3123663294.0	-3123880491.0	728.4	-275725.6
1Fuel-4HNO_3	0.80	-3860850793.0	-3861095518.0	820.9	-331372.8
1Fuel-6HNO_3	0.86	-5335195316.0	-5335499680.0	1020.9	-412960.8
1Fuel-8HNO_3	0.89	-6809511477.0	-6809884090.0	1249.8	-465679.2
1Fuel-10HNO_3	0.91	-8283838070.0	-8284262606.0	1423.8	-529276
HNO_3	1.00	-737131601.9	-737210561.2	264.9	0

As in the nitric acid – water system, Redlich – Kister type expansion, two constant Margules equation and van Laar equation were utilized to fit the quantum chemical data on a polynomial. In addition, the regular solution theory was the theoretical basis for the thermodynamic calculations. For the fuel – oxidizer system, the resulting polynomial coefficients were given in Table 5.7.

Table 5.7 Coefficients of the polynomials for molar excess Gibbs free energy for fuel – oxidizer system

	Coefficients	Value
	A_1	51.8
Redlich – Kister	A_2	-1005.6
Expansion[a]	A_3	-22.4
(for $n = 4$)	A_4	1030.5
Two – Constant	A	-446.1
Margules Equation	B	-1455.7
van Laar	A	-149.3
Equation	B	5000

The excess molar Gibbs energies with different fitting methods were given in Appendix D for comparison.

The resulting activity coefficients are given in Table 5.8.

Table 5.8 Resulting activity coefficients of fuel - oxidizer system.

		Redlich Kister Fit		Two Constant Margules Fit		Van Laar Fit	
Fuel Mole Fraction	**G^{ex}** (J/mol)	γ_{Fuel}	γ_{HNO_3}	γ_{Fuel}	γ_{HNO_3}	γ_{Fuel}	γ_{HNO_3}
0.00	0.0	1.0	1.0	0.0	1.0	-	1.0
0.09	-529276.0	1.4E-50	2076.3	0.0	8.2E-16	-	1E-133
0.11	-465679.2	2.5E-55	8503.7	0.0	1.2E-22	1.5E+220	2E-113
0.14	-412960.8	1.9E-59	13605.0	0.00	9.3E-35	3.1E+109	6.3E-98
0.20	-331372.8	6.2E-60	13.1	1.2E-205	4.1E-64	8.4E+39	2.6E-84
0.25	-275725.6	1.3E-55	6.4E-06	1.1E-109	7.4E-92	1.0E+21	6.3E-79
0.33	-221333.6	1.6E-45	9.5E-22	7.0E+03	1.7E-137	1.1E+09	3.5E-74
0.40	-308486.3	3.0E-37	7.2E-38	6.5E+66	2.5E-173	59061.1	9.1E-72
0.50	-117570.4	1.9E-29	2.6E-55	4.1E+109	3.3E-207	113.7	1.3E-69
0.60	-276980.8	1.2E-25	2.5E-55	4.1E+110	5.0E-207	7.9	3.3E-68
0.67	-146440.0	1.7E-23	1.9E-41	3.67E+94	1.6E-178	3.0	1.7E-67
1.00	0.0	1.0	1.0	1.00E+00	-	1.0	1.5E-65

For the fuel – oxidizer system, the minimum excess molar Gibbs free energy is observed at the point where the mixture contains 91% of oxidizer by moles. This represents the structure having ten oxidizer molecules are interacting with a single fuel molecule.

5.2.3 Comparison of Experimental and Quantum Chemical Heat of Mixing Data

The experimental heat of mixing data is compared with DFT results for the nitric acid – water system in a double y-axis plot. Both data are in J/mol HNO_3 basis.

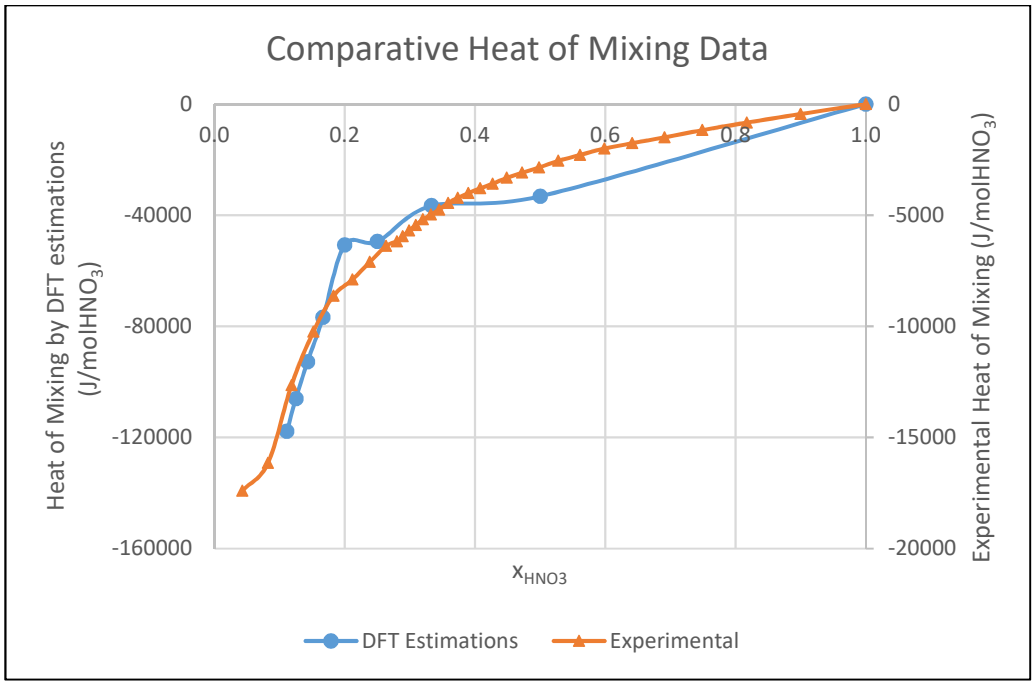

Figure 5.6 Comparative plot of heats of mixing for nitric acid – water system by calorimetry and DFT estimations.

Even though the large difference in magnitude, for nitric acid – water system, DFT heat of mixing shows very similar trend with the experimental heat of mixing data on a double y-axis plot.

5.3 Results of van Laar Method

It was mentioned before, that the binary mixture of nitric acid – water system gives a maximum boiling azeotrope at 120.5 ˚C at atmospheric pressure. This is because the system exhibits a negative deviation from the Raoult's Law, hence, stronger interactions between unlike molecules than like molecules. Therefore, for the case of negative deviation, activity coefficient of at least one mixture component should be less than 1, $\gamma_i < 1$.

As explained before, to calculate activity coefficient of each component as a function of liquid composition, the required parameters α and β were obtained from the azeotrope data.

Table 5.9 α and β parameters calculated from azeotrope data

Parameter	**Calculated value**
α	-4.36
β	-2.81

With the azeotrope data given in Table 5.9. Vapor pressures of both components, the bubble and dew point temperatures were calculated. By the use of the boiling, bubble and dew point temperatures, the phase diagram for the binary nitric acid – water system were constructed in Figure 5.7 below.

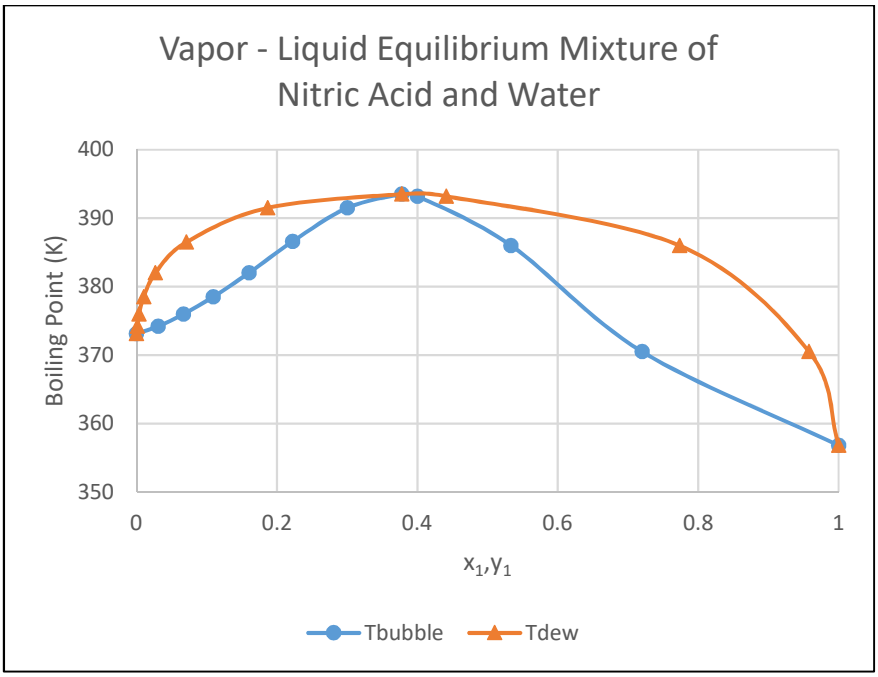

(a)

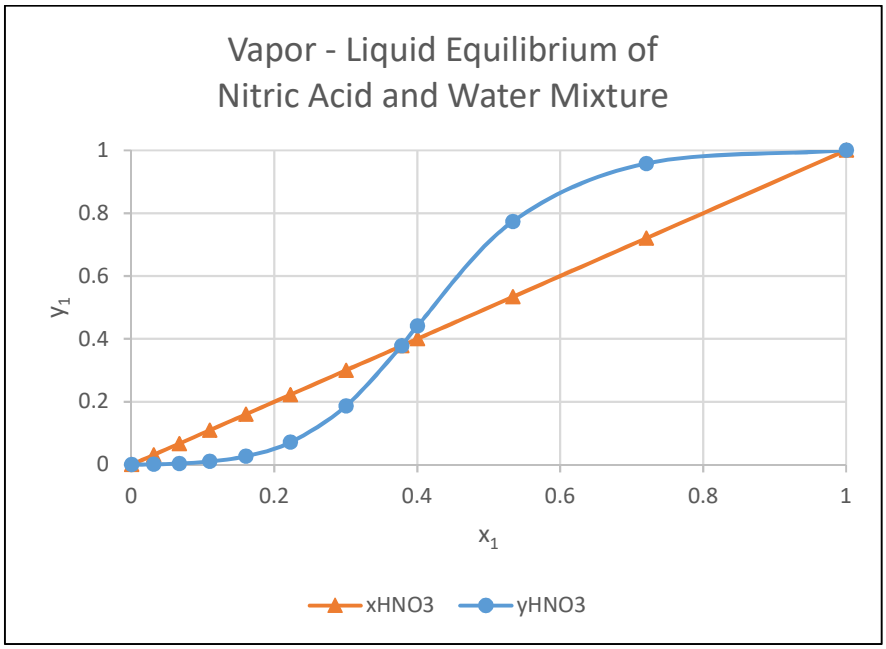

(b)

Figure 5.7. Nitric acid – water binary phase diagrams at 1 bar pressure

As already given in the work of Matheswaran et al. (2007) with a nitric acid – water azeotropic mixture of 68% nitric acid by mass, it can be seen from the Figure 5.7, binary mixture of nitric acid - water yields an azeotrope at 120.5 ˚C at atmospheric pressure with a composition of $x_1 = y_1 = 0.38$ and $x_2 = y_2 = 0.62$ which is the molar equivalent of the reference mixture (Matheswaran, Kwon, Kim, & Moon, 2007).

Using the van Laar model in calculation, in addition to construction of binary mixture phase diagram, the excess Gibbs free energy, therefore, taking into account the regular solution theory, the excess enthalpy of the binary mixture and the activity coefficients of the components as a function of composition could be also estimated and shown in Figure 5.8 and Figure 5.9.

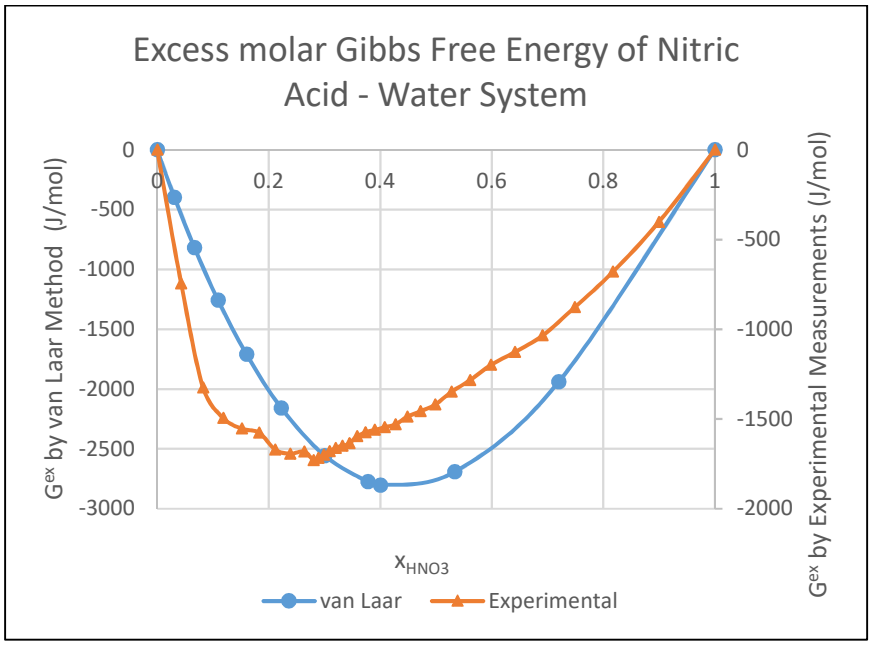

Figure 5.8. Comparative plot of excess molar Gibbs free energy (excess molar enthalpy) of the binary nitric acid – water system as a function of composition at atmospheric pressure by van Laar method and experimental measurements

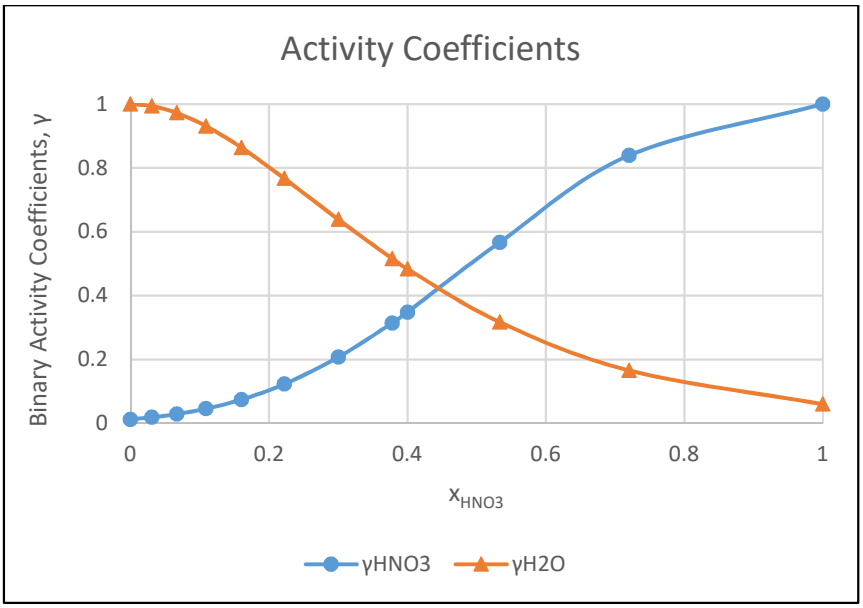

Figure 5.9. Activity coefficients of nitric acid and water in the binary system as a function of composition at atmospheric pressure

As seen from the Figure 5.9, the activity coefficients of the components are increasing with increasing composition in the mixture. From the Figure 5.8, it can be inferred that the minimum of the excess molar Gibbs free energy of the binary mixture of nitric acid – water system; therefore, the maximum heat release upon mixing is observed at the composition where the mixture contains 40% nitric acid by moles. According to this model, the maximum heat release is around 2800 J/mol.

From the data on α and β values, the infinite dilution activity coefficients of the nitric acid and water in the binary mixture were determined. As it is indicated in van Laar model,

$$ln\gamma_1^{\infty} = \alpha \tag{125}$$

$$ln\gamma_2^{\infty} = \beta \tag{126}$$

The calculated infinite dilution activity coefficients for the nitric acid – water system is given in Table 5.10.

Table 5.10 Infinite dilution activity coefficients of nitric acid – water system from the azeotrope point data

For HNO_3, γ_1^{∞}	0.013
For H_2O, γ_2^{∞}	0.060

Since it could be applied to the nitric acid – water binary system, and yielded very similar results with the resource work of Matheswaran et al (2007), the van Laar method can be regarded as a good model for estimation of activity coefficients, vapor – liquid equilibria and the excess molar Gibbs energy for binary systems (Matheswaran, Kwon, Kim, & Moon, 2007).

The infinite dilution activity coefficient for water is very small in magnitude, in other words approaching to zero. This outcome can be a signal to point out that using azeotrope point data may not be a suitable method for estimating excess Gibbs free energy.

5.4 Results of UNIFAC Group Contribution Binary Activity Coefficient Model

In order to check the ability to estimate VLE data of UNIFAC binary activity coefficient model, an example system of methanol and water was selected and the estimated VLE data with UNIFAC was compared with the reference VLE data. The comparison chart is given in the Appendix H.

The UNIFAC calculations on methanol – water system very well represented the reference vapor – liquid equilibrium data for water with an error of around 0.42 %, and for methanol with an error of around 7.1. Therefore, regarding the reliability of the methanol – water system representation, it was concluded that UNIFAC binary

activity coefficient model could be used for the VLE estimation of binary nitric acid – water and fuel – oxidizer systems.

5.4.1 Results of Nitric Acid – Water System

As in the methanol – water system, UNIFAC binary activity coefficient model is very successful to produce estimated data very similar to reference experimental data. Based on this inference, UNIFAC binary activity coefficient model is used for nitric acid – water and fuel – oxidizer binary systems, for which there are not enough experimental VLE data. For the calculations, the surface and area parameters of the functional groups given in Table 4.2 were used. For both nitric acid – water and fuel – oxidizer systems, activity coefficients, vapor – liquid equilibrium and excess molar Gibbs free energies were calculated. The required functional group interaction parameters, a_{mn}, are calculated using CI-index method as explained before.

For the nitric acid – water system, the functional groups are assigned as the HNO_3 and _OH groups. The resulting of the UNIFAC calculations at 20 ˚C are given in Table 5.11.

Table 5.11 Results of the UNIFAC activity coefficient model calculations for nitric acid – water binary system

Nitric Acid Mole Fraction, x_1	γ_1	γ_2	**Excess Molar Gibbs Free Energy** (J/mol mixture)	**Excess Molar Gibbs Free Energy** (J/mol HNO_3)	y_1	y_2
0.00	0.00	1.00	0.00	-29024.5	0.00	1.00
0.10	0.05	0.61	-1838.67	-18386.7	0.01	0.99
0.20	0.17	0.43	-2498.21	-12491.1	0.15	0.85
0.30	0.35	0.33	-2625.64	-9062.6	0.44	0.56
0.40	0.54	0.28	-2475.88	-8752.2	0.69	0.31
0.50	0.70	0.24	-2172.41	-8453.1	0.83	0.17
0.60	0.82	0.22	-1783.23	-6189.7	0.91	0.09
0.70	0.91	0.20	-1349.22	-4344.8	0.95	0.05
0.90	0.99	0.18	-442.75	-1927.5	0.99	0.01
1.00	1.00	0.17	0.00	-1120.7	1.00	0.00

The resulting excess molar Gibbs free energy of the nitric acid – water system is visualized in Figure 5.10.

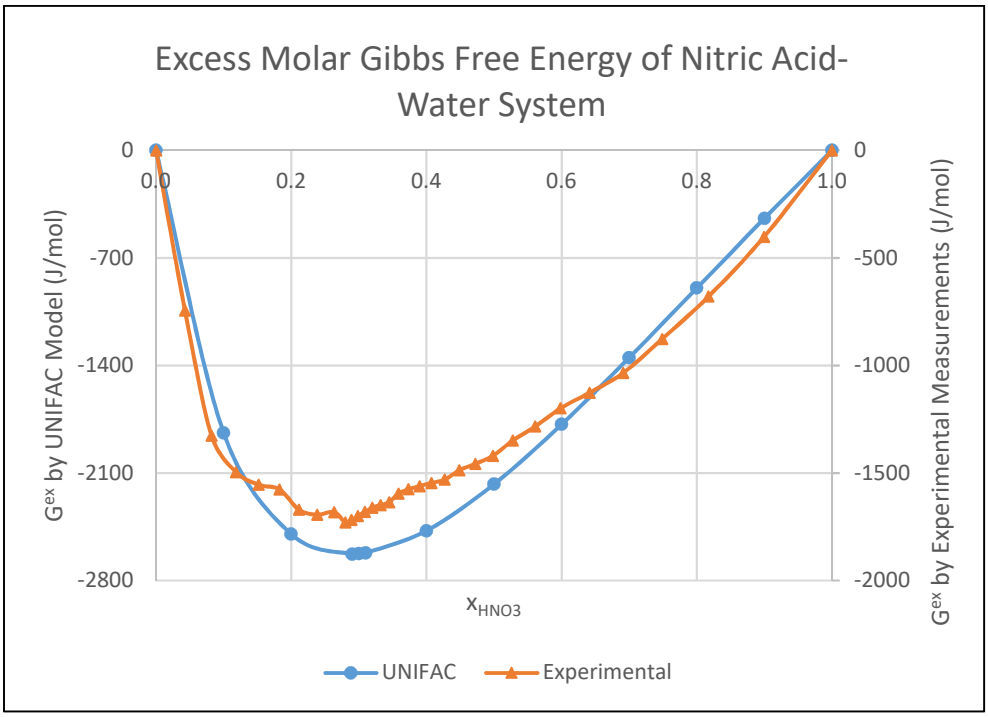

Figure 5.10. Comparative plot of excess molar Gibbs free energy (excess molar enthalpy) of the binary nitric acid – water system as a function of composition at atmospheric pressure by UNIFAC model and experimental measurements

Because of the very small values of activity coefficients, from the aspect of determination of activity coefficients and vapor – liquid equilibria, UNIFAC method does not seem to be suitable enough for nitric acid – water system. This disparity can be a consequence of the scope of UNIFAC method, as the method covers liquid mixtures of non-electrolytes while nitric acid is a strong electrolyte. With the very small values and rough vapor – liquid equilibria, the molar Gibbs free energy calculations with UNIFAC shows that the maximum heat release is observed at the point where the mixture contains nearly 30% of nitric acid. This result claims a similar condition to that of van Laar model results which gives the maximum heat release at 40% nitric acid concentration. While the minimum excess molar Gibbs free energy is around -2800 J/mol for van Laar model, it is nearly -2626 J/mol for the UNIFAC results.

The resulting excess molar Gibbs free energy trend obtained by quantum chemical method shows very similar trend with that of UNIFAC model. In DFT results, the minimum excess molar Gibbs free energy is observed when the fuel molecule is surrounded by ten oxidizer molecules. However, in the UNIFAC results, the minimum excess molar Gibbs free energy is observed at the fuel rich side. As mentioned before, the UNIFAC is actually used for the non-polar, non-electrolyte liquids. If a comparison is made, the quantum chemical method results can be preferred due to be more reliable than UNIFAC for the unknown case of the mixing of fuel – oxidizer system.

Although the UNIFAC model would have been sufficient enough to estimate the excess molar Gibbs free energy, the computation of group interaction parameters, a_{mn}, can be possibly a reason the errors included in the calculations. The same non-electrolyte issue is valid for the CI-index method, too. In addition, the group interaction parameter, a_{mn}, is temperature dependent in real systems. However, for the sake of simplicity, it was considered as temperature independent in this work.

5.4.2 Results of Fuel – Oxidizer System

For the fuel - oxidizer system, the functional groups were assigned as the G1, G2 and HNO_3 groups. The resulting of the UNIFAC calculations at 20 ˚C are given in Table 5.12.

Table 5.12 Results of the UNIFAC activity coefficient model calculations for fuel - oxidizer binary system

Fuel Mole Fraction, x_1	γ_1	γ_2	**Excess Molar Gibbs Free Energy** (J/mol mixture)	**Excess Molar Gibbs Free Energy** (J/mol fuel)	y_1	y_2
0.00	0.00	1.00	0.00	-29024.54	0.00	1.00
0.10	0.03	0.78	-1364.24	-18386.65	0.00	1.00
0.20	0.22	0.57	-1830.84	-12491.05	0.05	0.95
0.30	0.46	0.45	-1942.79	-9062.62	0.20	0.80
0.40	0.66	0.37	-1876.76	-8752.15	0.41	0.59
0.50	0.80	0.31	-1689.88	-8453.08	0.60	0.40
0.60	0.89	0.27	-1443.16	-6189.71	0.74	0.26
0.70	0.95	0.24	-1143.46	-4344.81	0.84	0.16
0.80	0.98	0.21	-801.66	-2972.05	0.92	0.08
0.90	1.00	0.18	-422.26	-1927.46	0.97	0.03
1.00	1.00	0.13	0.00	-1120.69	1.00	0.00

The resulting excess molar Gibbs free energy of the fuel - oxidizer binary system is visualized in Figure 5.11.

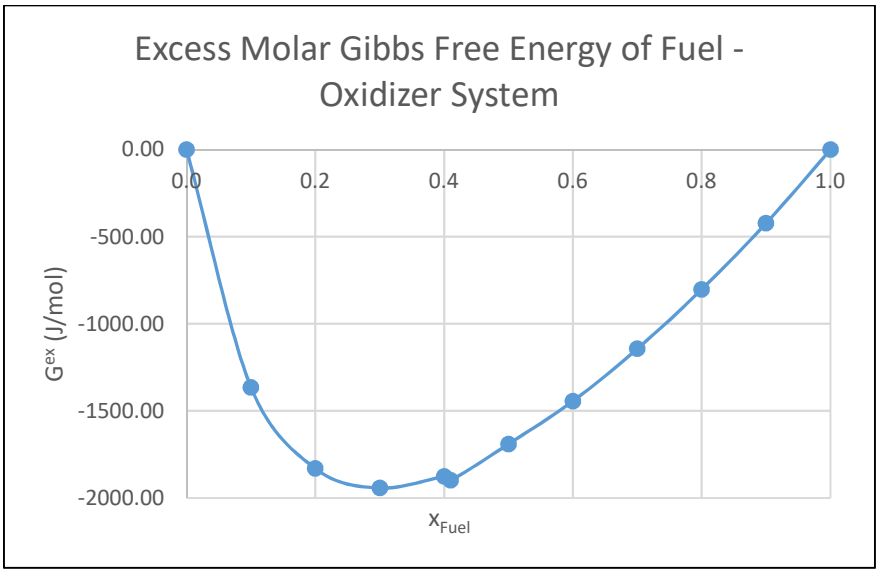

Figure 5.11 The resulting UNIFAC excess molar Gibbs free energy of fuel - oxidizer system changing with fuel mole fraction

Looking at the Figure 5.11, using UNIFAC binary activity coefficient model, it can be seen that the minimum excess molar Gibbs free energy for the fuel – oxidizer system is observed at the point where the mixture contains 31% fuel by moles. In addition, the excess molar Gibbs free energy is approximately -1836 J/mol.

The resulting binary activity coefficients and vapor – liquid equilibrium are also plotted in Figure 5.12 below.

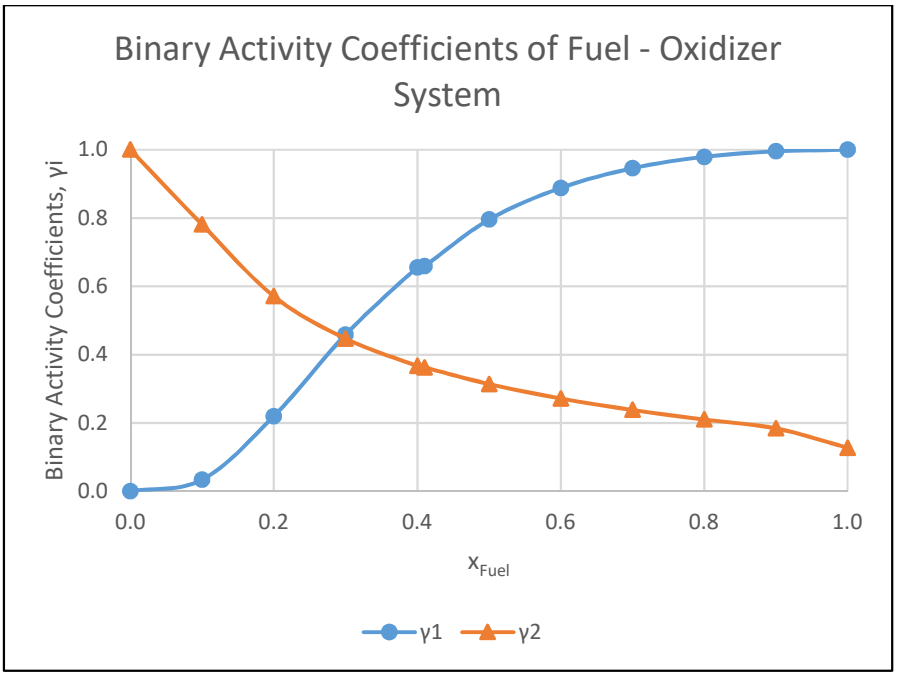

Figure 5.12 The resulting UNIFAC binary activity coefficients of fuel - oxidizer system changing with fuel mole fraction.

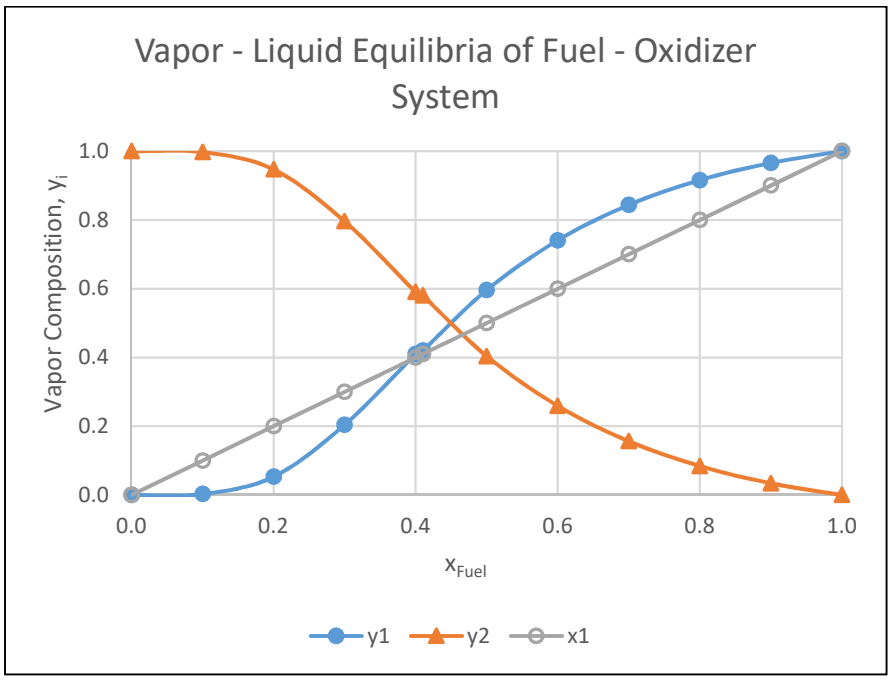

Figure 5.13 The resulting vapor – liquid equilibrium of fuel - oxidizer system changing with fuel mole fraction.

The UNIFAC results for the fuel and oxidizer system show the maximum heat release upon mixing is observed in the fuel rich region. The activity coefficients exhibit a similar trend with the activity coefficients of nitric acid – water system obtained by van Laar and UNIFAC models.

UNIFAC binary activity coefficient model is actually used to estimate the activity coefficients and the excess molar Gibbs free energy of non-polar liquids. However, the oxidizer used in this work is polar as water. Although the resulting activity coefficients and the excess molar Gibbs free energies does not offer a high accuracy in prediction, the results give a sight to the research where should be the mixture composition lie, in the fuel rich side or the oxidizer rich side.

5.5 Results of Ignition Delay Time Experiments

The ignition delay time measurement experiments were conducted for observing the ignition behavior of the amine based hypergolic fuel and the strong acidic oxidizer. In the experimental setup, these parameters were kept constant for all of the runs,

- Injection drop height
- Volume of the stationary oxidizer
- Volume of the fuel drop

The experiments were scheduled to examine the pressure and temperature effects on the ignition delay time of the hypergolic amine based fuel and the acidic oxidizer. Although it was tried to conduct a great number of experiments, because of the limitations of the custom designed IDT experimental setup, only a few experiments were completed successfully.

The experimental results obtained at different pressure and different temperature conditions are firstly grouped in two groups: constant temperature and constant pressure cases. The refined results at constant temperatures are given in Appendix G and Figure 5.14 below. The data includes the arithmetic averages of multiple results at

the same temperature and pressure conditions. Therefore, each point of ignition time delay is represented by a single pressure and temperature dimension.

Ignition delay time experimental results are tabulated in Appendix G. The results with changing pressures at different temperatures are also shown in Figure 5.14.

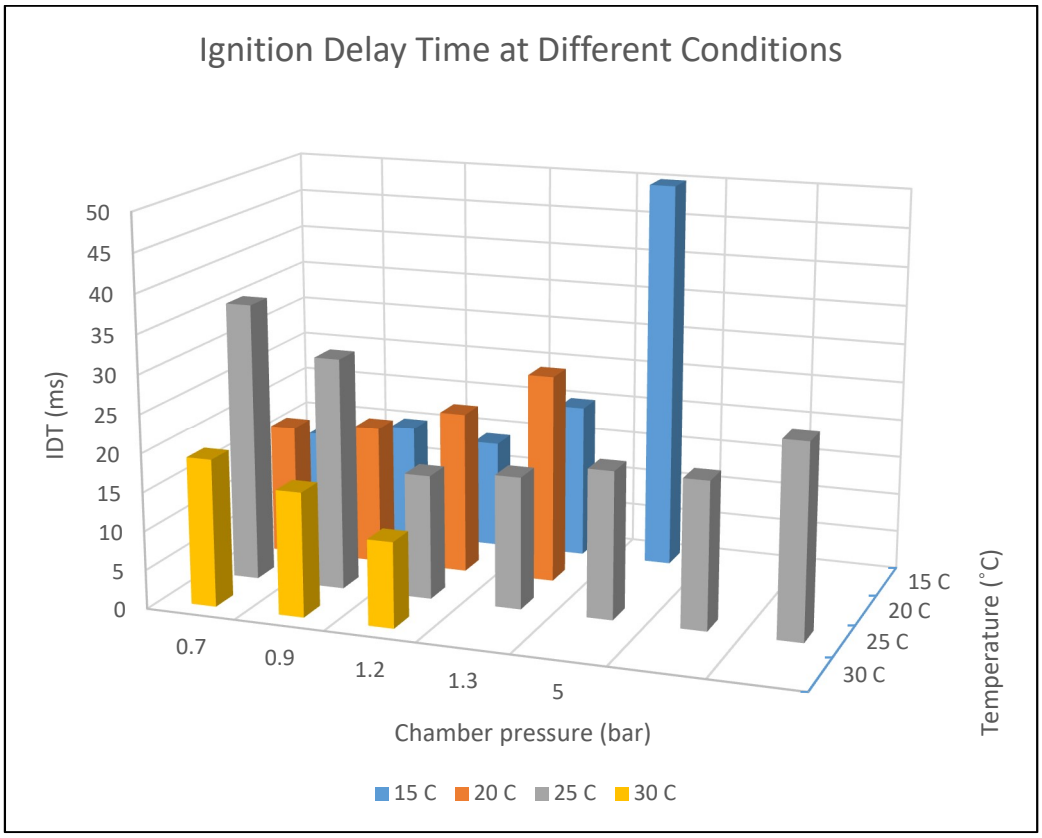

Figure 5.14 Comparison of ignition delay times of fuel and oxidizer drop test at different temperature and chamber pressure conditions

In the issue of ignition time delay, there are two phenomena leap to the eye. First of them is related to the vapor pressure of the liquids, in other words, the ease of the evaporation of the fluids at low pressures. The second one is the ease of mixing of liquids that the ease of breaking the surface tension barrier at relatively high pressures.

The experimental data exhibits an increasing trend of ignition delay time with increasing pressure conditions at low temperatures, i.e. in the 15 – 20 ˚C temperature

interval. On the contrary, the ignition delay time shows a decreasing trend with increasing pressure values at relatively high pressures, i.e. in the temperature interval of 25 – 30 ˚C.

When the interest is concentrated on the data at 25 ˚C, it can be said that there is some point where these two phenomena are equally dominant on the ignition delay time. Because the data gives a curvature at 25 ˚C. Furthermore, while ignition delay time decreases with increasing chamber pressure at temperatures less than 25 ˚C, it seems to be decreasing with increasing chamber pressure at temperatures greater than 25 ˚C.

According to Rice (1947), due to the gas adsorption on the liquid surface, the increase in pressure decreases the surface tension of the liquid (Rice, 1947). It is because of that the gas molecules penetrate into the liquid surface and interfere with the cohesive forces on the liquid surface. Therefore, it can be explained to observe a decrease in ignition delay time at relatively higher temperatures as pressure increases, i.e. in the case of IDT experiments at 25 – 30 ˚C. The other feature to have smaller ignition delay time at these relatively high temperatures is the larger vapor pressures of the liquids. At higher temperatures, the vapor pressure of the liquids gets higher and facilitates the breakage of the cohesive forces on the liquid surface. Consequently, relatively high vapor pressures facilitates the transformation to gas phase and gas phase mixing; thus, facilitates the initial gas phase reactions. According to Pourpoint and Anderson (2005), for combustible materials, initial ambient pressure has an important effect on their ignition delay times. When increasing the chamber pressure, a small decrease is observed in ignition delay time (Pourpoint & Anderson, 2005).

From the Figure 5.14, it can be seen that the ignition delay time increases with increasing pressure. This could be a result of that the increasing pressure exerts force onto the liquid surface, which is larger than the kinetic energies of the molecules at that temperature. Since the molecular kinetic energy is the phenomenon behind the vapor pressure which is essential for the phase change from liquid to gas, for the

relatively smaller temperature cases it can be said that the surface tension dominates the vapor pressure. Therefore, the phase change would be larger and would cause longer ignition delay times. According to Warren (1958), the low initial pressure may affect the ignition and may change the liquid phase reactions, thus may prevent gas phase reactions (Warren, 1958).

According to Pourpoint and Anderson (2005), the experiments on ignition delay time of hydrogen peroxide with a mixture of methanol, manganese dioxide, acetic acid and water showed an inversely proportional pressure dependence of ignition delay time. Then for hypergolic liquids, it was claimed that the ignition delay time is inversely proportional to the logarithm of the pressure (Pourpoint & Anderson, 2005).

5.6 Comparison of Methods Used for Excess Mixture Enthalpy Estimation

In the scope of this work, in order to explore the thermodynamic and kinetic interactions of the fuel – oxidizer system, activity coefficients and the excess mixing enthalpy were studied and modeled for the nitric acid – water and fuel – oxidizer binary systems. Since there were not sufficient experimental data and available parameters, the methods presented theoretical calculations for the excess mixing enthalpy except direct mixing for the nitric acid – water system. For all of the methods the regular solution theory was the initial assumption.

van Laar theory, gave an opportunity to calculate the activity coefficients and excess molar Gibbs free energy for a whole range of mixture composition using only the azeotrope point and the vapor pressure data of components. Using van Laar theory with azeotrope point data gave the maximum heat release at the water rich region of the mixture of the composition $x_{HNO_3} = 0.40$.

UNIFAC group contribution activity coefficients model was also another way to estimate both activity coefficients and excess molar Gibbs free energy of the nitric acid – water and fuel – oxidizer system. The missing functional group interaction param-

eters were also calculated by CI-index method. The resulting UNIFAC model facilitated to obtain excess molar Gibbs energy for a whole composition range for both two systems. In the nitric acid – water system, on the contrary to van Laar azeotrope method, with UNIFAC, the minimum excess molar Gibbs energy was obtained in the water rich region of the mixture of composition $x_{HNO_3} = 0.30$. Similarly, the interaction thermodynamics data from quantum chemical methods showed the minimum excess molar Gibbs free energy at the water rich region of the mixture of composition $x_{HNO_3} = 0.11$. The experimental heat of mixing data yielded the maximum heat release at the water rich region of composition $x_{HNO_3} = 0.29$. In the results section, the experimental heat of mixing data and DFT complexation energy data were compared in J/mol-HNO_3 basis and showed very similar trends even though the difference in magnitude. Similarly, the excess molar Gibbs free energies obtained from estimation methods, van Laar and UNIFAC, were also compared graphically in Figure 5.15 below.

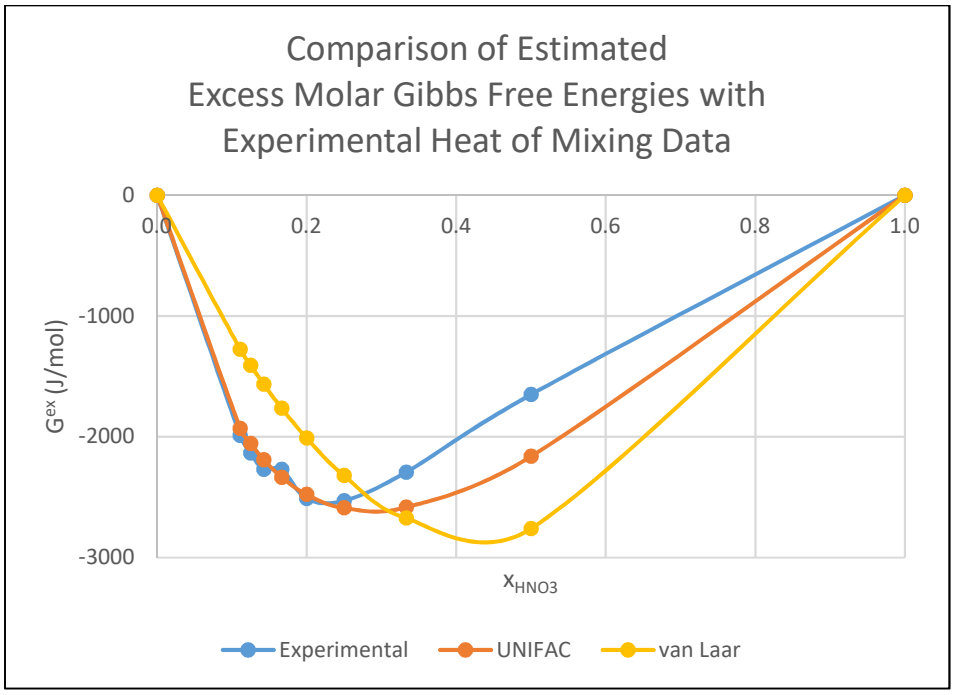

Figure 5.15 Comparative plot of excess molar Gibbs free energies of four different methods.

Pearson correlation coefficient is used to test the linear association between two variables, in other words it tests how two separate data is related to each other. This method was used for the results of these four prediction models for the same composition interval. The excess molar Gibbs free energies were tested as pairs. When the correlation coefficient is 1, that means the two data are linearly related to each other; thus, they are said to be perfectly correlated. When it is -1, then the data are perfectly negatively correlated, that is they seem to be very poorly related. When these four methods are compared utilizing Pearson correlation method, the resulting correlation coefficients shows how these data for the same composition interval are related to each other. The correlation coefficients are given in Table 5.13.

.

Table 5.13 Pearson correlation coefficients for four different model results for excess molar Gibbs free energy

	Experimental	**UNIFAC**	**DFT**	**van Laar**
Experimental	1.00	0.97	0.55	0.82
UNIFAC	0.97	1.00	0.53	0.91
DFT	0.55	0.53	1.00	0.27
van Laar	0.82	0.91	0.27	1.00

From Table 5.13, it can be inferred that among all four methods, the experimental heat of mixing data and UNIFAC model excess molar Gibbs free energy data are reasonably related to each other with a PCC (Pearson Correlation Coefficient) of 0.97. Similarly, van Laar excess Molar Gibbs free energy data are highly correlated to both UNIFAC model excess molar Gibbs free energy data and experimental heat of mixing data by PCC's of 0.91 and 0.82 respectively.

For the fuel – oxidizer system, UNIFAC model showed the minimum excess molar Gibbs free energy at the oxidizer rich region of the mixture of composition $x_{fuel} = 0.31$. Similarly, the quantum chemical interaction data also showed the minimum excess molar Gibbs free energy at the oxidizer rich region of the composition $x_{fuel} = 0.11$. which is also a coincidence with the stoichiometric fuel/oxidizer ratio of $x_{fuel} \cong 0.12$ for complete combustion. When the Pearson correlation test is done for UNIFAC and DFT results, the data showed a PCC of 0.55.

CONCLUSIONS

This work has shown mainly the effect of composition on excess mixture enthalpy of the thermodynamic system of nitric acid and water as the model system for hypergolic fuel and oxidizer, which is directly related to the vapor-liquid equilibrium and ignition delay time. Calorimetry experiments and DFT calculations were done to obtain the heat of mixing data for binary systems. This work has also shown that, satisfying heat of mixing data can be collected even with a very simply constructed calorimeter system. In addition, heat of mixing of these binary systems were estimated by using van Laar and UNIFAC models. For all of the methods, the regular solution theory was the initial assumption.

Two different liquid mixtures were explored for the excess mixing enthalpies as a function of composition. For nitric acid – water system, the experimental heat of mixing and DFT complexation energy data exhibited very good relation with each other, although the difference in magnitude is almost 8 times. The possible causes for this difference is still being investigated. For the estimations, UNIFAC activity coefficient model and van Laar theory have very good relations with each other and the experimental heat of mixing data and showed that the maximum heat release is observed at the water rich region of the mixture of composition around $x_{HNO_3} = 0.29 - 0.30$ and $x_{HNO_3} = 0.40$ respectively. At the end, experimental heat of mixing, DFT binding energy and heat of mixing estimations by UNIFAC and van Laar show a very good coherence.

For the fuel – oxidizer system, both UNIFAC and DFT results showed that the minimum excess Gibbs free energy is observed at the oxidizer rich region of the mixture. The composition at which DFT gives the minimum excess Gibbs free energy also coincides with the molar composition at which the stoichiometric ratio is satisfied

for the complete combustion. The aim of the study was to make predictions consistent with the DFT results. The resemblance of the DFT results with estimation models has supported the objective.

This study constructed a very good algorithm to estimate heat of mixing in relation with vapor-liquid equilibrium to determine the effective parameters on ignition delay time of different possible hypergolic propellant couples. At the end, this study brought the unpredictable mixing behavior of liquids giving spontaneous reactions to a possibly predictable point by offering an applicable route of calculations.

RECOMMENDATIONS

Firstly, a more reliable and robust calorimetry system is required to do the heat of mixing experiments for less heat loss; therefore, a more accurate data and better relations of methods. Heat loses might be misleading for the estimations of heats of mixing and ignition delay time.

The selected binary activity coefficient model, UNIFAC, is a very good VLE estimation tool for the non-polar and non-electrolyte systems. In this work, it was utilized for a strong electrolyte solution, too. In the literature, in order to work with electrolyte solutions, there are modifications of UNIFAC and UNIQUAC models called LIFAC and LIQUAC. These group contribution models can be used to predict the vapor – liquid equilibria, mean ionic coefficients and osmotic coefficients for aqueous solutions of strong electrolytes even with high concentrations. These models are widely used for several industrial applications with systems including salt solutions such as extraction processes, salt crystallization, coal gasification and petroleum refining (Kiepe, Noll, & Gmehling, 2006). Therefore, with offering model parameters and interaction parameters for ions, it might be a more developed solution to estimate the excess enthalpy and vapor – liquid equilibria for the nitric acid – water and fuel – oxidizer systems for future works.

In order to estimate the excess Gibbs free energy, a quantum chemical method, DFT, was also used to predict the interaction energies of the complexes that were the atomic scale representations of the mixtures. In order to estimate the equilibrium thermodynamic properties in a better way and more accurate, another quantum chemical method called COSMO-RS (Conductor like Screening Model for Real Solvents) can be utilized. Both of the methods belong to dielectric continuum models class. COSMO-RS is an equilibrium thermodynamics method to predict chemical potential, μ, in liquids, which is directly related to the excess molar Gibbs free energy by definition. The calculated chemical potentials provides calculations for the other

required properties of thermodynamic equilibrium such as activity coefficients, vapor pressure, solvation energy and solubility. COSMO-RS has been used to estimate activity coefficients of binary ionic liquid-neutral solvent mixtures and neutral compounds in ionic liquids with very satisfying qualitative and quantitative results (Diedenhofen & Klamt, 2010). The energy calculations in COSMO-RS includes hydrogen bonding, dispersion and electrostatic interactions. Therefore, it might be a better tool to give more accurate interaction energies for the liquids in the mixture. Hence, it might give an opportunity to estimate more accurate excess mixing energies.

Among the recommendations for future work in doing more reliable experiments, modeling and maximizing the excess mixture enthalpy; thus, minimizing of the ignition delay time are:

- Detailed investigation of the effect of temperature on ignition delay time
- Detailed investigation of the effect of pressure
- Design and use of ideal calorimetry systems as possible
- Design of an experimental setup which will enable to collect experimental mixing data and VLE data for the fuel and oxidizer mixture
- New sets of ignition delay time measurements using Impinging Jets Reactor test setup. The new test setup is an example of impinging test technique as explained before. This experimental setup is now being constructed. In principle, it is designed to capture the ignition time like in the case of drop test technique. Besides, our test setup has some other useful features. It is composed of a glass windowed stainless steel reactor body, four thermocouple inserting ports to measure temperature from different coordinates of the combustion region, four gas sampling ports and sample tubes to collect combustion gases from different coordinates of the combustion region in order to analyze the combustion products changing with combustion zone length. The uncompleted setup of the impinging jets reactor that will be used in future studies is given in Figure 7.1 below.

Figure 7.1 The Impinging jets reactor experimental setup

In addition to experimental methods and thermodynamic models, some modifications on quantum chemical methods can also be done. As stated before, since assumes molecules at static conditions. In future works, dynamic methods can be used to simulate interactions between molecules and compared with DFT results in order to check the consistency of data.

REFERENCES

Atkins, P., & de Paula, J. (2006). *Atkins' Physical Chemistry.* W.H. Freeman & Co.

Bennett, G. W. (1929). A Laboratory Experiment on the Boiling Point Curves of Non-azeotropic Binary Mixtures. *Journal of Chemical Education*, 6(9), 1544.

Black, A. T., Drolet, M. P., & Pourpoint, T. L. (2018). Early Liquid and Gas Phase Hypergolic Reactions between. *Combustion Science and Technology, 191(11)*, 1990-2005.

Blevins, J., Gostowski, R., & Chianese, S. (2004). An Experimental Investigation of Hypergolic Ignition Delay of Hydrogen Peroxide with Fuel Mixtures. *American Institute of Aeroneutics and Astronautics*.

Bretonnet, J. L. (2017). Basics of the density functional theory. *AIMS Materials Science, 4*(6), 1372-1405.

Britannica, T. E. (1998). *Britannica*. Retrieved from https://www.britannica.com/science/propellant/additional-info#history

Carreón-Calderón, B., Uribe-Vargas, V., & Aguayo, J. P. (2020). *Thermophysical Properties of Heavy Petroleum Fluids.* Cham: Springer International Publishing AG.

Chapra, S. C., & Canale, R. P. (2006). *Numerical Methods for Engineers, 6th ed.* New York: McGraw-Hill.

Davis, S. M., & Yılmaz, N. (2014). *Advances in Hypergolic Propellants: Ignition, Hydrazine, and Hydrogen Peroxide Research.* Socorro: Hindawi Publishing Corporation.

Dennis, J. D., Son, S. F., & Pourpoint, T. L. (2012). *Critical Ignition Criteria for Monomethylhydrazine and Red Fuming Nitric Acid in an Impinging Jet Apparatus.* Atlanta: American Institute of Aeronautics and Astronautics.

Diedenhofen, M., & Klamt, A. (2010). COSMO-RS as a tool for property prediction of IL mixtures—A review. *Fluid Phase Equilibria*, 31-38.

Dortmund Data Bank. Parameters of the original UNIFAC model. Retriewed from:

http://www.ddbst.com/published-parameters-unifac.html

Duisman, J. A., & Stern, S. A. (1969). Vapor pressure and boiling point of pure nitric acid. *Journal of Chemical and Engineering Data*, 457-459.

Fredenslund, A., Jones, R., & Praustnitz, J. (1975). Group-contribution estimation of activity coefficients in nonideal liquid mixtures. *AIChE Journal, 21(6)*, 1086-1099.

Gani, R., Harper, P., & Hostrup, M. (2005). Automatic creation of missing groups through connectivity index for pure-component property prediction. *Industrial & Engineering Chemistry Research, 44(18)*, 7262-726.

Gmehling, J., Rasmussen, P., & Fredenslund, A. (1982). Gmehling, J., Rasmussen, P., & Fredenslund, A. (1982). Vapor-liquid equilibriums by UNIFAC group contribution. Revision and extension. 2. *Industrial & Engineering Chemistry Process Design and Development*, 118-127.

Gonzalez, H., Abildskov, J., Gani, R., Rousseaux, P., & Le Bert, B. (2007). A method for prediction of UNIFAC group interaction parameters. *AIChE journal, 53(6)*, 1620-1632.

Gosh, S., Verma, P., Cramer, C. J., Gagliardi, L., & Truhlar, D. G. (2018). Combinig Wave Function Methods with Density Functional Theory for Excited States. *Chemical Reviews*, 7249-7292.

Holtzmann, R. (1969). *Chemical Rockets.* New York: Marcel Dekker.

ILO. (2009, November). Retrieved from International Labor Organization: http://www.ilo.org/dyn/icsc/showcard.display?p_lang=en&p_card_id=0281&p_version=1

Incropera, F. P., Lavine, A. S., Bergman, T. L., & Dewitt, D. P. (2011). *Fundamentals of Heat and Mass Transfer, 7th ed.* Hoboken: John Wiley & Sons.

Izato, Y. I., Shiota, K., & Miyake, A. (2021). A detailed mechanism for the initial hypergolic reaction in liquid hydrazine/nitrogen tetroxide mixtures based on quantum chemistry calculations. *Combustion and Flame*, 111389.

Kiepe, J., Noll, O., & Gmehling, J. (2006). Modified LIQUAC and Modified LIFACsA Further Development of Electrolyte Models for the Reliable Prediction of Phase Equilibria with Strong Electrolytes. *Industrial & Engineering Chemistry Research*, 2361-2373.

Kier, L. B., & Hall, H. L. (1986). *Molecular Connectivity in Structure Acivity Analysis.* New York: John Wiley & Sons.

Kilpatrick, M., & Baker Jr., L. L. (1955). A study of fast reactions in fuel-oxidant systems: Anhydrous hydrazine with 100 per cent nitric acid. *Symposium (International) on Combustion*, 196-205.

Lai, K. Y., Zhu, R., & Lin, M. C. (2012). Why mixtures of hydrazine and dinitrogen tetroxide are hypergolic? *Chemical Physics Letters*, 33-37.

Larsen, B. L., Rasmussen, P., & Fredenslund, A. (1987). A modified UNIFAC group-contribution model for prediction of phase equilibria and heats of mixing. *Industrial & Engineering Chemistry Research*, 2274-2286.

Li, S., Qian, W., Haoyang, L., Guijun, L., & Zhu, M. (2021). Autoignition and flame lift-off behavior of a fuel jet mixing with turbulent hot air coflow. *Proceedings of the Combustion Institute*, 6385-6392.

Lide, D. R. (2004). *CRC handbook of chemistry and physics.* Boca Raton: CRC Press.

Lide, D. R. (2007). *CRC Handbook of Chemistry and Physics 88TH Edition.* Boca Raton: CRC Press, Taylor & Francis.

Liu, W. G., Dashgupta, S., Zybin, S. V., & Goddard, W. A. (2011). First Principles Study of the Ignition Mechanism for Hypergolic Bipropellants: N,N,N',N'-Tetramethylethylenediamine (TMEDA) and N,N,N',N'-Tetramethylmethylenediamine (TMMDA) with Nitric Acid. *The Journal of Physical Chemistry,115(20)*, 5221-5229.

Matheswaran, M., Kwon, T. O., Kim, J. W., & Moon, I. S. (2007). Factors Affecting Flux and Water Separation Performance in Air Gap Membrane Distillation. *Journal of Industrial and Engineering Chemistry*, 965-970.

Mays, L. O., Farmer, M. J., & Smith, J. E. (2010). A Laser DiagnosticTechnique to Measure Chemical DelayTime in Hypergolic Combustion. *Combustion Science and Technology, 134:1-6*, 127-138.

Modell, M., & Reid, R. C. (1974). *Thermodynamics and Its Applications.* London: Prentice-Hall.

NA. (n.d.). *Parameters of the Original UNIFAC Model*. Retrieved from Dortmund Data Bank: http://www.ddbst.com/published-parameters-unifac.html

Naidja, A., Krishna, C. R., Butcher, T., & Mahajan, D. (2002). *Oxidation of Fuels in the Cool Flame Regime for Combustion and Reforming for Fuel Cells (No. BNL-69349).* Upton, New York: Brookhaven National Lab.

NIST. (n.d.). NIST Webbook.

Nolan, D. P. (2014). *Handbook of Fire and Explosion Protection Engineering Principles: for Oil, Gas,Chemical and Related Facilities, 3rd Ed.* William Andrew.

Pourpoint, T., & Anderson, W. (2005). Environmental Effects on Hypergolic Ignition. *41st AIAA/ASME/SAE/ASEE Joint Propulsion Conference & Exhibit.* Tucson, Arizona: American Institute of Aeronautics and Astronautics.

Prausnitz, J. (1958). Regular Solution Theory for Gas-Liquid Solutions. *AIChE Journal, 4(3)*, 269-272.

Raatikainen, T., & Laaksonen, A. (2005). Application of several activity coefficient models to water-organic-electrolyte aerosols of atmospheric interest. *Atmospheric Chemistry and Physics, 5*(9), 2475-2495.

Rice, O. K. (1947). The Effect of Pressure on Surface Tension. *The Journal Of Chemical Physics*, 333-335.

Sandler, S. I. (2006). *Chemical, Biological and Engineering Thermodynamics.* John Wiley & Sons Inc.

Sangiovanni, J. J., & Kesten, A. S. (1977). A Theoretical and Experimental Investigation of the Ignition of Fuel Droplets. *Combustion Science and Technology*, 59-70.

Sardeshmukh, V., Heister, S., Wang, H., & Sankaran, V. (2013). Kinetics Modeling of Hypergolic Propellants. *49th AIAA/ASME/SAE/ASEE Joint Propulsion Conference.* San Jose, CA: American Institute of Aeronautics and Astronautics.

Sasahira, A., Hoshikawa, T., Nakamura, T., Fukasawa, T., & Kawamura, F. (1994). Activities of Water and Nitric Acid in Simulated Reprocessing Waste Solutions. *Journal of Science and Technology*, 321-328.

Simon, J., & McQuarrie, D. (1997). *Physical Chemistry: A Molecular Approach.* University Science Books.

Singh, R. P., & Pathanjali, G. A. (1987). UNIFAC Interaction Parameters for Excess Enthalpies of Mixing. *Thermochimica Acta*, 267-274.

Skjold-Jorgensen, S., Kolbe, B., Gmehling, J., & Rasmussen, P. (1979). Vapor-Liquid Equilibria by UNIFAC Group Contribution. Revision and Extension. *Industrial & Engineering Chemistry Process Design and Developement*, 714-722.

Sutton, G. P., & Biblarz, O. (2016). *Rocket propulsion elements.* New York: John Wiley & Sons.

Takano, Y., & Houk, K. N. (2005). Benchmarking the conductor-like polarizable continuum model (CPCM) for aqueous solvation free energies of neutral and ionic organic molecules. *Journal of Chemical Theory and Computation*, 70-77.

Thiemann, M., Scheibler, E., & Wiegand, K. W. (2000). *Ullmann's Encyclopedia of Industrial Chemistry: Nitric acid, nitrous acid, and nitrogen oxides.* Wiley.

Thomas, A., & Cantwell, B. (2017). Hypergolic Ionic Liquids: Ignition with 70% Nitric Acid at Various Pressures. *American Institute of Aeronautics and Astronautics.* Atlanta, GA: American Institute of Aeronautics and Astronautics.

Tosun, İ. (2012). *Thermodynamics of Phase and Reaction Equilibria.* Elsevier.

Turns, S. (2000). *An Introduction to Combustion: Concepts and Applications.* Boston: McGraw-Hill.

Wadhwani, P., & Saha, P. (2021). *Rocket Propulsion Market Size, Global Forecast Report 2027.* Global Market Insights.

Warren, F. A. (1958). *Rocket Propellants.* Reihold Publishing Corporation.

Zarbo, N., Belal, H., & Pourpoint, T. (2015). Effect of Water and Humidity on Hypergolic Propellant. *51st AIAA/SAE/ASEE Joint Propulsion Conference, Propulsion and Energy Forum.* American Institute of Aeronautics and Astronautics.

APPENDICES

A. An Example Calculation for HNO_3 – H_2O System with UNIFAC including a_{mn} Calculations

Functional Groups CI-Interaction Parameters (i-j):

$b_{CC} := 977,87$ $c_{CC} := -108,11$ $d_{CC} := 104,61$ $e_{CC} := -109,42$

$b_{CO} := -1134,83$ $c_{CO} := -17,44$ $d_{CO} := 45,25$ $e_{CO} := 61,83$

$b_{CN} := 20,04$ $c_{CN} := 9,94$ $d_{CN} := 47,79$ $e_{CN} := -6,45$

$b_{NC} := 45,41$ $c_{NC} := -32,91$ $d_{NC} := 333,83$ $e_{NC} := 108,41$

$b_{NN} := 43,47$ $c_{NN} := -38,85$ $d_{NN} := 327,89$ $e_{NN} := 83,23$

$b_{NO} := 1,83$ $c_{NO} := 11,81$ $d_{NO} := 6,27$ $e_{NO} := 30,51$

$b_{OC} := -11028,5$ $c_{OC} := -3913,23$ $d_{OC} := -633,11$ $e_{OC} := 2128,63$

$b_{ON} := 0$ $c_{ON} := 10,82$ $d_{ON} := 47,79$ $e_{ON} := -2,8$

$b_{OO} := 11347,17$ $c_{OO} := 14250,92$ $d_{OO} := 329,24$ $e_{OO} := -2150,65$

Functional Group CI-Interaction Parameters (j-i):

$bi_{CC} := -145,02$ $ci_{CC} := -208,54$ $di_{CC} := 321,40$ $ei_{CC} := 261,28$

$bi_{CO} := 401,21$ $ci_{CO} := 358,76$ $di_{CO} := -69,53$ $ei_{CO} := 66,83$

$bi_{CN} := -52,78$ $ci_{CN} := -117,17$ $di_{CN} := -212,21$ $ei_{CN} := 20,01$

$bi_{NC} := 194,75$ $ci_{NC} := 450,73$ $di_{NC} := -251,60$ $ei_{NC} := -283,58$

$bi_{NN} := -4,63$ $ci_{NN} := -69,02$ $di_{NN} := -65,09$ $ei_{NN} := 20,0$

$bi_{NO} := -395,38$ $ci_{NO} := -91,91$ $di_{NO} := 27,47$ $ei_{NO} := -283,66$

$bi_{OC} := 63,32$ $ci_{OC} := -34,0$ $di_{OC} := 195,52$ $ei_{OC} := -30,87$

$bi_{ON} := -1,121$ $ci_{ON} := 2,27$ $di_{ON} := -3,85$ $ei_{ON} := 18,62$

$bi_{OO} := -515,78$ $ci_{OO} := -472,59$ $di_{OO} := 1026,39$ $ei_{OO} := -398,08$

Conditions

$T := 293\,K$
$P := 1\ bar$
$x1 := 0,3$
$x2 := 1 - x1 = 0,7$

Surface Area and Volume Parameters

$R_{HNO3} := 1,64$ $R_{H2O} := 0,92$

$Q_{HNO3} := 1,6$ $Q_{H2O} := 1,4$

Fractions of Functional Groups

$u1_{H2O} := 1$ $u1_{HNO3} := 0$

$u2_{H2O} := 0$ $u2_{HNO3} := 1$

for HNO3 (N):

$Z_{NN} := 7 \quad Z_{NO1} := 8 \quad Z_{NO2} := 8 \quad Z_{NO3} := 8$

$ZV_{NN} := 5 \quad ZV_{NO1} := 6 \quad ZV_{NO2} := 6 \quad ZV_{NO3} := 6$

$NH_{NN} := 0 \quad NH_{NO1} := 0 \quad NH_{NO2} := 1 \quad NH_{NO3} := 0$

$$\delta_{NN} := \frac{ZV_{NN} - NH_{NN}}{Z_{NN} - ZV_{NN} - 1} = 5 \qquad \delta_{NO2} := \frac{ZV_{NO2} - NH_{NO2}}{Z_{NO2} - ZV_{NO2} - 1} = 5$$

$$\delta_{NO1} := \frac{ZV_{NO1} - NH_{NO1}}{Z_{NO1} - ZV_{NO1} - 1} = 6 \qquad \delta_{NO3} := \frac{ZV_{NO3} - NH_{NO3}}{Z_{NO3} - ZV_{NO3} - 1} = 6$$

$\beta_{Na} := \delta_{NN} \cdot \delta_{NO1} = 30 \qquad \beta_{Nb} := \delta_{NN} \cdot \delta_{NO2} = 25 \qquad \beta_{Nc} := \delta_{NN} \cdot \delta_{NO3} = 30$

$\varepsilon_N := \beta_{Na} \cdot \beta_{Nb} \cdot \beta_{Nc} = 22500$

$$\chi 0_N := \frac{1}{\sqrt{\delta_{NN}}} + \frac{1}{\sqrt{\delta_{NO1}}} + \frac{1}{\sqrt{\delta_{NO2}}} + \frac{1}{\sqrt{\delta_{NO3}}} = 1,7109$$

$$\chi 1_N := \frac{1}{\sqrt{\beta_{Na}}} + \frac{1}{\sqrt{\beta_{Nb}}} + \frac{1}{\sqrt{\beta_{Nc}}} = 0,5651$$

$$\chi 2_N := \frac{1}{\sqrt{\varepsilon_N}} = 0,0067$$

for H2O (W):

$Z_{WO} := 8$

$ZV_{WO} := 6$

$NH_{WO} := 2$

$$\delta_{WO} := \frac{ZV_{WO} - NH_{WO}}{Z_{WO} - ZV_{WO} - 1} = 4$$

$\beta_W := \delta_{WO} = 4$

$\varepsilon_W := \beta_W = 4$

$$\chi 0_W := \frac{1}{\sqrt{\delta_{WO}}} = 0,5$$

$$\chi 1_W := \frac{1}{\sqrt{\beta_W}} = 0,5$$

$$\chi 2_W := \frac{1}{\sqrt{\varepsilon_W}} = 0,5$$

CI Interaction Coefficients, amn

H2O : $nN_W := 0$ $nO_W := 1$

HNO3 : $nC_N := 0$ $nN_N := 1$ $nH_N := 1$ $nO_N := 3$

Interactions, HNO3 - H2O:

$$A0NO_{NW} := \frac{nN_N}{\chi 0_N} - \frac{nO_W}{\chi 0_W} = -1,4155 \qquad A0OO_{NW} := \frac{nO_N}{\chi 0_N} - \frac{nO_W}{\chi 0_W} = -0,042$$

$$A1NO_{NW} := \frac{nN_N}{\chi 0_N} - \frac{nO_W}{\chi 1_W} = -1,4155 \qquad A1OO_{NW} := \frac{nO_N}{\chi 0_N} - \frac{nO_W}{\chi 1_W} = -0,042$$

$$A2NO_{NW} := \frac{nN_N}{\chi 1_N} - \frac{nO_W}{\chi 1_W} = -0,2306 \qquad A2OO_{NW} := \frac{nO_N}{\chi 1_N} - \frac{nO_W}{\chi 1_W} = 3,9276$$

$$A3NO_{NW} := \frac{nN_N}{\chi 0_N} - \frac{nO_W}{\chi 2_W} = -1,4155 \qquad A3OO_{NW} := \frac{nO_N}{\chi 0_N} - \frac{nO_W}{\chi 2_W} = -0,042$$

Interactions, H2O - HNO3:

$$A0ON_{WN} := \frac{nO_W}{\chi 0_W} - \frac{nN_N}{\chi 0_N} = 1,4155 \qquad A0OO_{WN} := \frac{nO_W}{\chi 0_W} - \frac{nO_N}{\chi 0_N} = 0,042$$

$$A1ON_{WN} := \frac{nO_W}{\chi 0_W} - \frac{nN_N}{\chi 1_N} = 0,2306 \qquad A1OO_{WN} := \frac{nO_W}{\chi 0_W} - \frac{nO_N}{\chi 1_N} = -3,9276$$

$$A2ON_{WN} := \frac{nO_W}{\chi 1_W} - \frac{nN_N}{\chi 1_N} = 0,2306 \qquad A2OO_{WN} := \frac{nO_W}{\chi 1_W} - \frac{nO_N}{\chi 1_N} = -3,9276$$

$$A3ON_{WN} := \frac{nO_W}{\chi 0_W} - \frac{nN_N}{\chi 2_N} = -148 \qquad A3OO_{WN} := \frac{nO_W}{\chi 0_W} - \frac{nO_N}{\chi 2_N} = -500,5$$

$$aNO_{NW} := b_{NO} \cdot A0NO_{NW} = -2,5904$$

$$aOO_{NW} := b_{OO} \cdot A0OO_{NW} = -476,5065$$

$$a_{NW} := aNO_{NW} + aOO_{NW} = -479,0969$$

$$aON_{WN} := bi_{ON} \cdot A0ON_{WN} = -1,5868$$

$$aOO_{WN} := bi_{OO} \cdot A0OO_{WN} = -21,6594$$

$$a_{WN} := aON_{WN} + aOO_{WN} = -23,2462$$

$a_{11} := 0$ $a_{12} := a_{WN} = -23,2462$

$a_{21} := a_{NW} = -479,0969$ $a_{22} := 0$

Combinatorial Activity Coefficient:

$r1 := \upsilon 1_{H2O} \cdot R_{H2O} = 0,92 \quad r2 := R_{HNO3} \cdot \upsilon 2_{HNO3} = 1,64$

$q1 := \upsilon 1_{H2O} \cdot Q_{H2O} = 1,4 \quad q2 := Q_{HNO3} \cdot \upsilon 2_{HNO3} = 1,6$

$\Phi 1 := \frac{r1 \cdot x1}{r1 \cdot x1 + r2 \cdot x2} = 0,1938 \qquad \Phi 2 := \frac{r2 \cdot x2}{r1 \cdot x1 + r2 \cdot x2} = 0,8062$

$\Theta 1 := \frac{q1 \cdot x1}{q1 \cdot x1 + q2 \cdot x2} = 0,2727 \qquad \Theta 2 := \frac{q2 \cdot x2}{q1 \cdot x1 + q2 \cdot x2} = 0,7273$

$I1 := 1 - r1 + 5 \cdot (r1 - q1) = -2,32$

$I2 := 1 - r2 + 5 \cdot (r2 - q2) = -0,44$

$\gamma 1_C := \exp\left(\ln\left(\frac{\Phi 1}{x1}\right) + 5 \cdot q1 \cdot \ln\left(\frac{\Theta 1}{\Phi 1}\right) + I1 - \frac{\Phi 1}{x1} \cdot (x1 \cdot I1 + x2 \cdot I2)\right) = 1,3266$

$\gamma 2_C := \exp\left(\ln\left(\frac{\Phi 2}{x2}\right) + 5 \cdot q2 \cdot \ln\left(\frac{\Theta 2}{\Phi 2}\right) + I2 - \frac{\Phi 2}{x2} \cdot (x1 \cdot I1 + x2 \cdot I2)\right) = 1,034$

Residual Activity Coefficients:

$Q_1 := Q_{H2O} = 1,4 \qquad Q_2 := Q_{HNO3} = 1,6$

$R_1 := R_{H2O} = 0,92 \qquad R_2 := R_{HNO3} = 1,64$

$X_1 := \frac{\upsilon 1_{H2O} \cdot x1}{\upsilon 1_{H2O} \cdot x1 + \upsilon 2_{H2O} \cdot x2} = 1 \qquad X_2 := \frac{\upsilon 2_{HNO3} \cdot x2}{\upsilon 1_{HNO3} \cdot x1 + \upsilon 2_{HNO3} \cdot x2} = 1$

$\Theta_1 := \frac{Q_1 \cdot X_1}{Q_1 \cdot X_1 + Q_2 \cdot X_2} = 0,4667 \qquad \Theta_2 := \frac{Q_2 \cdot X_2}{Q_1 \cdot X_1 + Q_2 \cdot X_2} = 0,5333$

$\Psi_{11} := \exp\left(-\frac{a_{11}}{T}\right) = 1 \qquad \Psi_{22} := \exp\left(-\frac{a_{22}}{T}\right) = 1$

$\Psi_{12} := \exp\left(-\frac{a_{12}}{T}\right) = 1,0826 \qquad \Psi_{21} := \exp\left(-\frac{a_{21}}{T}\right) = 5,1302$

$$\Gamma_1 := \exp\left(Q_1 \cdot \left(1 - \ln\left(\Theta_1 \cdot \Psi_{11} + \Theta_2 \cdot \Psi_{21}\right) - \left(\frac{\Theta_1 \cdot \Psi_{11}}{\Theta_1 \cdot \Psi_{11} + \Theta_2 \cdot \Psi_{21}} + \frac{\Theta_2 \cdot \Psi_{12}}{\Theta_1 \cdot \Psi_{12} + \Theta_2 \cdot \Psi_{22}}\right)\right)\right) = 0,2976$$

$$\Gamma_2 := \exp\left(Q_2 \cdot \left(1 - \ln\left(\Theta_1 \cdot \Psi_{12} + \Theta_2 \cdot \Psi_{22}\right) - \left(\frac{\Theta_2 \cdot \Psi_{22}}{\Theta_2 \cdot \Psi_{22} + \Theta_1 \cdot \Psi_{12}} + \frac{\Theta_1 \cdot \Psi_{12}}{\Theta_2 \cdot \Psi_{21} + \Theta_1 \cdot \Psi_{12}}\right)\right)\right) = 1,5975$$

Since only main groups exist in both HNO3 and H2O;

$\Gamma 1_1 := 1 \quad \Gamma 1_2 := 1$

$$\gamma 1_R := \exp\left(\upsilon 1_{H2O} \cdot \left(\ln\left(\Gamma_1\right) - \ln\left(\Gamma 1_1\right)\right)\right) = 0,2976$$

$$\gamma 2_R := \exp\left(\upsilon 2_{HNO3} \cdot \left(\ln\left(\Gamma_2\right) - \ln\left(\Gamma 1_2\right)\right)\right) = 1,5975$$

$$\gamma_1 := \exp\left(\ln\left(\gamma 1_C\right) + \ln\left(\gamma 1_R\right)\right) = 0,3948$$

$$\gamma_2 := \exp\left(\ln\left(\gamma 2_C\right) + \ln\left(\gamma 2_R\right)\right) = 1,6519$$

Gibbs-Duhem Equation for consistency check:

$$x_1 \cdot \frac{d}{d\, x_1} \ln\left(\gamma_1\right) + x_2 \cdot \frac{d}{d\, x_2} \ln\left(\gamma_2\right) = 0$$

B. Structures of Nitric Acid – Water Complexes Used In DFT Calculations

a) 1 HNO_3 – 1 H_2O Complex

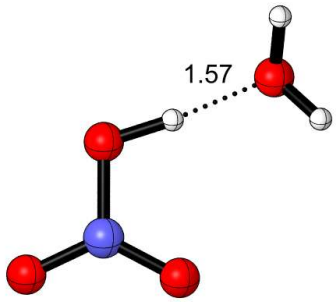

b) 1 HNO_3 – 2 H_2O Complex

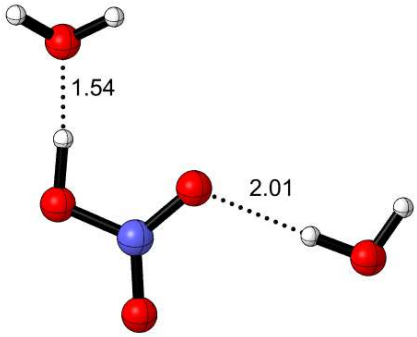

c) 1 HNO_3 – 3 H_2O Complex

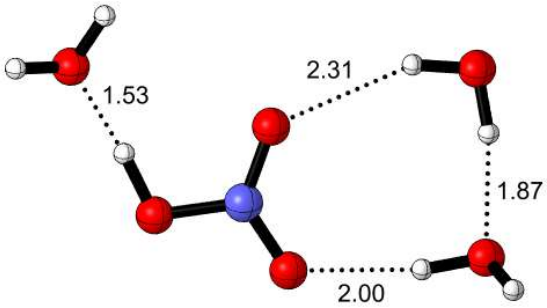

d) 1 HNO_3 – 4 H_2O Complex

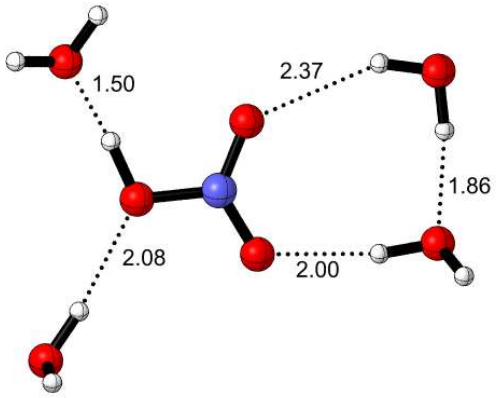

e) 1 HNO_3 – 5 H_2O Complex

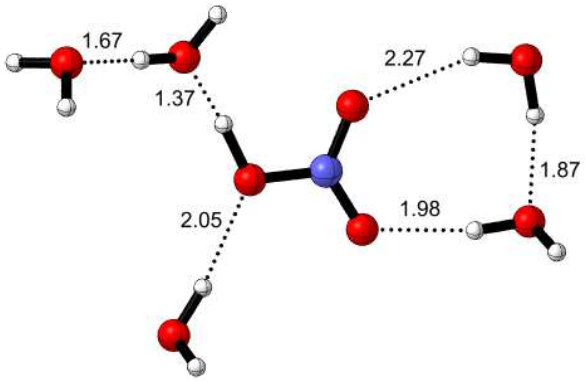

f) 1 HNO_3 – 6 H_2O Complex

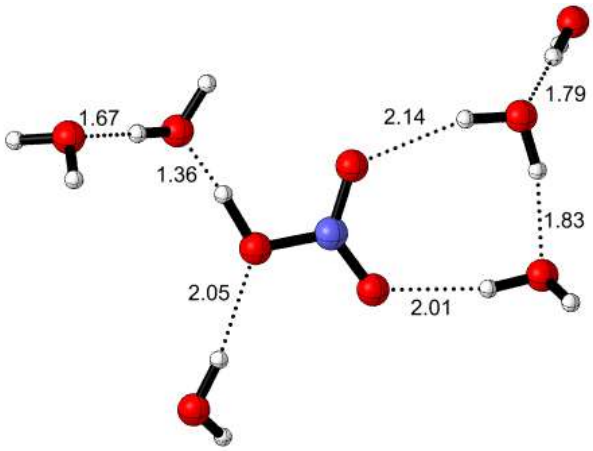

g) 1 HNO_3 – 7 H_2O Complex

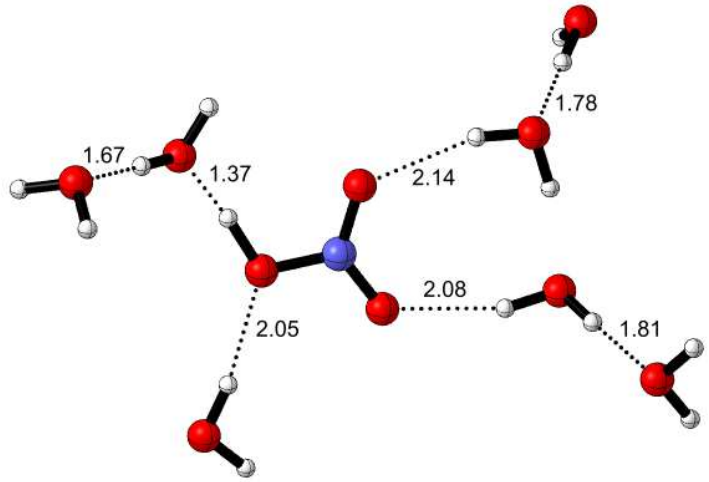

h) 1 HNO_3 – 7 H_2O Complex

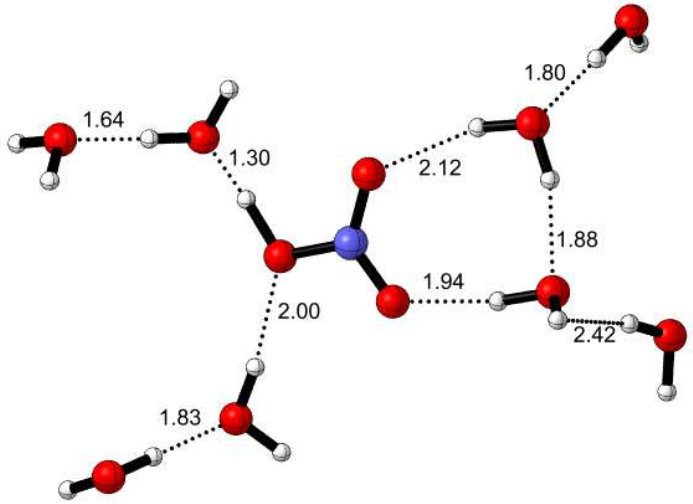

C. Polynomial Fitting and Data Regression

Redlich-Kister Type Polynomial Expansion

In many fields of engineering, the experimental data are not often represented by a linear equation, a straight line. A curve can be suited much better to fit the experimental data for these kind of engineering cases. An alternative for mathematical modeling is to fit the polynomials to the experimental data using polynomial regression (Chapra & Canale, 2006).

Another alternative is to fit polynomials to the data using polynomial regression. The excess Gibbs free energy data of nitric acid – water mixture, obtained by quantum chemical methods, was modeled as a function of x_1 and x_2. The sample calculation to find Redlich-Kister expansion coefficients, A_i, is given in this appendix.

$$G^{ex} = x_1 x_2 (A_1 + A_2(x_1 - x_2) + A_3(x_1 - x_2)^2 + A_4(x_1 - x_2)^3)$$

Table C.1 Experimental excess Gibbs energy values at constant temperature and pressure

x_{HNO_3}	G^{ex} (J/mol)
0.00	0.00
0.11	-117750.94
0.13	-106038.60
0.14	-92703.70
0.17	-76740.67
0.20	-50677.36
0.25	-49430.24

Table C.2 (continued)

0.33	-36546.93
0.50	-33165.29
1.00	0.00

To model $G^{ex}(x_1, x_2)$, a substituent, y is used to linearize the equation.

$$y = \frac{G^{ex}(x_1, x_2)}{x_1 x_2} = A_1 + A_2(x_1 - x_2) + A_3(x_1 - x_2)^2 + A_4(x_1 - x_2)^3$$

The substituent z represents,

$$z = x_1 - x_2$$

then Redlich-Kister expansion for the excess molar Gibbs free energy becomes,

$$y = A_1 + A_2 z_1 + A_3 {z_2}^2 + A_4 {z_3}^3$$

In the estimations of polynomial parameters, A_i,

In order to obtain the correct values of A_i, the sum of squares of deviation of y, should be minimized.

$$S = \sum_{i=1}^{n} (y_i - (A_1 + A_2 z_i + A_3 {z_i}^2 + A_4 {z_i}^3))^2$$

The derivatives of the square deviation equation with respect to each unknown coefficient, A_i, in the polynomial are taken,

$$\frac{\partial S}{\partial A_1} = -2 \sum_{i=1}^{n} y_i - (A_1 + A_2 z_i + A_3 {z_i}^2 + A_4 {z_i}^3)$$

$$\frac{\partial S}{\partial A_2} = -2 \sum_{i=1}^{n} z_i (y_i - (A_1 + A_2 z_i + A_3 {z_i}^2 + A_4 {z_i}^3))$$

$$\frac{\partial S}{\partial A_3} = -2 \sum_{i=1}^{n} {z_i}^2 (y_i - (A_1 + A_2 z_i + A_3 {z_i}^2 + A_4 {z_i}^3))$$

$$\frac{\partial S}{\partial A_4} = -2 \sum_{i=1}^{n} {z_i}^3 (y_i - (A_1 + A_2 z_i + A_3 {z_i}^2 + A_4 {z_i}^3))$$

As the criteria for the best fit, the derivatives above can be set to equal to zero, then the equations can be rearranged to form a set of equations.

$$A_1 n + A_2 \sum_{i=1}^{n} z_i + A_3 \sum_{i=1}^{n} {z_i}^2 + A_4 \sum_{i=1}^{n} {z_i}^3 = \sum_{i=1}^{n} y_i$$

$$A_1 \sum_{i=1}^{n} z_i + A_2 \sum_{i=1}^{n} {z_i}^2 + A_3 \sum_{i=1}^{n} {z_i}^3 + A_4 \sum_{i=1}^{n} {z_i}^4 = \sum_{i=1}^{n} z_i y_i$$

$$A_1 \sum_{i=1}^{n} {z_i}^2 + A_2 \sum_{i=1}^{n} {z_i}^3 + A_3 \sum_{i=1}^{n} {z_i}^4 + A_4 \sum_{i=1}^{n} {z_i}^5 = \sum_{i=1}^{n} {z_i}^2 y_i$$

$$A_1 \sum_{i=1}^{n} {z_i}^3 + A_2 \sum_{i=1}^{n} {z_i}^4 + A_3 \sum_{i=1}^{n} {z_i}^5 + A_4 \sum_{i=1}^{n} {z_i}^6 = \sum_{i=1}^{n} {z_i}^3 y_i$$

where, n is the number of data points and all of the summations are from $i = 1$ to n. From that point on, the equations above are linear and having four unknowns: A_1, A_2, A_3, A_4. should be solved by linear algebra calculations. For this set of equations, determinations of a third order least squares polynomial is simply equivalent to solving a set of four linear equations simultaneously.

$$\begin{pmatrix} A_1 \\ A_2 \\ A_3 \\ A_4 \end{pmatrix} = \begin{pmatrix} n & \sum_{i=1}^{n} z_i & \sum_{i=1}^{n} {z_i}^2 & \sum_{i=1}^{n} {z_i}^3 \\ \sum_{i=1}^{n} z_i & \sum_{i=1}^{n} {z_i}^2 & \sum_{i=1}^{n} {z_i}^3 & \sum_{i=1}^{n} {z_i}^4 \\ \sum_{i=1}^{n} {z_i}^2 & \sum_{i=1}^{n} {z_i}^3 & \sum_{i=1}^{n} {z_i}^4 & \sum_{i=1}^{n} {z_i}^5 \\ \sum_{i=1}^{n} {z_i}^3 & \sum_{i=1}^{n} {z_i}^4 & \sum_{i=1}^{n} {z_i}^5 & \sum_{i=1}^{n} {z_i}^6 \end{pmatrix}^{-1} \begin{pmatrix} \sum_{i=1}^{n} y_i \\ \sum_{i=1}^{n} z_i y_i \\ \sum_{i=1}^{n} {z_i}^2 y_i \\ \sum_{i=1}^{n} {z_i}^3 y_i \end{pmatrix}$$

Two – Constant Margules Equation

In the case of two constant Margules equation, the excess molar Gibbs free energy is not symmetric for the mole fractions. Similarly, the activity coefficients as a function of concentration, don't have to be necessarily a mirror image of each other (Sandler, 2006). In two constant Margules equation, the excess Gibbs free energy is a function of both $x_1$and x_2 and has two polynomial constants, A and B;

$$\frac{G^{ex}}{RT} = x_1 x_2 [A + B(x_1 - x_2)]$$

It is simply a type of Redlich – Kister polynomial expansion of order two. In order to get the constants, it is required to linearize the excess molar Gibbs free energy equation. Therefore,

$$\frac{G^{ex}/RT}{x_1 x_2} = 2Bx_1 + (A - B)$$

When the linearized function is plotted, the slope and the intercept will help to find the polynomial constants, A and B. The activity coefficients can also be calculated as a functions of $x_1$and x_2,

$$ln\gamma_1 = x_2^2[-4Bx_2 + (A + 3B)]$$

$$ln\gamma_2 = x_1^2[4Bx_1 + (A - 3B)]$$

van Laar Equation

In van Laar model, the excess molar Gibbs free energy is given by,

$$\frac{G^{ex}}{RT} = x_1 x_2 \left[\frac{AB}{Ax_1 + Bx_2}\right]$$

A linearization is required to obtain the polynomial parameters,

$$\frac{x_1}{G^{ex}/RT} = \frac{1}{B}\frac{x_1}{x_2} + \frac{1}{A}$$

When the linearized function is plotted as $\frac{x_1}{G^{ex}/RT}$ versus $\frac{x_1}{x_2}$, the resulting slope and the intercept helps to calculate the polynomial constants, A and B. The activity coefficients can also be calculated as functions of $x_1$and x_2,

$$ln\gamma_1 = \frac{A}{\left(1 + \frac{A}{B}\frac{x_1}{x_2}\right)^2}$$

$$ln\gamma_2 = \frac{B}{\left(1 + \frac{B}{A}\frac{x_2}{x_1}\right)^2}$$

D. Comparative Plots of DFT Heat of Mixing Results by Polynomial Fits

a. Nitric Acid – Water System

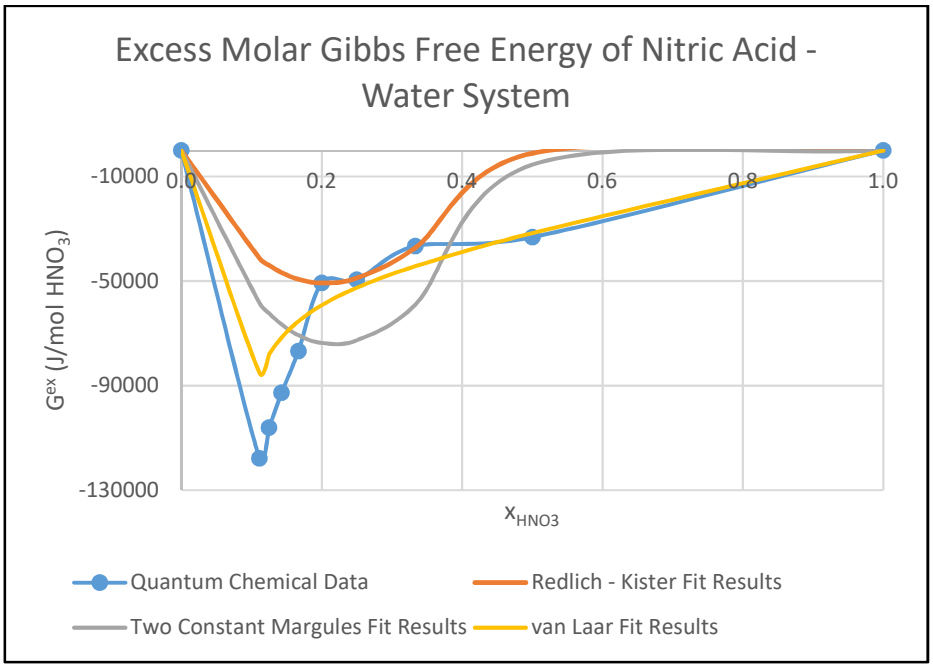

b. Fuel – Oxidizer System

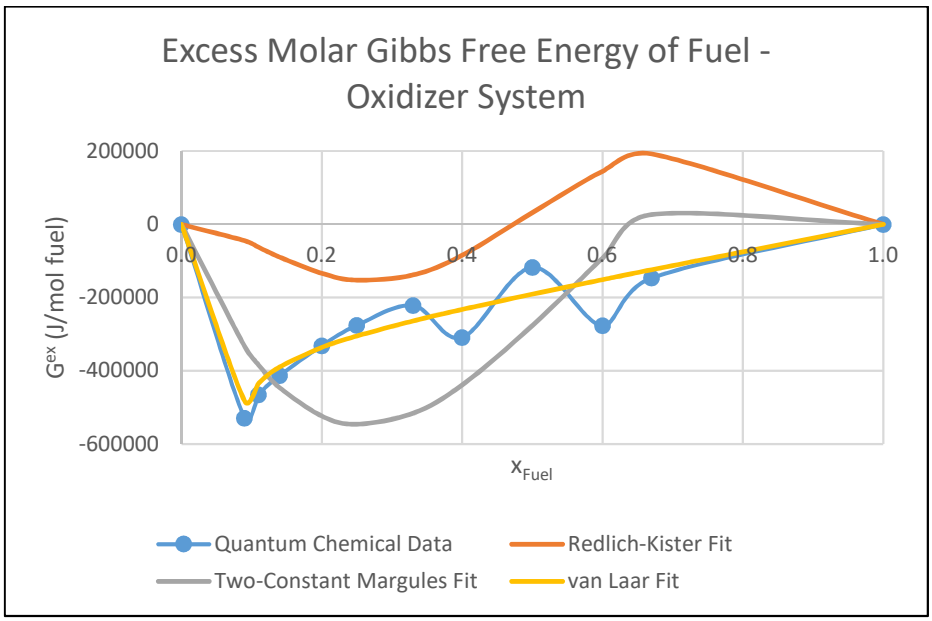

E. Phyton Code of the Algorithm to Estimate Antoine Constants for Pure Liquids from Experimental Vapor Pressure Data

```python
import sys
import math

# global range settings for A B C factors
A_range_min = 1
A_range_max = 15

B_range_min = 500
B_range_max = 5000

C_range_min = -50
C_range_max = -10


def optimize_params(T, P, target_precision):
    global A_range_min
    global A_range_max
    global B_range_min
    global B_range_max
    global C_range_min
    global C_range_max

    abs_min_diff = math.inf
    min_diff = math.inf
    found_A = 0
    found_B = 0
    found_C = 0

    step = 1

    while step >= target_precision:
        print(f"\tSearching with step: {step}")

        curr_A = A_range_min

        # brute-force search for best option
        while curr_A < A_range_max:
            curr_B = B_range_min

```

```python
import sys
import math

# global range settings for A B C factors
A_range_min = 1
A_range_max = 15

B_range_min = 500
B_range_max = 5000

C_range_min = -50
C_range_max = -10


def optimize_params(T, P, target_precision):
    global A_range_min
    global A_range_max
    global B_range_min
    global B_range_max
    global C_range_min
    global C_range_max

    abs_min_diff = math.inf
    min_diff = math.inf
    found_A = 0
    found_B = 0
    found_C = 0

    step = 1

    while step >= target_precision:
        print(f"\tSearching with step: {step}")

        curr_A = A_range_min

        # brute-force search for best option
        while curr_A < A_range_max:
            curr_B = B_range_min

```

```
            while curr_B <= B_range_max:
                curr_C = C_range_min

                while curr_C <= C_range_max:
                    diff = antoine_difference(T, P, A=curr_A, B=curr_B, C=curr_C)

                    if abs(diff) < abs_min_diff:
                        abs_min_diff = abs(diff)
                        min_diff = diff

                        found_A = curr_A
                        found_B = curr_B
                        found_C = curr_C

                    curr_C += step
                curr_B += step
            curr_A += step

        # zoom in and change ranges
        A_range_min = found_A - step
        A_range_max = found_A + step

        B_range_min = found_B - step
        B_range_max = found_B + step

        C_range_min = found_C - step
        C_range_max = found_C + step

        # increase sensitivity
        step = step / 10

    result = { "A": found_A, "B": found_B, "C": found_C, "diff": min_diff }
    print("\t", result)
    return result

def antoine_difference(T, P, A, B, C):
    log_P = math.log10(P)

    return T*log_P + C*log_P -A*C -A*T + B

```

```
79
80
81  def main():
82      global A_range_min
83      global A_range_max
84      global B_range_min
85      global B_range_max
86      global C_range_min
87      global C_range_max
88
89      # check number of parameters
90      if len(sys.argv) != 3:
91          print("You entered wrong parameters! You should run as: .\\antoine.py <input_file_name> <output_file_name>")
92
93      else:
94          # read experiments
95          input_file_name = sys.argv[1]
96          output_file_name = sys.argv[2]
97          experiments = []
98
99          with open(input_file_name, "r") as inp_file:
100             lines = inp_file.readlines()
101
102             for line in lines:
103                 values = [x.strip().replace(",", ".") for x in line.split("\t")]
104                 experiments.append({ "temperature": float(values[0]), "pressure": float(values[1]) })
105
106         with open(output_file_name, "w") as out_file:
107             out_file.write("T\tP\tA\tB\tC\tDiff\n")
108
109             for experiment in experiments:
110                 T = experiment["temperature"]
111                 P = experiment["pressure"]
112
113                 print(f"Temperature(K): {T}\tPressure(bar): {P}")
114
115                 opt_result = optimize_params(T=T, P=P, target_precision=0.0001)
116
117                 out_file.write(f"{T}\t{P}\t{opt_result['A']}\t{opt_result['B']}\t{opt_result['C']}\t{opt_result['diff']}\n")
118
```

F. Experimental Data of Coffee-Cup Heat of Mixing Experiments

a. Oxidizer and Water Heat of Mixing Experiments

Table F.1 Experimental data on the adiabatic coffee-cup calorimeter heat of mixing experiment of the oxidizer and water system – 1 μL water injection

Water Addition to the Mixture (μL)	**# of Moles of Water in the Mixture**	**Mole Fraction of Oxidizer in the Mixture**	**Equilibrium Mixture Temperature** (˚C)	**Temperature Elevation** (˚C)
50	0.003	0.95	25.5	2.5
100	0.006	0.90	27.5	4.5
150	0.008	0.86	28.9	5.9
200	0.011	0.82	30.0	7.0
250	0.014	0.78	31.2	8.2
300	0.017	0.75	32.3	9.3
350	0.019	0.72	33.1	10.1
400	0.022	0.69	34.0	11.0
450	0.025	0.67	34.7	11.7
500	0.028	0.64	35.0	12.0
550	0.031	0.62	35.3	12.3
600	0.033	0.60	35.6	12.6
650	0.036	0.58	36.3	13.3
700	0.039	0.56	38.4	15.4
750	0.042	0.54	41.3	18.3
800	0.044	0.53	44.6	21.6

Table F.2 Experimental data on the adiabatic coffee-cup calorimeter heat of mixing experiment of the oxidizer and water system – 5 mL oxidizer injection

Oxidizer Addition to the Mixture (mL)	**# of Moles of Oxidizer in the Mixture**	**Molar Fraction of Oxidizer in the Mixture**	**Equilibrium Mixture Temperature** (˚C)	**Temperature Elevation** (˚C)
5	0.12	0.04	32	10
10	0.25	0.08	40	18
15	0.37	0.12	42.5	20.5
20	0.50	0.15	43.5	21.5
25	0.62	0.18	44	22
30	0.74	0.21	45.5	23.5
35	0.87	0.24	46	24
40	0.99	0.26	46	24

b. Fuel and Water Heat of Mixing Experiments

Table F.3 Experimental data on the adiabatic coffee-cup calorimeter heat of mixing experiment of the fuel and water system – 1 mL fuel injection

Fuel Addition to the Mixture (mL)	**# of Moles of Fuel in the Mixture**	**Molar Fraction of Fuel in the Mixture**	**Equilibrium Mixture Temperature** (˚C)	**Temperature Elevation** (˚C)
1	0.007	0.002	22.7	1.7
2	0.013	0.005	24.0	3.0
3	0.020	0.007	25.4	4.4
4	0.027	0.009	26.6	5.6
5	0.033	0.012	27.8	6.8
6	0.040	0.014	28.9	7.9
7	0.046	0.016	30.2	9.2
8	0.053	0.019	31.3	10.3
9	0.060	0.021	32.3	11.3
10	0.066	0.023	33.4	12.4
11	0.073	0.026	34.2	13.2
12	0.080	0.028	35.2	14.2
13	0.086	0.030	36.0	15.0
14	0.093	0.032	36.9	15.9
15	0.099	0.035	37.6	16.6
16	0.106	0.037	38.2	17.2
17	0.113	0.039	38.8	17.8
18	0.119	0.041	39.3	18.3
19	0.126	0.043	39.8	18.8
20	0.133	0.046	40.3	19.3
21	0.139	0.048	40.7	19.7

Table F.3 (continued)

22	0.146	0.050	41.2	20.2
23	0.152	0.052	41.5	20.5
24	0.159	0.054	41.9	20.9
25	0.166	0.056	42.3	21.3
26	0.172	0.058	42.6	21.6
27	0.179	0.061	42.9	21.9
28	0.186	0.063	43.0	22.0
29	0.192	0.065	43.1	22.1
30	0.199	0.067	43.1	22.1

Table F.4 Experimental data on the adiabatic coffee-cup calorimeter heat of mixing experiment of the fuel and water system – 5 mL fuel injection

Fuel Addition to the Mixture (mL)	**# of Moles of Fuel in the Mixture**	**Molar Fraction of Fuel in the Mixture**	**Equilibrium Mixture Temperature** (˚C)	**Temperature Elevation** (˚C)
5	0.033	0.012	28.0	7.0
10	0.066	0.023	33.0	12.0
15	0.099	0.035	37.0	16.0
20	0.133	0.046	39.9	18.9
25	0.166	0.056	42.2	21.2
30	0.199	0.067	43.7	22.7
35	0.232	0.077	44.9	23.9
40	0.265	0.087	45.8	24.8
45	0.298	0.097	46.5	25.5
50	0.331	0.107	47.1	26.1
55	0.364	0.116	47.3	26.3
60	0.398	0.125	47.4	26.4
65	0.431	0.134	47.5	26.5
70	0.464	0.143	47.6	26.6
75	0.497	0.152	47.6	26.6

Table F.5 Experimental data on the adiabatic coffee-cup calorimeter heat of mixing experiment of the fuel and water system – 1 mL water injection

Water Addition to the Mixture (mL)	**# of Moles of Fuel in the Mixture**	**Molar Fraction of Fuel in the Mixture**	**Equilibrium Mixture Temperature** (˚C)	**Temperature Elevation** (˚C)
1	0.33	0.856	23.4	2.4
2	0.33	0.749	26.2	5.2
3	0.33	0.665	28.7	7.7
4	0.33	0.599	31.0	10.0
5	0.33	0.544	33.0	12.0
6	0.33	0.499	34.9	13.9
7	0.33	0.460	36.3	15.3
8	0.33	0.427	37.8	16.8
9	0.33	0.399	39.1	18.1
10	0.33	0.374	40.2	19.2
11	0.33	0.352	40.9	19.9
12	0.33	0.332	41.8	20.8
13	0.33	0.315	42.6	21.6
14	0.33	0.299	43.2	22.2
15	0.33	0.285	43.7	22.7
16	0.33	0.272	44.2	23.2
17	0.33	0.260	44.7	23.7
18	0.33	0.249	45.0	24.0
19	0.33	0.239	45.3	24.3
20	0.33	0.230	45.6	24.6
21	0.33	0.221	45.8	24.8
22	0.33	0.213	46.0	25.0
23	0.33	0.206	46.2	25.2

Table F.5 (continued)

24	0.33	0.199	46.5	25.5
25	0.33	0.193	46.6	25.6
26	0.33	0.187	46.7	25.7
27	0.33	0.181	46.8	25.8
28	0.33	0.176	46.8	25.8
29	0.33	0.171	46.8	25.8
30	0.33	0.166	46.8	25.8
31	0.33	0.161	46.8	25.8
32	0.33	0.157	46.8	25.8
33	0.33	0.153	46.8	25.8
34	0.33	0.149	46.7	25.7
35	0.33	0.146	46.6	25.6
36	0.33	0.142	46.5	25.5
37	0.33	0.139	46.4	25.4
38	0.33	0.136	46.4	25.4
39	0.33	0.133	46.3	25.3
40	0.33	0.130	46.3	25.3
41	0.33	0.127	46.2	25.2
42	0.33	0.124	46.0	25.0
43	0.33	0.122	46.0	25.0
44	0.33	0.119	45.9	24.9
45	0.33	0.117	45.8	24.8
46	0.33	0.115	45.7	24.7
47	0.33	0.113	45.6	24.6
48	0.33	0.111	45.5	24.5
49	0.33	0.109	45.4	24.4
50	0.33	0.107	45.2	24.2

Table F.6 Experimental data on the adiabatic coffee-cup calorimeter heat of mixing experiment of the fuel and water system – 5 mL water injection

Water Addition to the Mixture (mL)	**# of Moles of Fuel in the Mixture**	**Molar Fraction of Fuel in the Mixture**	**Equilibrium Mixture Temperature** (˚C)	**Temperature Elevation** (˚C)
5	0.33	0.544	34.3	13.4
10	0.33	0.374	39.7	18.7
15	0.33	0.285	44.3	23.3
20	0.33	0.230	46.7	25.7
25	0.33	0.193	48.4	27.4
30	0.33	0.166	48.6	27.6
35	0.33	0.146	48.5	27.5
40	0.33	0.130	48.2	27.2
45	0.33	0.117	47.8	26.8
50	0.33	0.107	47.4	26.4
55	0.33	0.098	46.8	25.8
60	0.33	0.090	46.4	25.4
65	0.33	0.084	45.7	24.7
70	0.33	0.079	45.2	24.2
75	0.33	0.074	44.7	23.7
80	0.33	0.069	44.2	23.2

c. Diluted Fuel – Diluted Oxidizer Mixing Experiments

Table F.7 Experimental data on the adiabatic coffee-cup calorimeter heat of mixing experiment of the diluted fuel and diluted oxidizer system

Fuel Addition to the Mixture (mL)	**# of Moles of Fuel in the Mixture**	**Molar Fraction of Fuel in the Mixture** (X_{fuel})	**Equilibrium Mixture Temperature** (˚C)	**Temperature Elevation** (˚C)
5	0.00	0.03	24.10	0.70
10	0.01	0.05	24.80	1.40
15	0.01	0.07	25.30	1.90
20	0.01	0.10	25.80	2.40
25	0.02	0.12	26.20	2.80
30	0.02	0.14	26.60	3.20
35	0.02	0.16	26.70	3.30
40	0.03	0.18	27.10	3.70
45	0.03	0.19	27.30	3.90
50	0.03	0.21	27.60	4.20
55	0.04	0.23	27.80	4.40
60	0.04	0.24	27.90	4.50
65	0.04	0.26	28.10	4.70
70	0.05	0.27	28.20	4.80
75	0.05	0.29	28.30	4.90
80	0.05	0.30	28.40	5.00
85	0.06	0.31	28.60	5.20
90	0.06	0.32	28.70	5.30
95	0.06	0.34	28.70	5.30
100	0.07	0.35	28.70	5.30
105	0.07	0.36	28.40	5.00

Table F.7 (continued)

110	0.07	0.37	28.30	4.90
115	0.08	0.38	28.10	4.70
120	0.08	0.39	27.90	4.50
125	0.08	0.40	27.80	4.40
130	0.09	0.41	27.70	4.30
135	0.09	0.42	27.60	4.20
140	0.09	0.43	27.40	4.00
145	0.10	0.44	27.30	3.90
150	0.10	0.44	27.20	3.80

G. Ignition Delay Time Experimental Results

Table G.1 Ignition delay time experimental results.

P (bar)	**T** (˚C)	**Ignition Delay Time** (ms)
0.7	15	13
0.9	15	15
1.2	15	14
1.3	15	20
5.0	15	50
0.6	20	17
0.7	20	18
3.0	20	21
4.0	20	27
0.6	25	36
0.7	25	30
0.9	25	16
1.0	25	17
1.2	25	19
2	25	19
3	25	25
0.5	30	19
0.6	30	16
3.0	30	11

H. An Example Model of Methanol – Water Binary System VLE Estimation with UNIFAC

As the test model, for the sake of simplicity and the availability of very broad range of data, the methanol – water system was selected. The required parameters for all parameters _CH_3, _OH and H_2O were taken from Dortmund Data Bank, as already given in Table 4.2. The reference data on vapor – liquid equilibrium of methanol – water system is taken from the work of Bennett (1929) (Bennett, 1929) . The comparison of the calculated and reference binary vapor – liquid equilibrium data on methanol – water system is given in the figure below.

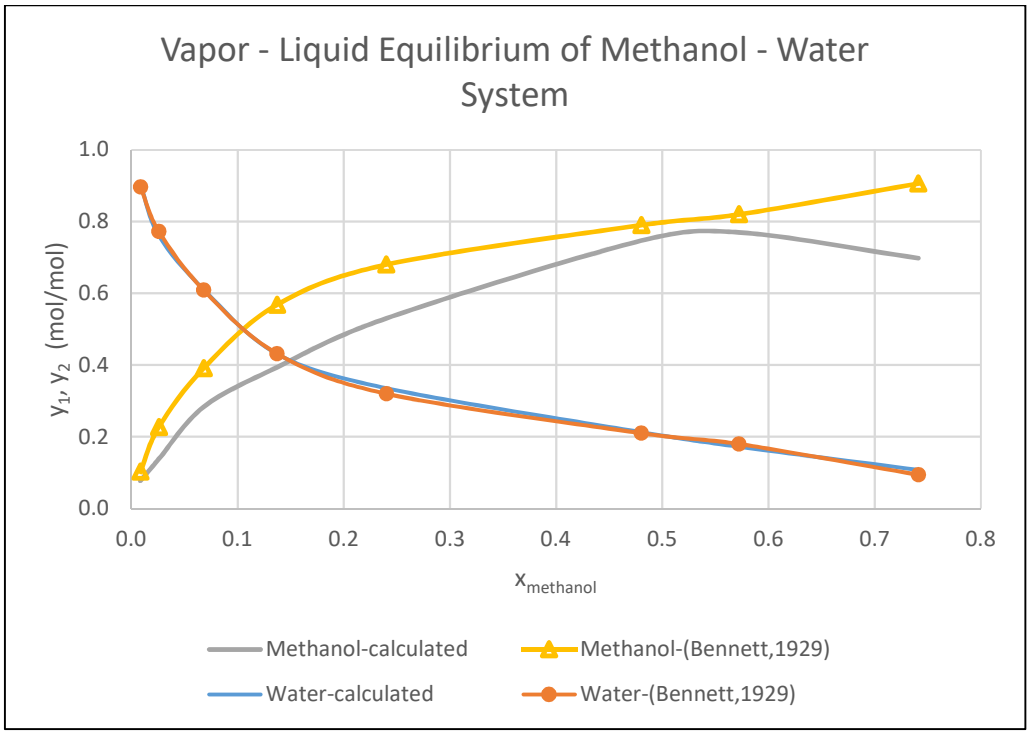

Figure H.1. Comparative plot of calculated and reference vapor – liquid equilibrium data of methanol – water system by UNIFAC group contribution activity coefficient model.